SANDIA REPORT

SAND96–1460 • UC–700
Unlimited Release
Printed July 1996

Validation of EMP Bounds

Larry K. Warne, Kimball O. Merewether, Kenneth C. Chen, Roy E. Jorgenson,
Marvin E. Morris, James E. Solberg, Jeanne G. Lewis, William Derr

Prepared by
Sandia National Laboratories
Albuquerque, New Mexico 87185 and Livermore, California 94550
for the United States Department of Energy
under Contract DE-AC04-94AL85000

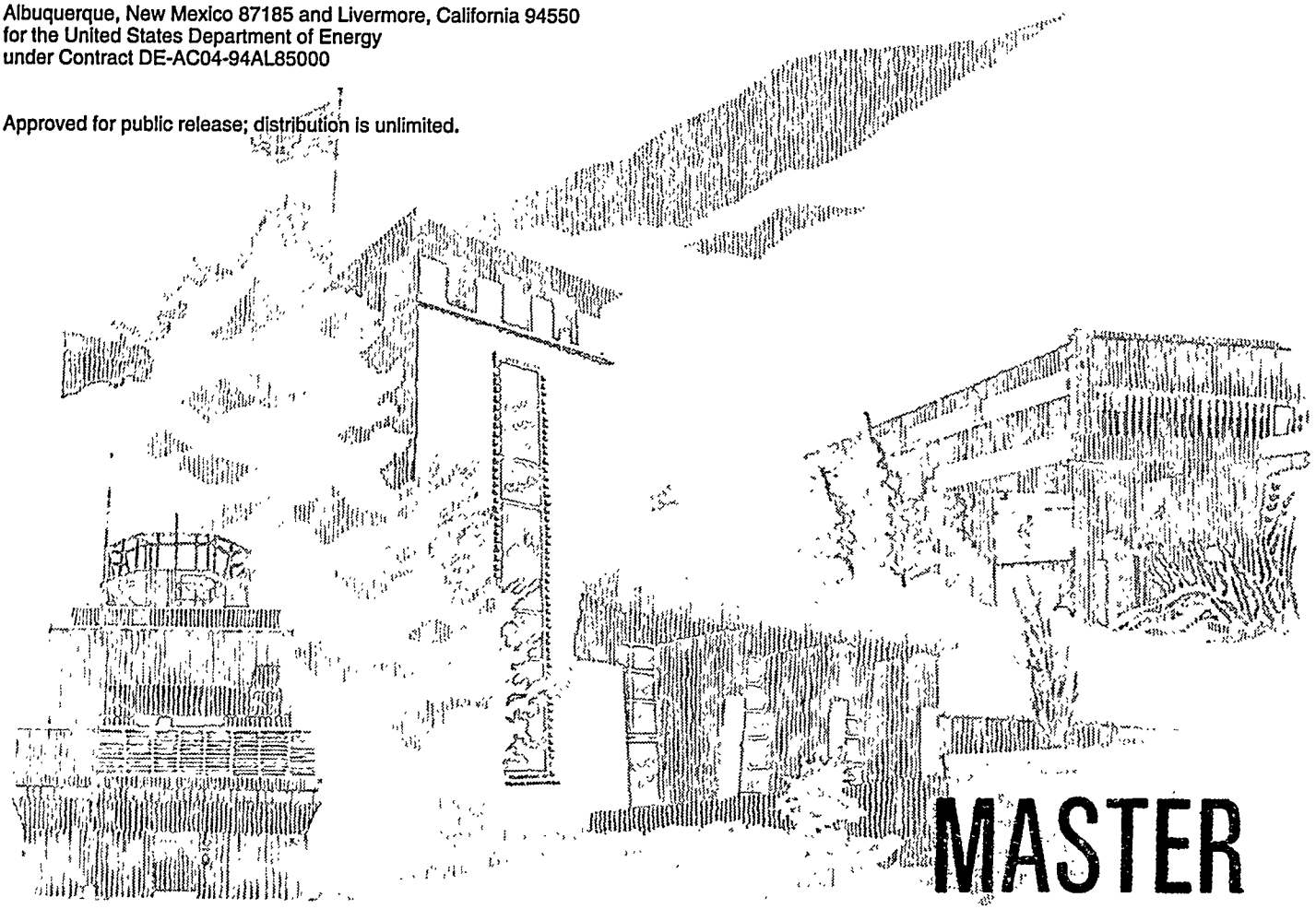

SF2900Q(8-81)

Issued by Sandia National Laboratories, operated for the United States Department of Energy by Sandia Corporation.

Available to DOE and DOE contractors from
Office of Scientific and Technical Information
PO Box 62
Oak Ridge, TN 37831

Prices available from (615) 576-8401, FTS 626-8401

Available to the public from
National Technical Information Service
US Department of Commerce
5285 Port Royal Rd
Springfield, VA 22161

NTIS price codes
Printed copy: A06
Microfiche copy: A01

SAND96-1460
Unlimited Distribution
Printed July 1996

Distribution
Category UC-700

Validation of EMP Bounds

Larry K. Warne, Kimball O. Merewether, Kenneth C. Chen,
Roy E. Jorgenson, Marvin E. Morris, and James E. Solberg
Electromagnetic Analysis and Test Department

Jeanne G. Lewis
Engineering and Process Department
Sandia National Laboratories
Albuquerque, NM 87185

William Derr
Derr Enterprises
507 Montaño Rd. N.W
Albuquerque, NM 87107

Abstract

Test data on canonical weapon-like fixtures are used to validate previously developed analytical bounding results. The test fixtures were constructed to simulate (but be slightly worse than) weapon ports of entry but have known geometries (and electrical points of contact.) The exterior of the test fixtures exhibited exterior resonant enhancement of the incident fields at the ports of entry with magnitudes equal to those of weapon geometries. The interior consisted of loaded transmission lines adjusted to maximize received energy or voltage but incorporating practical weapon geometrical constraints. New analytical results are also presented for bounding the energies associated with multiple bolt joints and for bounding the exterior resonant enhancement of the exciting fields.

Acknowledgment

The authors express their thanks to John Stake and Parris Holmes for careful operation of the Electromagnetic Environments Simulator (EMES) test facility, conducting the EMP tests, and data processing the results.

Contents

1 Introduction 7

2 EMP Waveform 7

3 Test Fixture Concept and Design 8

4 EMP Energy Bounds 12

5 Reduction in Energy Bounds 16

6 Voltage Predictions 21

7 EMP Test Data and Comparison 22

8 Exterior Resonance Drive 29

9 Numerical Analysis Using PATCH Code 31

10 Summary and Conclusions 32

References 35

Validation of EMP Bounds

1 INTRODUCTION

Nuclear electromagnetic pulse (EMP) is a required environment for weapon systems (by weapon system we mean here the nuclear weapon only). However past experimental evidence and analyses (using models that can be found in [1]) have shown that typical weapon apertures (excluding exposed cabling) are penetrated efficiently only by frequencies above those typically present in the EMP spectrum. Comparisons [2] with typical electromagnetic radiation (EMR) requirements have demonstrated that the threats posed by EMP are relatively small at the higher frequencies.

Determining the limits of energy penetration from EMP is a useful criterion to rule out the possibility of electro-explosive device (EED) initiation and damage to older electronic devices. Thus a step function energy bound was developed [3], [4]. This result bounds the energy which can be coupled to an object or through an aperture in a ground plane from a step function waveform. The spectrum of the step function bounds the spectrum of the corresponding double exponential description of realistic EMP. Application of the energy bound to the exterior of a weapon system results in too large a result to rule out damage. Applications to typical ports of entry (POEs) (excluding exterior cabling) results in coupled energies below typical EED activation or older electronics damage thresholds. Furthermore the effects of nonzero rise time, POE dimensions, POE-cable clearance, and cable-load impedance often result in substantially reduced energies [5]. On the other hand POEs on weapon systems are not on ground planes. The POE may be small enough to approximate the surrounding conductor as a ground plane, but the exciting exterior field is enhanced at certain frequencies (exterior resonant frequencies) over the field on a ground plane [6]. One brute force way to apply the step function bound in this situation is to increase the step amplitude by an appropriate factor so the spectrum of the step bounds the actual spectrum of the exterior field of the POE [7]. This increase can be substantial, and thus it would be useful to find an alternative.

The model validation project proposal [8] described a multi-year program to address both EMP and EMR bounds. The first half year is devoted to EMP. A driver for its priority is the projected decommissioning of the EMP facility at Sandia National Laboratories. The first half year objectives [9] and tasks are: 1) provide experimental benchmark of EMP bounds with weapon-like geometries which are geometrically and electrically known, 2) optimize experimental energy reception in realistic weapon geometry, 3) demonstrate reduction in received energy resulting from nonzero rise time, POE dimensions, POE-cable clearance, and cable-load impedance, 4) demonstrate exterior resonance enhancement of received energy, 5) find an alternative bound to apply for the exterior resonant enhancement of the POE exciting field, 6) provide experimental data on interior voltage limits for use in second year voltage bound analysis, and 7) provide numerical modeling for validation purposes.

2 EMP WAVEFORM

The Electromagnetic Environments Simulator (EMES) test facility was used in the EMP tests. The electromagnetic pulse provided by EMES is somewhat more severe in rise rate than typical requirements. Figure 1 shows a typical EMES waveform. A double exponential fit of the waveform is

$$E(t) = E_0 \left(e^{-\alpha t} - e^{-\beta t} \right) u(t) \tag{1}$$

where $u(t)$ is the unit step function. The fall time to half maximum is controlled by the time constant α. The nominal EMES parameters are approximately $\alpha \approx 3 \times 10^7$ sec^{-1} (fall to half maximum

is approximately 25 nsec, peak to half peak is approximately 23 nsec), $\beta \approx 4 \times 10^9$ sec^{-1} (10% to 90% of peak rise time is approximately 0.5 nsec), $E_0 \approx 60$ kV/m (peak level of approximately 57 kV/m). The late time behavior and the opposite polarity pulse at 30 nsec deviate from the typical EMP requirement. Steps will be taken in the energy comparisons to ignore contributions beyond the 25 nsec time when deviations of the facility environment become significant.

Unfortunately the double exponential fit (1) overestimates the rise rate of the EMES waveform by more than a factor of two near $t = 0$. This results from the discontinuity in slope of the waveform (1) at $t = 0$. An improved fit can be obtained by use of the inverse double exponential waveform

$$E(t) = E_0 \frac{U e^{\alpha t}}{1 + e^{\beta(t-t_p)}} \tag{2}$$

where

$$U = \beta(\beta - \alpha)^{\alpha/\beta - 1} \alpha^{-\alpha/\beta} e^{-\alpha t_p}$$

The nominal values of these parameters are $t_p = 5$ nsec, $\alpha \approx 8.552 \times 10^9$ sec^{-1} and $\beta \approx 8.58 \times 10^9$ sec^{-1} (peak to half peak fall time is approximately 25 nsec and the 10% to 90% of peak rise time is 0.5 nsec). The value of E_0 is set to the peak amplitude, for example, $E_0 \approx 60$ kV/m. Many of the EMES waveforms exhibit rise times near 0.4 nsec. A set of parameters for this rise time are $\alpha \approx 10.725 \times 10^9$ sec^{-1} and $\beta \approx 10.753 \times 10^9$ sec^{-1} (10% to 90% rise time of 0.4 nsec and peak to half peak fall time of approximately 25 nsec). The peak rate of rise and its time of occurrence for the waveform (2) can be found from $E_p' = E_0\beta(\beta-\alpha)^{\alpha/\beta-1}(e_p/\alpha)^{\alpha/\beta}\{\alpha+(\alpha-\beta)e_p\}/(1+e_p)^2$ and $e_p = e^{\alpha(t-t_p)} = \{(\beta^2 + 2\alpha\beta - 2\alpha^2) - \sqrt{(\beta^2+2\alpha\beta-2\alpha^2)^2 - 4(\alpha-\beta)^2\alpha^2}\}/\{2(\alpha-\beta)^2\}$. The peak rise rate of the waveform (2) for $\alpha \to \beta$ is thus approximately

$$\frac{\partial E}{\partial t} \approx E_0\beta/4 \tag{3}$$

3 TEST FIXTURE CONCEPT AND DESIGN

Budget and schedule constraints limit the number of tests and test fixtures. Three test fixtures were constructed. Figure 2 shows the design concept from the test plan [9]. Figure 2a shows the cylindrical geometry of the test fixtures which captures field enhancements of the exterior resonances of an isolated weapon. Note that the rectangular plate forms part of the ground plane floor of EMES. The cylinder above the plate thus images to form an exterior with twelve to one aspect ratio (most weapons have roughly a ten to one aspect ratio or less). The aspect ratio determines the magnitude of the resonant field enhancement. (Of course if the weapon is stood end to ground, the imaged system will have an order twenty to one aspect ratio and slightly larger field enhancements.) The region below the plate allows measurement signals to be easily removed by coaxial cables without interfering with the exterior field. The actual cylinder dimensions used in the test were $2b_o = 2(b + \Delta) = 6$ in (outside diameter), $\Delta = 0.25$ in (wall thickness of stock pipe), $h_c = 36$ in (height to top of end cap plate), $h_b = 17\frac{5}{8}$ in (height below ground plane plate to bottom of end cap plate), the ground plane plate was a square with side length $26\frac{11}{16}$ in and thickness 0.25 in, the end cap plate thicknesses were 0.25 in. The aluminum alloy is 6061.

Figure 2b shows the slot test fixture which is a canonical POE representing a single opening (between bolts) in a more complicated bolted joint POE. The slot was constructed with a saw cut of the cylinder wall having actual depth $d = \Delta = 0.25$ in, width $w = 0.018$ in (cut width), $\ell = 2h = 2.35$ in (average of cut arc lengths at inner, 2.25 in, and outer, 2.45 in, radii of cylinder, note that the slot ends approximately align with the cylinder radius vector), and height above the ground plane plate $h_s = 6$ in. (The cut width used here is 0.001 in greater than that marked on the

drawings because it is possible to insert a 0.018 in wire through the majority of the slot with some sticking at certain points. The electrical inductance is an average of the slot width rather than the minimum value, and furthermore for bounding calculations it better to make errors on the large side for this parameter.) The slot is placed near the ground plane so that it receives the majority of the exterior field enhancement resulting from the exterior resonance of the cylinder. Figure 2c shows pick up cable locations to be used interior to the fixture with both the slot and bolted joint fixtures. The center conductor has diameter $2a = 3/16$ in and is made of hollow brass stock. The center location is an obvious choice for symmetry reasons. The characteristic impedance in the center case is [10]

$$Z_c = \sqrt{L/C} = \frac{\eta_0}{2\pi} \ln(b/a) \approx 202.7 \text{ ohms} \tag{4}$$

where L is the inductance per unit length, C is the capacitance per unit length, $LC = \mu_0 \epsilon_0 = 1/c^2$ when no dielectrics are present (c is the vacuum velocity of light) and the transmission line is uniform along its length, and $\eta_0 = \sqrt{\mu_0/\epsilon_0} \approx 120\pi$ ohms is the free space impedance. An approximately matched configuration was achieved at both ends by the series combination of a 150 ohm resistor in series with a 50 ohm coaxial termination (on the bottom the 50 ohm termination is the coaxial cable to the measurement system). The eccentric location increases flux linkage of the cable by the slot penetrant field and thus increases the induced voltage. The spacing $D = 1.25$ in $\approx \ell/2$ is about the smallest distance where we can expect the dipole moment approximations for the slot penetrant field to yield valid results. (This is also a convenient distance from the cylinder walls for the terminating loads and connectors at the end caps.) The impedance per unit length in the eccentric case is also somewhat reduced [11]

$$Z_c = \frac{\eta_0}{2\pi} \text{Arccosh} \left\{ \left(a^2 + b^2 - (b-D)^2 \right) / (2ab) \right\} \approx 181.5 \text{ ohms} \tag{5}$$

An approximately matched configuration was achieved at both ends by the series combination of a 120 ohm resistor in series with a 50 ohm coaxial termination (on the bottom the 50 ohm termination is the coaxial cable to the measurement system).

Figure 2d shows a stripline conductor behind the slot POE (and bisecting the slot). This structure simulates a flat signal cable near the wall of a weapon system. The stripline width w_{sl} was restricted to be small compared to the slot length ℓ to maximize magnetic flux linkage; it was also chosen to be equal to or larger than typical stripline cable widths. The stripline characteristic impedance can be made low so it is comparable with the slot inductive reactance. Thus the energy received by the loaded stripline is larger than the wire cases above. Note also that the stripline is so close to the slot that it can be considered as a slot center load (there is no appreciable reduction factor from slot penetrant magnetic flux lines not linking the stripline). The stripline characteristic impedance is approximately ($g_{sl} << w_{sl}$)

$$Z_c \approx \eta \frac{g_{sl}}{w_{sl}} \approx 10.4 \text{ ohms} \tag{6}$$

where the dielectric gap is approximately $g_{sl} \approx 0.025$ in, the width is approximately $w_{sl} \approx 0.625$ in, the impedance of the dielectric spacer is $\eta = \eta_0 \sqrt{\epsilon_0/\epsilon}$, where for a Teflon spacer $\epsilon \approx 2.1\, \epsilon_0$. The stripline is constructed of copper tape and is shorted to the fixture approximately 3/8 in above the slot and $21\frac{3}{4}$ in below the slot. The load coax enters the cylinder side wall 1.75 in from the end cap. The stripline is terminated by three 50 ohm surface mount (with small length of $< \frac{1}{16}$ in to reduce inductance) parallel resistors in parallel with the 50 ohm measurement system at a distance of 3/16 in above the short at $21\frac{3}{4}$ in below the slot. The total load is thus

$$Z_L \approx 12.5 \text{ ohms} \tag{7}$$

The reason that only three rather than four surface mount 50 ohm resistors were used to construct an approximate matched load is because the time domain reflectometer (TDR) indicated that the characteristic impedance of the stripline was $Z_c \approx 12.5$ ohms. This result was accepted because several thousandths of an inch of silicon seal (RTV) were used to adhere the Teflon dielectric spacer to the fixture wall.

The inductance per unit length of the slot is [12], [13]

$$L \approx \mu_0 \pi / \Omega_e \tag{8}$$

where we can take the expansion parameter to be $\Omega_e = \Omega + 2(\ln 2 - 7/3)$ and the fatness parameter is approximately $\Omega \approx 2\ln(4\ell/w) + \pi d/w$. The total slot center inductance is

$$L_{slot} = \frac{1}{2} hL \approx 1.11 \text{ nH} \tag{9}$$

The exterior short circuit center slot current is

$$I_{sc} \approx h K_z^{sc} \tag{10}$$

where $K_z^{sc} = H_\varphi^{sc}$ is the exterior short circuit axial current density. Noting from (3) the peak value of the derivative of the incident magnetic field is $\frac{\partial}{\partial t} H^{inc} \approx H^{inc}\beta/4$ we can see that the peak inductive reactance is roughly $X_L \approx L_{slot}\beta/4 \approx 3$ ohms for ($t_r = 0.4$ nsec) $\beta = 10.753 \times 10^9$ sec^{-1}. Thus the stripline characteristic impedance, (6) or (7), is far closer to the slot inductive reactance than the wire characteristic impedance, (4) or (5); thus the stripline circuit absorbs more energy.

An unmatched load was also used on the stripline configuration to simulate low impedance loads associated with EEDs. Six 10 ohm surface mount parallel resistors in parallel with the 50 ohm measurement system were used to obtain

$$Z_L \approx 1.6 \text{ ohms} \tag{11}$$

Six surface mount resistors were a convenient number to insert across the stripline; parasitic inductance also limits how small this load can be made and still remain a reliably known value. The value (11) is also more closely matched to the slot inductive reactance although it is time isolated (by several nanoseconds) from the slot. Thus we expect the energy deposition to build up by means of several round trip reflections from the slot to the load. Another reason for the low impedance load is an attempt to match the value of the slot inductive reactance at the exterior length resonant frequency of $f_r \approx 67$ MHz, which is $\omega_r L_{tot} \approx 0.47$ ohms. Thus the low impedance load (11) may exhibit some exterior resonant enhancement of the energy since the load impedance is not too far above the inductive reactance at this frequency. It should be noted that with typical single point ground interior circuits, a stray capacitive element will always appear in series with the EED resistance.

The bolted joint fixture of Figure 2e more closely resembles bolted step joints of weapon systems. The step in a typical weapon bolt joint does not change the penetration (unless more points of electrical contact are created by the step) relative to the joint of Figure 2e (provided the width w and depth d are the same). The joint construction of Figure 2e has two important advantages for the model validation project: unlike bolted step joints the gap geometry (or slot width w) of the Figure 2e joint can be easily verified by insertion of a gauge, and secondly it is inexpensive to construct. Eight bolts were used to achieve a similar slot length $\ell \approx 2.36$ in (between bolts) to the

single slot fixture. The collar was welded on without a spacer unlike the planned construction in Figure 2e. The collar thickness was 0.25 in. The collar was milled out to create the same slot width $w \approx 0.018$ in as in the single slot. The slot depth was $d \approx 0.625$ in. This depth was convenient for the bolt penetrations and is smaller than the overlap depth on weapon joints. Stainless steel 0.245 in diameter bolts were used with steel capture nuts similar (except somewhat smaller diameter and thus more inductance) to weapon construction. The bolt hole diameter was 0.261 in. Care was taken on assembly to make the gaps uniform around the bolted joint. The wire and stripline configurations discussed previously for the slot fixture were also used in the joint fixture. The center inductance of the bolted joint is approximately

$$L_{tot} \approx L_{slot} + \frac{1}{2} L_{bolt} \tag{12}$$

where from (8) and (9) $L_{slot} \approx 0.5$ nH, and from [14] the bolt inductance can be found approximately from $L_{bolt} \approx \frac{\mu_0}{2\pi}(2\Delta)\ln(b_{hole}/b_{bolt}) \approx 0.16$ nH, where the bolt hole diameter is $2b_{hole} \approx 0.261$ in, and the bolt diameter is $2b_{bolt} \approx 0.245$ in. (The effect of the other bolts and slots on this inductance L_{tot} can be incorporated as a continued fraction but because of the large slot inductance $4L_{slot}$ compared with the bolt inductance L_{bolt} this has little effect on the result.) The bolt inductance given here assumes that the bolt is centered in the hole and does not make electrical contact with the hole except at the head and threaded end; it thus represents an overestimate. However added inductances at the nut plate are thought to be of this same range of value. Thus we will use the value $L_{bolt} \approx 0.2$ nH to represent a nominal level of bolt inductance including the nut plate. The center inductance of the bolted joint is thus somewhat greater than half that of the slot fixture and therefore a greater mismatch exists. (However, the open circuit voltage of the joint slot is similar to the slot fixture as shown in the next section.) Ferrous steel bolts were also used in the final test to check on their effect (which was negligible).

The final cable configuration in Figure 2f was used for induced voltage bounding purposes. A transmission line transformer is used to change the characteristic impedance from its nominal value (7) (note that a strip width of $w_{sl} \approx 0.562$ in was used here because the Teflon sheet material from which the transformer insulating wedge was constructed has this standard thickness) to the characteristic impedance of a wire of radius $a_{sl} \approx 1/16$ in, a height g_{sl} above a ground plane

$$Z_c \approx \frac{\eta_0}{2\pi}\text{Arccosh}(g_{sl}/a_{sl}) \approx 173 \text{ ohms} \tag{13}$$

The strip line gap is tapered from the original gap to $g_{sl} \approx 0.562$ in. The characteristic impedance of the stripline at this height is approximately 100 ohms [15]. A two dimensional finite element calculation was also used to check the effect of the finite width dielectric insulator (the insulator in [15] covers the entire ground plane) below the stripline and the effect of the cylindrical geometry. Figure 3a shows the finite element mesh used; the results were approximately the same as those in [15]. The transition from the 100 ohm stripline impedance to the wire impedance (13) was made by means of a stripline width taper of the copper tape over about a 1.25 in length. The height also tapered over this section from g_{sl} to 1.25 in at the eccentric connector at which point the impedance was approximately (5). An approximate matching resistor of 120 ohms was used in series with the 50 ohm coaxial measurement cable. A second high impedance load resistor of 1 kohm was also used to simulate a high impedance load and thus obtain a higher voltage (more will be said about this high impedance resistor in the results section).

Figure 2g shows the third and final test fixture. A monopole antenna with height $h_m \approx 1$ in and diameter $2a \approx 3/16$ in penetrates the center of the end cap. This geometry simulates (in a simple way) the situation of a connector insulated from the weapon case (although the capacitance

of such a connector to case is substantially higher than the monopole). It also simulates the pins in a connector (although the effective height for the monopole will be larger than typical recessed pins). The monopole conductor penetrates the end cap through a $2b_m = 0.290$ in diameter hole lined with a Teflon sleeve. This conductor also forms the center conductor of the test fixture with characteristic impedance (4). The monopole capacitance is given approximately by the formula [16]

$$C_{mono} \approx \frac{4\pi\epsilon_0 h_m}{\Omega - 2 - 2\ln 2} \approx 1 \text{ pF} \tag{14}$$

where the fatness parameter is $\Omega = 2\ln(2h_m/a)$. Figure 3b shows a surface PATCH Code grid used to check the accuracy of this capacitance; the numerical value was approximately the same as (14). The Teflon sleeve capacitance is approximately

$$C_{sleeve} \approx \frac{2\pi\epsilon\Delta}{\ln(b_m/a)} \approx 1.7 \text{ pF} \tag{15}$$

The parallel combination thus has capacitance $C_{tot} \approx 2.7$ pF and capacitive reactance $X_C \approx 1/(C_{tot}\beta/4) \approx 138$ ohms for the $t_r \approx 0.4$ nsec rise time value of β. The characteristic impedance of the centered transmission line has a value well suited for receiving large energies from the monopole (as opposed to a low impedance load). The capacitive reactance at the exterior resonant frequency is $X_C \approx 1/(\omega_r C_{tot}) \approx 880$ ohms. We expect to receive substantial energies from the exterior resonant mode in the case of the monopole POE since the mismatch is not too pronounced. The interior coaxial transmission line was terminated with three loads. A 50 ohm load (directly into the measurement coax) was used for a relatively low impedance load, a 150 ohm resistor in series with the 50 ohm measurement system was used for an approximate matched case, and a 1 kohm resistor in series with the 50 ohm measurement system was used for a high impedance load (again comments will be made in the results section on the high impedance load).

Figure 4 shows detailed drawings of the test fixtures and the stripline geometries. Figure 5 comprises photographs of the test fixtures, wire geometry, stripline geometry, load resistors, and the EMES facility test volume. Figure 6 shows TDR measurements of the striplines in the test fixtures.

4 EMP ENERGY BOUNDS

This section applies the energy bound in [4] to the POEs of the test fixtures. The energy bound applies to either an object in space or to an aperture on a ground plane with a step function incident wave. The step function wave spectrum bounds the more realistic spectrum described by the double exponential or the inverse exponential waveform. The electric vector of the incident wave is polarized in unit vector direction $\underline{e}_1$, the step amplitude is E_0, and the direction of propagation is $\underline{e}_3$ (the magnetic vector is thus in direction $\underline{e}_2$). The energy that can be absorbed or received by an object is then given by [4]

$$W_{rec} \le \frac{1}{2}V\left(\epsilon_0 \underline{E}_0 \cdot \underset{\leftrightarrow}{P} \cdot \underline{E}_0 + \mu_0 \underline{H}_0 \cdot \underset{\leftrightarrow}{M} \cdot \underline{H}_0\right) = \frac{1}{2}V\left(\epsilon_0 E_0^2 P_{11} + \mu_0 H_0^2 M_{22}\right) \tag{16}$$

where for a plane wave $E_0 = \eta_0 H_0$, the static normalized polarizability tensors $\underset{\leftrightarrow}{P}$ and $\underset{\leftrightarrow}{M}$ on the right hand side of (16) (the $\underline{e}_1\underline{e}_1$ component of the electric tensor and the $\underline{e}_2\underline{e}_2$ component of the magnetic tensor are used) are defined by the equations

$$\underline{p} = \epsilon_0 V \underset{\leftrightarrow}{P} \cdot \underline{E}_0$$

$$\underline{m} = V \underset{\leftrightarrow}{M} \cdot \underline{H}_0 \tag{17}$$

where V is the object volume, $\underline{p}$ is the induced static electric dipole moment, $\underline{m}$ is the induced magnetic dipole moment, and the unperturbed plane static fields at the object are $\underline{E}_0$ and $\underline{H}_0$. The formula (16) gives too large a result (to be useful) when applied to the entire weapon system. However the same arguments can be applied to an aperture in a ground plane [4] to yield

$$W_{rec} \leq \frac{1}{2} 2^2 \left(\mu_0 H_0^2 \alpha_{m_{22}} - \epsilon_0 E_0^2 \alpha_{e_{11}} \right) \tag{18}$$

where for a plane wave $E_0 = \eta_0 H_0$. The polarizability tensors $\underset{\leftrightarrow}{\alpha_e}$ and $\underset{\leftrightarrow}{\alpha_m}$ here are defined by

$$\underline{p} = -2\epsilon_0 \underset{\leftrightarrow}{\alpha_e} \cdot \underline{E}_{sc}$$

$$\underline{m} = 2\underset{\leftrightarrow}{\alpha_m} \cdot \underline{H}_{sc} \tag{19}$$

where the short circuit plane fields at the aperture are $\underline{E}_{sc}$ and $\underline{H}_{sc}$. The polarizability tensors and the dipole moments used here are associated with the incident side of the aperture, not the transmitted side. (The usual relation [1] where the dipole moments reverse sign and the polarizability tensors remain unchanged on the transmitted side of the aperture fails to hold rigorously if the ground plane is thick or if a cavity exists on the transmitted side, etc.)

The POEs on the test fixtures are not on infinite ground planes. Nevertheless the POE dimensions (the slot half length h and monopole height h_m) are typically smaller than the surface radius of curvature. Thus the local fields have approximately the same form as the ground plane fields except the level is enhanced at certain frequencies by the exterior resonance of the test fixture. Figure 7 shows the axial current density ($K_z = H_\varphi$) on the surface, and at the center (facing the direction from which the incident wave impinges), of a perfectly conducting cylinder of length 6 ft (includes the image in the ground plane of the test object) and diameter 6 in for unit incident electric field level. Figure 7a gives the total current density and shows the high frequency limit $2H_{inc}$ (for unit amplitude incident electric field); Figure 7b gives the zero mode (azimuth independent and proportional to total current on the cylinder) current density; Figure 7c shows the amplitudes of azimuthal modes one through four; Figures 7d and 7e (from [6]) show the total current at the center of a cylinder in both the frequency and time domains. The low frequency limit and high frequency limits in Figure 7a are equal to the result on a ground plane $H_{sc} = 2H_{inc} = 2(1 \text{ V/m})/\eta_0 = 0.0053$ A/m. The first resonance occurs at $f_r \approx 67$ MHz (the cylinder plus image is somewhat less than one half wavelength) and the magnetic field is $H_{sc} \approx 8.6\,(2H_{inc})$. The third resonance (even numbered resonances are absent as a result of the symmetry of the cylinder about its center) occurs at roughly 200 MHz with level of approximately $H_{sc} \approx 2.3\,(2H_{inc})$. The fifth resonance occurs at 380 MHz with level $H_{sc} \approx 1.9\,(2H_{inc})$. Above this resonance there is little further enhancement of the magnetic field (above the $2H_{inc}$ level). Thus to apply the above result (18) to the slot POE we can take $H_0 = H_{inc}$ for the high frequencies (as if the slot is in an infinite ground plane) or we can bound the resonant enhancement of the driving field by taking $H_0 = 8.6H_{inc}$ (only $\alpha_{m_{22}}$ contributes significantly for a narrow slot aperture). However because the first exterior resonance occurs at a relatively low frequency and thus does not couple well through the slot to the interior circuit we could consider a compromise value of $H_0 = 2H_{inc}$ which bounds the other resonances (above the first) and consider the large first resonance separately later in the report. The length directed magnetic polarizability of a narrow slot aperture with depth (here we use results which require $\ell >> d, w$ although general results are known [4]) is given by

$$\alpha_{m_{22}} \approx \frac{\ell^3 \pi}{12\Omega_e} \approx 1.05 \times 10^{-6} \text{ m}^3 \tag{20}$$

Using an incident electric field level of 60 kV/m and the corresponding magnetic field $H_0 = H_{inc}$ we obtain

$$W_{rec} \leq 67 \text{ nJ} \tag{21}$$

The resonance bounding result using $H_0 = 8.6H_{inc}$ is 4.96 μJ. The compromise value $H_0 = 2H_{inc}$ gives 268 nJ.

Before treating the bolted joint POE, it is useful to give an alternative derivation of the energy bound for the slot POE $W_{rec} \leq \frac{1}{2}2^2\mu_0 H_0^2 \alpha_{m_{22}}$. The simple inductance-conductance circuit shown in Figure 8 gives the motivation. The energy absorption is invariant under the action of a time reversal transformation (allowing time to run in the reverse direction). Thus if the current source represents a step current waveform $I_0 u(t)$, then under time reversal it is $I_0 u(-t)$ and it is clear that the energy that is absorbed in the conductance is simply the energy stored in the inductance. Now consider the low frequency transmission line model for the slot aperture shown in Figure 9 [13]. The distributed current source $K_{sc} = 2H_{inc}$ is the current density crossing the slot width when the slot is shorted; the incident magnetic field intensity doubles on an infinite ground plane (H_0 the step amplitude of H_{inc} can be interpreted differently on the fixture as discussed previously). The step function excitation establishes currents in the distributed inductance (8). The energy stored in the inductances is available for delivery to a load (for a single point load it is typically less). Thus the energy stored in the distributed transmission line inductance is

$$W_{rec} = \frac{1}{2} L \int_{-h}^{h} I^2 dz \tag{22}$$

The low frequency transmission line equation

$$\frac{dI}{dz} = K_{sc} \tag{23}$$

can be easily integrated (regarding K_{sc} as a constant along the slot with local coordinate z) to yield

$$I = zK_{sc} \tag{24}$$

Thus the energy is

$$W_{rec} = \frac{\ell^3}{24} L K_{sc}^2 = \frac{\pi \ell^3}{12\Omega_e} \frac{1}{2} \mu_0 (2H_0)^2 = \alpha_{m_{22}} \frac{1}{2} \mu_0 (2H_0)^2 \tag{25}$$

the expected result for the slot aperture energy bound.

We now apply this procedure to the bolted joint POEs. The bolted joint has eight slot apertures (eight bolts) around the circumference. The excitation has parts (the zero azimuthal modes) which are symmetric, and parts which are not symmetric (asymmetric azimuthal Fourier modes). We can achieve a bound by taking the entire excitation to be symmetric at a level equal to its peak value. Thus we can place perfect magnetic conductors (symmetry planes) through the center of the bolts and consider only one slot. Figure 10 shows the transmission line model for the symmetric bolted slot; the end loads of a single slot can be taken as twice the single bolt inductance because of the bisecting symmetry planes at the ends of a single slot. The transmission line current is identical to

(24) and thus the energy (25) is one part of the slot energy of the bolted joint. The second part of the energy results from the bolts yielding the total

$$W_{rec} = \frac{\ell^3}{24} L K_{sc}^2 + 2\frac{1}{2}(2L_{bolt})\, I^2(h) \tag{26}$$

Thus the energy bound for the bolt joint, per slot, can be written as

$$W_{rec} \leq \left(\frac{\pi \ell^3}{12\Omega_e} + \ell^2 L_{bolt}/\mu_0 \right) \frac{1}{2}\mu_0 (2H_0)^2 \tag{27}$$

Using the value $L_{bolt} \approx 0.2$ nH we obtain per slot

$$W_{rec} \leq (4.77 + 5.72)\, 6.4 \text{ nJ} \approx 67 \text{ nJ} \tag{28}$$

Note that when the slot depth d approaches the slot length ℓ these results become inaccurate and depth modes are needed to provide accurate results [17]. This arbitrary depth procedure can also be carried out with bolted joints and would slightly improve the accuracy of the above results. The value (28) corresponds to a short circuit field strength $H_{sc} = 2H_{inc}$ (and H_{inc} has step function amplitude H_0), which is the valid high frequency limit. Thus at high frequencies only the illuminated side of the fixture is excited and the driving magnetic field varies as $\cos(\varphi)$, where φ is the azimuthal coordinate. The average drive for the slots (for the square of the field or the energy) is

$$\left\langle \frac{H_\varphi^2}{H_{sc}^2} \right\rangle = \frac{1}{2\pi a} \int_{-\pi/2}^{\pi/2} \cos^2(\varphi) a d\varphi = \frac{1}{4} = \frac{1}{N} \sum_{n=-[N/4]}^{[N/4]} \cos^2(2n\pi/N) \tag{29}$$

where the continuous average is an approximate integration over the half cylinder and the discrete average is the approximate summation over half the slots on the cylinder at the slot centers (note that the notation $[N/4]$ means that the result is truncated to the nearest integer less than or equal to $N/4$). Thus the high frequency result for all the apertures is obtained by multiplying the single slot energy by $N/4 = 2$; giving $W_{rec} \leq 134$ nJ (the low frequency result would be multiplied by $N/2 = 4$ since there is no shadowing). The symmetric resonant modes couple to all slots equally and thus we multiply the single energy result by $N = 8$ times the resonant enhancement factor 8.6^2 arising from $H_0 = 8.6 H_{inc}$; giving $W_{rec} \leq 39.6$ μJ. This final result is a gross upper bound for two reasons. Reason one is that the first resonance does not couple well into the interior (the joint impedance is too low at this frequency) and thus the resonant enhancement factor is not representative (see the section on exterior resonance drive). Reason two results form the fact that a single cable only couples well when it is very near a slot (flux linkage is maximized and cable impedance is reduced, see the next section for reduction factors when the cable is not near one slot) and thus the remaining slots do not effectively drive the cable (the only exception again has to do with attaining a lower cable impedance than the bolts and thus providing a current path that several slots can feed, and even then only neighboring slots contribute unless the bolt inductance is significantly higher than the slot inductance, as discussed immediately following (12)). It is interesting to note that the worst case energy (when all slots are driven uniformly) involves only a multiplication by the number of slots N, instead of, for example, the square of the number. Rigorously, the inductive energies must, of course, be found with the load present (if the load has a significant effect on the slot current distribution). However this loading tends to decrease the stored static energy, and thus we can bound the energy without the presence of the load. (An intriguing issue has to do with possible small resistances of the bolts at late time; it is clear that if

the fall time were very long, the inductances in the circuit of Figure 10 could be replaced by short circuits, but if small series resistances were still present, any attached load would absorb some of the late time currents.)

The monopole fixture is discussed last. The polarizability of the monopole is given by [4]

$$VP_{11} \approx \frac{4h_m^3\pi}{3\Omega_e} \approx 2.4 \times 10^{-5} \text{ m}^3 \tag{30}$$

where again $\Omega_e = \Omega + 2(\ln 2 - 7/3)$ and the fatness parameter is $\Omega = 2\ln(2h_m/a)$. The energy is thus

$$W_{rec} \leq \frac{1}{2}\epsilon_0 (2E_0)^2 VP_{11} \approx 1.54 \ \mu\text{J} \tag{31}$$

where again this result represents the case of a monopole in an infinite ground plane (the exciting field at the monopole is thus $2E_{inc}$ where E_0 is the step function amplitude of E_{inc}). Figure 11a and Figure 11b (taken from the handbook [6]) show the normal electric field at the center of the end cap of a cylinder with ten-to-one aspect ratio excited by a unit amplitude electric plane wave. We see from this that the electric field enhancement at the first exterior length resonance is nearly sixteen times the incident unit field. Thus again we can bound the monopole POE on the test object by taking $E_0 = 8E_{inc}$ in (31); which yields $W_{rec} \leq 98.6$ μJ. The third resonance has an electric field that is less than three times the incident field. Thus little enhancement over the infinite ground plane results from anything but the first resonance.

5 REDUCTION IN ENERGY BOUNDS

This section incorporates further aspects of the test fixture geometry (aspects which are generic to interior weapon system geometry) into the energy bound results. The interior geometries are incorporated to show how the coupled energies are reduced from the worst case results given in the preceding section.

The nonzero rise time associated with the incident wave in relation to the POE dimensions, slot to cable clearance (and associated reductions in magnetic flux linkage), and impedance mismatch are the aspects which will be discussed that lead to reductions in coupled energy. The slot fixture is discussed first. Closed form results have been derived [5] for the reduced coupled energy for a slot in a ground plane with a wire behind it, excited by either a double exponential EMP waveform or an inverse exponential waveform. The received energy from the double exponential waveform (with long fall time $\alpha << \beta$) is [5]

$$W_{rec} = \frac{1}{2}\mu_0 H_0^2 \frac{3}{4}\alpha_{m_{22}} \frac{\pi}{\Omega_e} \left(\frac{\eta_0}{2Z_c}\right) \left(\frac{2\ell}{3\pi D}\right)^2 (\beta\ell/c) \tag{32}$$

where Z_c is the cable characteristic impedance, and D is the cable to POE distance, and the cable is assumed to bisect the slot. Using the values $D = 2.75$ in and (4) for the centered wire case we obtain

$$W_{rec} = 18.1 \text{ pJ} \tag{33}$$

where the value $\beta = 4 \times 10^9$ sec^{-1} was used for the double exponential (0.5 nsec rise time) and amplitude $E_0 = 60$ kV/m. The eccentric wire case with $D = 1.25$ in and characteristic impedance (5) gives

$$W_{rec} = 98 \text{ pJ} \tag{34}$$

The received energy for the inverse exponential waveform (with long fall time $\alpha \to \beta$) is [5]

$$W_{rec} = \frac{1}{2}\mu_0 H_0^2 \frac{1}{4}\alpha_{m_{22}} \frac{\pi}{\Omega_e}\left(\frac{\eta_0}{2Z_c}\right)\left(\frac{2\ell}{3\pi D}\right)^2 (\beta\ell/c) \tag{35}$$

Note that a factor of four was inadvertently left out of the integral identity used to arrive at (53) in [5]; hence the result (53) and results for W_{tot} subsequent to it in [5] must be multiplied by four. The result for the centered wire case using the value $\beta = 10.753 \times 10^9$ sec^{-1} (0.4 nsec rise time) is

$$W_{rec} = 16.2 \text{ pJ} \tag{36}$$

The result for the eccentric wire case is

$$W_{rec} = 88 \text{ pJ} \tag{37}$$

The required modification to cylindrical interior geometry is not difficult but will be carried out here only for the centered case (since the eccentric case is similar to the ground plane geometry and is bounded by, but is not very accurately modeled by, taking a constant field along the aperture when the wire is carrying a current). The effect is that the quantity [5] $f_I = 1/(\pi D)$ is replaced by $f_I = 1/(2\pi D)$ when a centered wire is at a distance D (equal to the radius of the cylinder) from the aperture. This quantity enters the energy as a square and thus we obtain one quarter the value of (32) or (35). The values for the centered wire case are thus

$$W_{rec} = 4.5 \text{ pJ} \tag{38}$$

for the double exponential waveform and

$$W_{rec} = 4 \text{ pJ} \tag{39}$$

for the inverse exponential waveform.

The stripline against the slot is now considered. We can consider the stripline as a center load on the slot since it is near enough that almost all of the magnetic field passing through the slot links the stripline. We assume here that the load impedance presented to the slot by the stripline (7) is substantially larger than the slot inductive reactance. The center load energy resulting from a double exponential waveform ($\alpha \to 0$) is [5]

$$W_{rec} = \frac{1}{2}\mu_0 H_0^2 \frac{3}{4}\alpha_{m_{22}} \frac{\pi}{\Omega_e}(\eta_0 G_L)(\beta\ell/c) \approx 17.9 \text{ nJ} \tag{40}$$

Note that the denominator factor $1 + \frac{\pi}{4}(\eta_0 G_L)(\beta\ell/c)/\Omega_e$ [5], which accounts for loading of the aperture, reduces this to 12.1 nJ.

The inverse exponential result for the slot center load is [5]

$$W_{rec} = \frac{1}{2}\mu_0 H_0^2 \frac{1}{4}\alpha_{m_{22}} \frac{\pi}{\Omega_e}(\eta_0 G_L)(\beta\ell/c) \approx 16 \text{ nJ} \tag{41}$$

Next we consider the bolted joint fixture. A bound on the joint polarizability per slot can be identified in (27) as

$$\alpha_{m_{22}} \leq \frac{\pi\ell^3}{12\Omega_e} + \ell^2 L_{bolt}/\mu_0 \approx 1.05 \times 10^{-6} \text{ m}^3 \tag{42}$$

However for multiple slots the magnetic flux coupling to the interior wire would be additive; hence superposition of the induced voltages holds (unlike the maximum case discussed in the previous

section). It is therefore more physical with the joint fixture to consider the symmetric voltage drive of the interior coax rather than directly using the polarizabilities. The symmetric part of the voltage can be found as

$$\langle V \rangle = \frac{1}{2\pi} \int_0^{2\pi} V d\varphi = \frac{1}{N} \sum_{n=1}^{N} \frac{1}{\ell} \int_{-h}^{h} V dz \tag{43}$$

where the second integral is over the local length coordinates of a single slot (for a given value of n). The transmission line model of Figure 10 is used to find the bolted joint voltage distribution. We will approximate the axial current drive as uniform over a single slot. Therefore from the transmission line of Figure 10 we find (23) and $\frac{dV}{dz} = i\omega I$ which can be integrated with the condition $V(h) = -i\omega 2 L_{bolt} I(h)$ to give the voltage distribution

$$V(z) \approx -i\omega K_{sc} \left[2hL_{bolt} + \frac{1}{2} L (h^2 - z^2) \right] \tag{44}$$

Integration over a single slot gives

$$\frac{1}{\ell} \int_{-h}^{h} V dz = -i\omega K_{sc} \frac{\mu_0}{\ell} \left[\ell^2 L_{bolt}/\mu_0 + \frac{\pi \ell^3}{12\Omega_e} \right] \tag{45}$$

Using the energy theorem [4] we thus find that

$$W_{rec} \approx \frac{G_L}{2\pi} \int_{-\infty}^{\infty} |\langle V(\omega) \rangle|^2 \, d\omega \tag{46}$$

where here we take the load G_L to be equal to $1/(2Z_c)$. Carrying this out for the double exponential (with $\alpha \to 0$) gives the reduced energy

$$\begin{aligned} W_{rec} &\approx \frac{1}{2} \mu_0 H_0^2 \left(\frac{2}{3} L_{slot}/\mu_0 + 2L_{bolt}/\mu_0 \right)^2 \ell \left(\frac{\eta_0}{2Z_c} \right) (\beta \ell / c) \left[\frac{1}{N} \sum_{n=1}^{N} \frac{K_{scn}}{2H_0} \right]^2 \\ &\approx 2\mu_0 H_0^2 \frac{1}{\ell^3} \left(\ell^2 L_{bolt}/\mu_0 + \frac{\pi \ell^3}{12\Omega_e} \right)^2 \left(\frac{\eta_0}{2Z_c} \right) (\beta \ell / c) \left[\frac{1}{N} \sum_{n=1}^{N} \frac{K_{scn}}{2H_0} \right]^2 \end{aligned} \tag{47}$$

where the center short circuit current on each slot is K_{scn}. Noting that one quarter (for the coaxial case) the result (32) can be written as $W_{rec} = 2\mu_0 H_0^2 \left(\alpha_{m_{22}}^2/\ell^3\right) \left(\frac{\eta_0}{2Z_c}\right) (\beta\ell/c) \left(\frac{\ell}{2\pi D}\right)^2$, and that in this centered wire case $N = 2\pi D/\ell$, we notice that the multiple slots enter the formula as the square of the number contributing $M^2 = \left[\sum_{n=1}^{N} \frac{K_{scn}}{2H_0}\right]^2$, as expected. The high frequency arguments leading to (29) here give the value $\left[1 + 1/\sqrt{2} + 1/\sqrt{2}\right]^2/64 \approx 0.091$ for the bracketed quantity in (47). The energy in this case is thus

$$W_{rec} \approx 22 \text{ pJ} \tag{48}$$

If all slots are excited at the level $K_{sc} = 2H_{inc}$ uniformly, the factor in brackets is unity and $W_{rec} \approx 241.5$ pJ. The inverse exponential results are given by (47) with 1/3 inserted and β replaced by the appropriate value (multiplication of the double exponential results by $10.753/12 \approx 0.896$) or

$$W_{rec} \approx 19.7 \text{ pJ} \tag{49}$$

The bolted joint center loaded cases are treated by noting that the preceding slot center load results, (40) and (41), can be arrived at by assuming that the open circuit voltage of the slot is applied to the center load G_L. Thus in the case of the bolted joint

$$V(0) = (L_{slot} + 2L_{bolt}) \frac{\partial}{\partial t} h K_{sc} = (L_{slot} + 2L_{bolt})\, h(-i\omega K_{sc}) \tag{50}$$

where $L_{slot} \approx 0.5$ nH is evaluated using the bolted joint slot dimensions and we again take $L_{bolt} \approx 0.2$ nH. Using the energy theorem [4] we thus find that

$$W_{rec} \approx \frac{G_L}{2\pi} \int_{-\infty}^{\infty} |V(\omega)|^2 \, d\omega \tag{51}$$

Carrying this out for the double exponential (with $\alpha \to 0$) gives the reduced energy per slot

$$W_{rec} \approx \frac{1}{2} \mu_0 H_0^2 \, (L_{slot}/\mu_0 + 2L_{bolt}/\mu_0)^2 \, \ell \, (\eta_0 G_L) \, (\beta \ell / c) \tag{52}$$

Inserting the values of the parameters gives

$$W_{rec} \approx 11.8 \text{ nJ} \tag{53}$$

The corresponding results for the inverse exponential are per slot

$$W_{rec} \approx \frac{1}{2} \mu_0 H_0^2 \frac{1}{3} \, (L_{slot}/\mu_0 + 2L_{bolt}/\mu_0)^2 \, \ell \, (\eta_0 G_L) \, (\beta \ell / c) \tag{54}$$

and

$$W_{rec} \approx 10.6 \text{ nJ} \tag{55}$$

The presence of multiple slots are not expected to be important in the strip line cases for a single cable.

Finally we consider the monopole fixture. The circuit model for the monopole fixture is shown in Figure 12. The low frequency open circuit voltage (again assuming that the vertical driving field at the monopole is $2E_{inc}$) is

$$V_{oc} \approx \frac{1}{2} h_m (2E_{inc}) \tag{56}$$

the capacitors C_{mono} and C_{sleeve} are given by (14) and (15), and the value of Z_c is given by (4) (the approximate matched value of $Z_L \approx 200$ ohms).

The capacitor C_{cap} results from the higher order modes in the vicinity of the coaxial transmission line end caps. An approximate analysis was used to determine its value (this capacitance approximately applies to all wire cases). Laplace's equation $\nabla^2 \phi = 0$ is solved in the coaxial region $(a < \rho < b)$ and $(0 < z < \infty$ where $z = 0$ is, say, the monopole sleeve end cap). The boundary conditions of the symmetrized problem $-\infty < z < \infty$ are taken as $(\phi(\rho = b) = 0$, $\phi(\rho = a) = \pm V$ for $z \gtrless 0)$. The solution is

$$\phi = \frac{2}{\pi} V \int_0^{\infty} \frac{I_0(\xi\rho)K_0(\xi b) - I_0(\xi b)K_0(\xi\rho)}{I_0(\xi a)K_0(\xi b) - I_0(\xi b)K_0(\xi a)} \sin(\xi z) \frac{d\xi}{\xi} \tag{57}$$

The charge per unit length $q = -2\pi a \epsilon_0 \frac{\partial \phi}{\partial \rho}(\rho = a)$ on the center conductor is thus

$$q = 4a\epsilon_0 V \int_0^\infty \frac{I_1(\xi a)K_0(\xi b) + I_0(\xi b)K_1(\xi a)}{I_0(\xi b)K_0(\xi a) - I_0(\xi a)K_0(\xi b)} \sin(\xi z) d\xi \tag{58}$$

We now approximate the Bessel functions with $a \to 0$ as $K_0(\xi a) \sim -\{\ln(\xi a/2) + \gamma\}$, $K_1(\xi a) \sim 1/(\xi a)$, $I_0(\xi a) \sim 1$, $I_1(\xi a) \sim \xi a/2$, where $\gamma \approx 0.5772$ is Euler's constant. This is equivalent to the Hallén filament approximation [18] and results in a finite charge density (this finite value is somewhat artificial but does not have a significant impact on the total integrated charge), as well as an extraneous pole at the large value $\xi_p \sim 2/(ae^\gamma) \to \infty$. Thus we can write

$$q \sim -4a\epsilon_0 V \int_0^\infty \frac{I_0(\xi b)}{I_0(\xi b)\{\ln(\xi a/2) + \gamma\} + K_0(\xi b)} \sin(\xi z) \frac{d\xi}{\xi} \tag{59}$$

where the $\xi a K_0(\xi b)$ numerator term has been dropped. As $z \to \infty$ the main contribution to the integral arises from the integrand in the limit $\xi \to 0$ and thus approximating the remaining Bessel functions for small argument gives

$$q \sim \frac{4\epsilon_0 V}{\ln(b/a)} \int_0^\infty \sin(\xi z) \frac{d\xi}{\xi} = \frac{2\pi\epsilon_0 V}{\ln(b/a)}, \; z \to \infty \tag{60}$$

This is the usual charge per unit length in a coaxial transmission line. Thus if we take a difference of (59) and (60) Δq and integrate from zero to infinity we obtain the total difference charge

$$\Delta Q = V C_{cap} \sim -4\epsilon_0 V \int_0^\infty \left[\frac{I_0(\xi b)}{I_0(\xi b)\{\ln(\xi a/2) + \gamma\} + K_0(\xi b)} + \frac{1}{\ln(b/a)} \right] \frac{d\xi}{\xi^2}$$

or

$$\ln(b/a) C_{cap}/(4\epsilon_0 b) \sim P \int_0^\infty \left[\frac{\ln(x/2) + \gamma + K_0(x)/I_0(x)}{\ln(b/a) - \ln(x/2) - \gamma - K_0(x)/I_0(x)} \right] \frac{dx}{x^2} \tag{61}$$

where the extraneous pole is to be treated by means of a principal value integral [18] (denoted by $P\int$). Because the extraneous pole is at a large distance $x_p = 2\frac{b}{a}e^{-\gamma} >> 1$ the Bessel functions can be expanded for large argument at this location. We can carry out the integral

$$P \int_{x_i}^\infty \left[\frac{\ln(x/2) + \gamma}{\ln(b/a) - \ln(x/2) - \gamma} \right] \frac{dx}{x^2} = -\frac{1}{x_i} + \frac{e^\gamma \ln(b/a)}{2(b/a)} \mathrm{Ei}\left[\ln(2\frac{b}{a}e^{-\gamma}\frac{1}{x_i}) \right] \tag{62}$$

where we choose the extraneous pole to be inside the integration interval $1 << x_i < x_p$ and $\mathrm{Ei}(x)$ is the exponential integral. Choosing $x_i = x_p - 1 \approx 31.94$ we find by means of numerical integration of (61) from 0 to x_i plus (62) gives $\ln(b/a)C_{cap}/(4\epsilon_0 b) \approx 0.52838$ or

$$C_{cap} \approx 0.4 \text{ pF} \tag{63}$$

(The value (63) has been checked and found consistent with the Thévenin impedance determined by the PATCH code model of the text fixture interior, discussed in the numerical modeling section.) This relatively small capacitance will be ignored. A Thévenin equivalent source can thus be formed as $V_T = V_{oc}\frac{C_{mono}}{C_T}$ and $C_T = C_{mono} + C_{sleeve}$ driving the load Z_c. The energy delivered to the matched load can thus be found as

$$W_{rec} \approx \frac{1}{2\pi Z_c} \int_{-\infty}^\infty |V_T(\omega)|^2 \frac{\omega^2\tau^2}{1 + \omega^2\tau^2} d\omega \tag{64}$$

where $\tau = Z_c C_T$ is the circuit time constant. Carrying this out for the double exponential (with long fall time $\alpha \to 0$) gives

$$W_{rec} \approx \frac{h_m^2 E_0^2}{2Z_c}\tau \left(\frac{C_{mono}}{C_T}\right)^2 \frac{\beta\tau}{(1+\beta\tau)} \approx 0.3\ \mu\text{J} \tag{65}$$

6 VOLTAGE PREDICTIONS

We now consider the peak voltages predicted by the models of the previous section. The slot fixture is considered first. The case of the coaxial geometry with centered wire gives [5] (with $f_I = 1/(2\pi D)$ where $D = 2.75$ in)

$$V = f_I \alpha_{m_{22}} \mu_0 \frac{\partial}{\partial t} K_{sc} \tag{66}$$

Taking the ground plane value $K_{sc} = 2H_{inc}$ we can write the peak value for the inverse exponential waveform as

$$V_p = \frac{1}{\pi D}\alpha_{m_{22}}(\beta/4)\mu_0 H_0 \approx 2.6 \text{ volts} \tag{67}$$

The eccentric wire case can also be treated by means of (66) for the ground plane (with $f_I = 1/(\pi D)$ where $D = 1.25$ in). The peak voltage in this case is thus

$$V_p = \frac{2}{\pi D}\alpha_{m_{22}}(\beta/4)\mu_0 H_0 \approx 11.3 \text{ volts} \tag{68}$$

The stripline case has voltage

$$V = L_{slot}\frac{\partial}{\partial t} h K_{sc} \tag{69}$$

where the slot inductance is given by (9). The peak voltage for the inverse exponential waveform, assuming $K_{sc} = 2H_{inc}$, is thus

$$V_p = L_{slot}\ell(\beta/4)H_0 \approx 28.3 \text{ volts} \tag{70}$$

The bolted joint fixture is considered next. The centered wire case gives (66) per slot where we can use the value (42) for the polarizability. Thus we obtain (67) for the value per slot. The high frequency limit discussed above (48) would have the multiplicative factor $M = \left[1 + 1/\sqrt{2} + 1/\sqrt{2}\right] \approx 2.4$ (for the number of slots contributing) times this value or

$$V_p \approx 6.3 \text{ volts} \tag{71}$$

A rough estimate of the eccentric wire voltage can be obtained by noting that in the ground plane case $f_I = D/(\pi r^2)$ where $D = 1.25$ in is the distance from the wire to the ground plane and r (which equals either D or $\sqrt{D^2 + \ell^2}$ for the three nearest slots) is the distance from the wire to the aperture (here we take it to be the distance to the center of the slot apertures). Thus we obtain the result (68) but with the multiplier $\left[1 + \sqrt{2}\frac{D^2}{D^2+\ell^2}\right] \approx 1.3$

$$V_p \approx 14.8 \text{ volts} \tag{72}$$

The stripline case is given by (50). The peak voltage is thus

$$V_p = (L_{slot} + 2L_{bolt})\,\ell(\beta/4)H_0 \approx 23.1 \text{ volts} \tag{73}$$

Finally the monopole fixture is considered. Because the time constant for the matched monopole $\tau \approx 0.55$ nsec is slightly larger than the rise time of the EMP waveform we cannot consider the

open circuit voltage alone as we did for the slot apertures where the time constants were much smaller $L_{slot}G_L \approx 0.089$ nsec. The double exponential waveform with long fall time $\alpha \to 0$ has transform Thévenin equivalent voltage $V_T = \frac{1}{2}h_m(C_{mono}/C_T)(2E_0)\beta/[-i\omega(\beta - i\omega)]$ (where again we have taken the ground plane field $E_{sc} = 2E_{inc}$). The voltage on the matched load Z_c of the coaxial transmission line is $V(\omega) = V_T(\omega)(-i\omega\tau)/(1 - i\omega\tau)$. Thus inverse transforming this result gives

$$V(t) = h_m \left(\frac{C_{mono}}{C_T}\right) E_0 \frac{\beta\tau}{\beta\tau - 1} \left(e^{-t/\tau} - e^{-\beta t}\right) u(t) \tag{74}$$

The peak time is $t_{peak} = \tau \ln(\beta\tau)/(\beta\tau - 1) \approx 0.36$ nsec (the double exponential waveform is reasonable to use here since the voltage peak does not occur at the initial time). Thus the peak value is

$$V_p \approx 292.6 \text{ volts} \tag{75}$$

The exterior resonance results in a spectral amplitude approximately 8 times the level $2E_{inc}$ (and Figure 11 shows that the step response of the electric field rises to approximately $8.3E_{inc}$, but the third time harmonic resonance is only $2.9E_{inc}$). However this peak of the step response occurs at approximately 7.6 nsec after the leading edge of the EMP pulse, which is considerably larger than the circuit time constant τ. Thus, although the energy is changed somewhat by the exterior resonance, the peak voltage should not be significantly affected.

Finally, the slot and joint fixtures were fitted with tapered stripline transformers in an attempt to generate the maximum voltages one would expect to see in a system resulting from joint penetrations. The transformer has a characteristic impedance near the nominal $Z_c = 12.5$ ohms at the slot to an approximate matched load value of $Z_L = 170$ ohms. Thus, if we take the transition to be gradual enough that little reflection occurs along its length, we obtain the load voltage

$$V \approx V_{slot}\sqrt{Z_L/Z_c} \tag{76}$$

Using the peak value of the voltage for the slot fixture (70) we obtain from (76) the result

$$V \approx 104.4 \text{ volts} \tag{77}$$

Using the peak value of the voltage for the joint fixture (73) we obtain from (76) the result

$$V \approx 85.2 \text{ volts} \tag{78}$$

7 EMP TEST DATA AND COMPARISONS

We now discuss the test results and the comparisons with the preceding analytical results. All test results (as well as Fourier transforms and incident waveforms) are included in the companion report [19]. Magnetic media are also available. Data are shown in this report on every test configuration, however only the short time base data are used (the long time base data can be found in the companion report). There are several reasons for concentrating on the short time base data: reflections in the EMES test facility occur near the end of the short time base data which provide drives to the test fixtures that are different from the typical EMP requirement (further data manipulations, involving deconvolution, may be able to reduce this effect), noise levels are higher on the long time base recording instrumentation and these noise levels appear to contribute in some cases to the integrated energy over long time periods. Several shots were conducted, for consistency reasons, on each configuration. Only one shot will be shown for each configuration in

this report. Shots were selected for 10% to 90% of peak rise times as near to 0.4 nsec as possible. The values selected from the curves will then be normalized to the nominal 60 kV/m peak level so they can be compared directly with analytical results of the previous sections.

Figure 1 shows the typical EMES incident EMP waveform. The waveform was detected by a magnetic field derivative sensor located up in the throat feed of the EMES facility (and normalized to the appropriate field level in the test volume). The incident waveforms on all shots are nearly identical except for variations in level and slight variations in rise time. The rise time, peak amplitude, shot number, etc. are shown at the bottom. The reflection that occurs at 27 nsec ($\approx$ 25 nsec from the peak and $\approx$ 0.5 times the peak level) results from a reflection at the peaking switch in the feed structure of EMES. Thus energy results definitely begin to differ at this point from those induced by the typical EMP requirement (this reflection acts as a second relatively fast excitation of the test fixture).

Figure 13a shows the time response of the slot fixture with centered wire and approximately matched load of 200 ohms (the characteristic impedance is (4) and the 200 ohm load consists of a 150 ohm resistor in series with the measurement system). This voltage appears across the fifty ohm measurement system attached at the bottom of the fixture. Matched loads exist on both ends of the fixture; thus to obtain the total source voltage on the coaxial transmission line we must multiply by four for the bottom voltage divider and by two for the two symmetrical loads. The peak voltage (we ignore the minus sign in the test data) is thus

$$V_p \approx 0.338 \text{ volts } (4 \times 2)(60/45.81) \approx 3.54 \text{ volts} \tag{79}$$

The coaxial prediction of the previous section (67) thus slightly underestimated this voltage (this underestimate likely results from slight exterior enhancements of the slot drive field above the ground plane value and possibly some coupling from higher order waveguide modes excited in the fixture, since the rise time of EMES is short enough to excite these). Figure 13b shows the time integral of the square of the measured voltage. We will take two values from this curve: the first is the fast rise value ($\approx$ 0.5 nsec into the curve from its break with the horizontal axis), the second is approximately at 27 nsec (just before the arrival of the second incident EMES pulse). The early time value captures the induced energy neglecting most of the first resonant enhancement of the drive field (of course since higher order resonances occur in the exterior spectrum there is still some enhancement at early time). The later time value captures most of the exterior resonant enhancements since from Figure 7d (the step function induced exterior current on a cylinder) 25 nsec corresponds to slightly more than 8 on the time axis of this Figure (more than one and one half cycles and significantly reduced amplitude). The early time value of the total absorbed energy is

$$W_{rec} \approx 4.8 \times 10^{-11} \text{ V}^2\text{-sec} \frac{(4 \times 2)}{50 \text{ ohms}} (60/45.81)^2 \approx 13.2 \text{ pJ} \tag{80}$$

This value is to be compared with the energy bound result (21) which clearly demonstrates the large reductions in received energy possible when the interior cable is not optimized. Comparing the value (80) with the more detailed models of a wire behind a ground plane (36) (the inverse exponential results will be referred to here whenever they are available) or the coaxial result (39), we see that the order of reduction is predicted. The square of the ratio of measured voltage (79) to predicted voltage (67) is less than the ratio of the measured energy (80) to the coaxial energy (39), however the first voltage pulse appears to be somewhat wider in time than would be expected from the derivative of a 0.4 nsec rise time excitation (the slot differentiates the drive). The later time energy value is given by

$$W_{rec} \approx 8 \times 10^{-11} \text{ V}^2\text{-sec} \frac{(4 \times 2)}{50 \text{ ohms}} (60/45.81)^2 \approx 22 \text{ pJ} \tag{81}$$

This increase in energy is likely in part due to the exterior resonance (although it should be noted that when the slot aperture, and all other possible leakage points on the test fixture were copper taped, 10% to 15% noise levels remained for these very small signal results).

Figure 14a shows the time response for the slot fixture with eccentric wire location. The approximate matched load in this case consists of a 120 ohm resistor in series with the 50 ohm measurement system ($170/50 = 3.4$). Thus the peak total coaxial source voltage is

$$V \approx 1.02 \text{ volts } (3.4 \times 2)(60/61.81) \approx 6.7 \text{ volts} \tag{82}$$

The wire behind ground plane result of the previous section (68) thus slightly overestimated this eccentric level. Figure 14b shows the integral of the square of the measured voltage in the eccentric wire case. The early time value of the total absorbed energy is

$$W_{rec} \approx 4.35 \times 10^{-10} \text{ V}^2\text{-sec} \frac{(3.4 \times 2)}{50 \text{ ohms}} (60/61.81)^2 \approx 55.7 \text{ pJ} \tag{83}$$

This value is again to be compared with the energy bound result (21). Comparing the value (83) with the more detailed model of a wire behind a ground plane (37) shows that the order of the reduction in energy was predicted well (although in the eccentric case the wire behind ground plane result slightly overestimated the measurement). The later time result from Figure 14b is

$$W_{rec} \approx 7.75 \times 10^{-10} \text{ V}^2\text{-sec} \frac{(3.4 \times 2)}{50 \text{ ohms}} (60/61.81)^2 \approx 99.3 \text{ pJ} \tag{84}$$

which is slightly above (37) but again negligible compared to the bound (21).

Figure 15a shows the time response of the slot fixture with matched stripline. There is only one load 12.5 ohms in this case (the stripline is shorted to the fixture just above the slot) and no voltage divider (thus the measured voltage is the load voltage). The peak voltage is thus

$$V \approx 35 \text{ volts } (60/65.55) \approx 32 \text{ volts} \tag{85}$$

This is to be compared to the peak result (70) which slightly underestimates the experimental level. Figure 15b shows the integral of the square of the voltage. The early time received energy is thus

$$W_{rec} \approx 5.3 \times 10^{-7} \text{ V}^2\text{-sec} \frac{(60/65.55)^2}{12.5 \text{ ohms}} \approx 35.5 \text{ nJ} \tag{86}$$

This value is again to be compared with the energy bound result (21). Comparing the value (86) with the center load model (41) (which includes mismatch of the load to the slot) we see that the more detailed model underestimated the experimental value by a factor of two. The square of the ratio of the measured peak voltage (85) to the predicted peak voltage (70) is again somewhat less than the ratio of energies (86) to (41). The later time energy value from Figure 15b is

$$W_{rec} \approx 12.3 \times 10^{-7} \text{ V}^2\text{-sec} \frac{(60/65.55)^2}{12.5 \text{ ohms}} \approx 82.4 \text{ nJ} \tag{87}$$

which is slightly above the slot bound result (21). The external resonance appears to be having some effect here and more will be said about this effect in the next section.

Figure 16a shows the time response of the slot fixture with stripline and a low impedance load (nominal 1.67 ohm termination, however even though surface mount resistors were used to reduce

inductive load effects, it is believed they are not negligible, and thus a slight overestimate of received energy will result) (some rough evidence for this inductance is provided by the TDR measurements of Figure 6). Figure 16b shows the integral of the square of the voltage. The later time value is

$$W_{rec} \approx 8.62 \times 10^{-8} \text{ V}^2\text{-sec} \frac{(60/62.56)^2}{1.67 \text{ ohms}} \approx 47.5 \text{ nJ} \tag{88}$$

Comparing (88) with the matched load result (87) we see a decrease in received energy even at the later time.

Figure 17a shows the time result for the slot fixture with tapered matched stripline. The stripline is again shorted just above the slot and the bottom approximate matched load is a series combination of a 120 ohm resistor and the 50 ohm measurement system. The total peak load voltage is thus

$$V \approx 33.5 \text{ volts } (3.4)(60/64.13) \approx 106.6 \text{ volts} \tag{89}$$

This level compares well with the prediction (77). It is interesting to examine the later time received energy in this case from Figure 17b

$$W_{rec} \approx 7.3 \times 10^{-7} \text{ V}^2\text{-sec} \frac{(3.4)}{50 \text{ ohms}} (60/64.13)^2 \approx 43.5 \text{ nJ} \tag{90}$$

which is again less than the uniform stripline matched case (87).

Figure 18 shows the time response of the slot fixture with tapered stripline and an attempt at a high impedance load (the nominal load consisted of a 1000 ohm resistor in series with the 50 ohm measurement system $1050/50 = 21$). The purpose was to see a doubling of the matched result (89) at the approximately open circuit of the high impedance load. The total peak voltage from Figure 18 appears to be

$$V \approx 18.9 \text{ volts } (21)(60/66.95) \approx 356 \text{ volts} \tag{91}$$

This large result was immediately held suspect; insertion loss measurements made on the resistors (to be discussed at the end of this section) indicated that a shunt capacitance was present at the resistor that invalidated the voltage divider extrapolation (use of this estimated capacitance from the insertion measurements was used to estimate the true voltage by some further data analysis). This shunt capacitance only affected the high impedance load results as discussed at the end of this section.

Figure 19a shows the time result for the joint fixture and centered matched wire. The total peak voltage is

$$V \approx 2.23 \text{ volts } (4 \times 2)(60/62.56) \approx 17.1 \text{ volts} \tag{92}$$

This level was underestimated by the coaxial result (71) (which included high frequency weighted excitations by the three slots facing the incident plane wave direction). The total received early time energy from Figure 19b is

$$W_{rec} \approx 2.1 \times 10^{-9} \text{ V}^2\text{-sec} \frac{(4 \times 2)}{50 \text{ ohms}} (60/62.56)^2 \approx 309 \text{ pJ} \tag{93}$$

This value is to be compared to the per slot bound result (28) which again shows the large reduction in energy possible when the interior cable is not optimized (obviously these reductions compared to the per slot bound are not as large when a symmetric array of slots are inducing voltage in

the cable as compared to the previous single slot fixture). The more detailed model result (49) substantially underestimates the level (93), indicating that symmetric resonant drive of the slots (discussed immediately above (49)) is a more reasonable model for the bolted joint fixture with center wire. The later time energy from Figure 19b is

$$W_{rec} \approx 10^{-8} \text{ V}^2\text{-sec} \frac{(4 \times 2)}{50 \text{ ohms}} (60/62.56)^2 \approx 1.47 \text{ nJ} \tag{94}$$

The exterior resonance appears to play a role here although these energies are still substantially below the bound per slot (28).

Figure 20a shows the time result for the matched eccentric wire in the joint fixture. The total peak voltage is

$$V \approx 2.8 \text{ volts} (3.4 \times 2) (60/63.55) \approx 17.8 \text{ volts} \tag{95}$$

which is only slightly underestimated by the peak result (72); symmetric drive of the slots has less impact for the eccentric wire than for the centered wire. The early time and later time total energies from Figure 20b are

$$W_{rec} \approx 3.6 \times 10^{-9} \text{ V}^2\text{-sec} \frac{(3.4 \times 2)}{50 \text{ ohms}} (60/63.55)^2 \approx 0.44 \text{ nJ} \tag{96}$$

$$W_{rec} \approx 9.4 \times 10^{-9} \text{ V}^2\text{-sec} \frac{(3.4 \times 2)}{50 \text{ ohms}} (60/63.55)^2 \approx 1.14 \text{ nJ} \tag{97}$$

which are again small compared to the per slot bound (28).

Figure 21a shows the time results for the joint fixture with matched stripline. The peak voltage is

$$V \approx 34 \text{ volts } (60/72.81) \approx 28 \text{ volts} \tag{98}$$

which is slightly underestimated by the result (73); the fact that multiple slots are present appears to have little effect. The early time energy from Figure 21b is

$$W_{rec} \approx 6 \times 10^{-7} \text{ V}^2\text{-sec} \frac{(60/72.81)^2}{12.5 \text{ ohms}} \approx 32.6 \text{ nJ} \tag{99}$$

This value is to be compared with the bound per slot (28). The center load model result (55) underestimates the experimental level (99). The late time energy from Figure 21b is

$$W_{rec} \approx 15.6 \times 10^{-7} \text{ V}^2\text{-sec} \frac{(60/72.81)^2}{12.5 \text{ ohms}} \approx 84.7 \text{ nJ} \tag{100}$$

which slightly exceeds the bound (28).

Figure 22a shows time response of the joint fixture with the low impedance load on the stripline. Figure 22b gives the corresponding integral of the square of the voltage. The later time energy is

$$W_{rec} \approx 8.1 \times 10^{-8} \text{ V}^2\text{-sec} \frac{(60/65.92)^2}{1.67 \text{ ohms}} \approx 40.2 \text{ nJ} \tag{101}$$

which is less than the matched energy (100).

The joint fixture stripline experimental results and analytical bound result are remarkable similar to the slot fixture stripline results. Thus, as the maximum levels are approached by moving the stripline near the wall, the presence of multiple slots play little role.

Figure 23a shows the time response of the joint fixture with matched tapered stripline. The peak voltage is

$$V \approx 27.5 \text{ volts}(3.4)(60/60.14) \approx 93.3 \text{ volts} \tag{102}$$

which compares quite well with the peak result (78). The later time energy from Figure 23b is

$$W_{rec} \approx 5.2 \times 10^{-7} \text{ V}^2\text{-sec} \frac{(3.4)}{50 \text{ ohms}} (60/60.14)^2 \approx 35.2 \text{ nJ} \tag{103}$$

which is smaller than the uniform matched case (100).

Figure 24 shows time response for the joint fixture with tapered stripline and high impedance load. The peak voltage is

$$V \approx 14.1 \text{ volts}(21)(60/63.44) \approx 280 \text{ volts} \tag{104}$$

but is regarded as incorrect because of the shunt load capacitance discussed previously in the slot fixture case.

Figure 25 shows the time response of the joint fixture with tapered stripline and high impedance load when the stainless steel bolts are removed one at a time and replaced with ferrous steel bolts. The peak level $V \approx 12.2$ volts$(21)(60/63.10) \approx 244$ volts thus did not show an appreciable increase from the stainless case (104). It should be noted that bolt replacement can easily change the air gaps surrounding the bolts and thus change the bolt inductance.

Figure 26a shows the time response for the matched monopole fixture. The single approximate matched load consists of a series combination of a 150 ohm resistor and the 50 ohm measurement system. Thus the total peak load voltage is

$$V \approx 48.4 \text{ volts}(4)(60/46.38) \approx 250.5 \text{ volts} \tag{105}$$

which is somewhat less than the result (75). The later time impact of the exterior resonance is obvious in this case (the oscillations in the time response). The later time received total energy from Figure 26b is

$$W_{rec} \approx 2 \times 10^{-5} \text{ V}^2\text{-sec} \frac{(4)}{50 \text{ ohm}} (60/46.38)^2 \approx 2.68 \ \mu\text{J} \tag{106}$$

The energy bound for the monopole is the result (31), which is slightly below the level (106). The fact that the exterior resonance is playing a role, is evident from a comparison of (106) with the more detailed model result (65).

Figure 27a shows the time response for the monopole with low impedance load (the 50 ohm measurement system only). The later time received energy from Figure 27b is

$$W_{rec} \approx 9.7 \times 10^{-5} \text{ V}^2\text{-sec} \frac{(60/64.64)^2}{50 \text{ ohms}} \approx 1.67 \ \mu\text{J} \tag{107}$$

which is smaller than the matched case (106) (the interior reflections may not have died out before truncation of the energy integration became necessary).

Figure 28a shows the time response of the monopole fixture with high impedance load. The peak voltage is

$$V \approx 19.5 \text{ volts}(21)(60/62.88) \approx 390.7 \text{ volts} \tag{108}$$

The parasitic shunt capacitance here has less impact because of the generally lower frequency content of the monopole response. It is interesting to calculate the later time received energy for this case from Figure 28b

$$W_{rec} \approx 2.25 \times 10^{-6} \text{ V}^2\text{-sec} \frac{(21)}{50 \text{ ohms}} (60/62.88)^2 \approx 0.86 \ \mu\text{J} \tag{109}$$

which is smaller than the matched case (106).

The high impedance results using the tapered stripline on both the slot and joint fixtures prompted calibration testing of the series resistors used in the tests. The network analyzer was used to perform $S_{21} = V_2/V_1$ measurements on GR 50 ohm insertion units containing the resistors. Figure 29 shows the results from the three types of resistors used (the relatively low impedance surface mount resistors used to terminate the uniform striplines were not checked). Figure 29a is the calibration curve for the 120 ohm resistor; Figure 29b is the calibration curve for the 150 ohm resistor; Figure 29c is the calibration curve for the 1000 ohm resistor. Frequencies near 500 MHz are certainly important in the tests. We see from Figure 29 that the 120 ohm and 150 ohm resistors provide reasonably flat responses up to this frequency. The $R_L = 1000$ ohm resistor obviously does not. Figure 30 shows a proposed circuit model involving an unknown shunt capacitor C_{shunt} across the resistor (the 50 ohm resistors represent the GR insertion unit and network analyzer transmission lines and $2V_1$ is the open circuit input voltage). The S parameter from this circuit is

$$S_{21} = \frac{2\,(50 \text{ ohms})}{2\,(50 \text{ ohms}) + R_L/\,(1 - i\omega C_{shunt} R_L)} = \frac{1 - i\omega C_{shunt} R_L}{1 + \frac{1}{2} R_L/\,(50 \text{ ohms}) - i\omega C_{shunt} R_L} \tag{110}$$

and thus defining $\zeta = \omega C_{shunt} R_L$ gives

$$|S_{21}|^2 = \frac{1 + \zeta^2}{\left\{1 + \frac{1}{2} R_L/\,(50 \text{ ohms})\right\}^2 + \zeta^2} \tag{111}$$

Taking the value $|S_{21}| = 0.2$ at $f = 500$ MHz from Figure 29c we find from (111) that $\zeta = 2$ and the shunt capacitance is

$$C_{shunt} \approx 0.64 \text{ pF} \tag{112}$$

Returning to the slot voltage with tapered stripline and high impedance load, Figure 18, we see that the first bipolar response pulse has a period of 1.52 nsec and thus a frequency of 658 MHz. The model of Figure 30, at this frequency gives

$$V_2/V_3 = \frac{1 - i\zeta}{1 + R_L/\,(50 \text{ ohms}) - i\zeta} \tag{113}$$

or

$$|V_3/V_2| = \sqrt{\frac{\{1 + R_L/\,(50 \text{ ohms})\}^2 + \zeta^2}{1 + \zeta^2}} \approx 7.5 \tag{114}$$

Thus replacing the factor 21 in (91) by 7.5 gives only $V \approx 127$ volts. Figure 24 for the joint fixture with tapered stripline and high impedance load has a period of roughly 1.61 nsec and thus a frequency of 621 MHz. The factor for the joint case is thus 7.9 which from (104) gives only $V \approx 105$ volts. These are very rough extrapolations, but they do show that the voltages are not significantly above the matched case (because the transition from the 100 ohm characteristic impedance at the

end of the tapered stripline, to the 170 ohm characteristic impedance at the connector, occurs over a short distance, it is possible that a high impedance load does not substantially increase the voltage, as these results indicate).

8 EXTERIOR RESONANCE DRIVE

To obtain more realistic estimates of the effect of the exterior resonances on the coupled energies (in particular the first resonance) we consider here the resonant mode expansion of the exterior current. The idea is basically to construct an expansion of damped sinusoids (singularity expansion) for the exterior field drive of the POE and then attempt to bound the coupled energies (here we focus primarily on the first resonance. To bound coupled energy in general structures thus requires one to consider the impedance transformation properties of the interior cable transmission lines so the load of the POE can be determined (for example if the cable characteristic impedance is large, the combination of cable load and cable transformation properties, could in principle lead to low impedance loads of the POE). The low quality factor of the exterior length resonances means that the transformation properties of the cable are quite limited as illustrated below. This section is a lead into future continuous wave electromagnetic radiation bounding calculations where the finite quality factors resulting from dissipation are used to limit power and voltage.

Time dependence $e^{-i\omega t} = e^{st}$ $(s = -i\omega)$ is used. The exterior current on a cylinder of half height h_c and exterior radius b_o, exposed to plane electromagnetic wave E_{inc} (polarized along the cylinder) has a center axial current resonant expansion [1]

$$I_{cyl}(t) = 2\mathrm{Re}\left[\sum_{n \text{ odd}} (-1)^{(n-1)/2}\eta(s_n)e^{s_n t}\right] \tag{115}$$

The special case $h_c/b_o = 10$ or $\Omega = 2\ln(2h_c/b_o) = 6$ gives [1]

$$(2h_c/c)s_1 = -0.4380 - i2.5849$$

$$(2h_c/c)s_3 = -0.7866 - i8.4120 \tag{116}$$

and

$$\eta_0\eta_1(s)/\left[cE_{inc}(s)\right] = 1.471 - i0.822$$

$$\eta_0\eta_3(s)/\left[cE_{inc}(s)\right] = 0.602 - i0.555 \tag{117}$$

where $E_{inc}(s)$ is the frequency domain form of the incident axial field and $\eta_0 = \sqrt{\mu_0/\epsilon_0} \approx 120\pi$ ohms. We will consider here the incident field to be a double exponential, with $\alpha \to 0$, having transform

$$E_{inc}(s) = \frac{E_0\beta}{s(\beta + s)} \tag{118}$$

The frequency domain form of the exterior current is [1]

$$I_{cyl}(s) = \sum_{n \text{ odd}} (-1)^{(n-1)/2}\left[\frac{s}{s_n(s - s_n)} + \frac{s}{s_n^*(s - s_n^*)}\right]\eta_n(s) \tag{119}$$

The short-circuit exterior circumferential magnetic field is thus

$$H_{sc}(s) = \frac{I_{cyl}(s)}{2\pi b_o} \tag{120}$$

Consider a slot aperture with center load G_L driven by the short circuit current $K_{sc} = H_{sc}$ given by (120). To simplify the calculation we assume that G_L is small enough that it does not load the aperture. Thus we can take the received energy to be

$$W_{rec} = \frac{G_L}{2\pi} \int_{-\infty}^{\infty} |V(\omega)|^2 \, d\omega \tag{121}$$

The center slot voltage is

$$V(\omega) = -i\omega L_{slot} I_{sc} = s L_{slot} h K_{sc} \tag{122}$$

Using the incident wave (118) and retaining only the leading resonant mode in (119) gives

$$W_{rec} = \frac{G_L}{2\pi} \left(\frac{E_0 L_{slot} h}{2\pi b_o \mu_0} \right)^2 |1.471 - i0.822|^2 \, \beta^2 \int_{-\infty}^{\infty} \left| \frac{s}{s_1(s - s_1)} + \frac{s}{s_1^*(s - s_1^*)} \right|^2 \frac{d\omega}{|s + \beta|^2} \tag{123}$$

The integral to be carried out is

$$I_{res} = \beta^3 \int_{-\infty}^{\infty} \left\{ \frac{1}{s_1(-i\omega - s_1)} + \frac{1}{s_1^*(-i\omega - s_1^*)} \right\} \left\{ \frac{1}{s_1^*(i\omega - s_1^*)} + \frac{1}{s_1(i\omega - s_1)} \right\} \frac{\omega^2 d\omega}{(-i\omega + \beta)(i\omega + \beta)} \tag{124}$$

and has poles at $\omega = \pm i s_1, \pm i s_1^*, \pm i\beta$. Closing the contour in the upper half ω plane and using the residue theorem with poles $\omega = -i s_1, -i s_1^*, i\beta$ we obtain

$$I_{res} = 2\pi\beta^3 \mathrm{Re} \left[\left\{ \frac{1}{s_1} + \frac{s_1}{s_1^* \mathrm{Re}(s_1)} \right\} \frac{1}{(\beta^2 - s_1^2)} \right] + 4\pi\beta^4 \mathrm{Re} \left(\frac{1}{s_1(\beta - s_1)} \right) \mathrm{Re} \left(\frac{1}{s_1(\beta + s_1)} \right) \tag{125}$$

The value of the integral using $\beta = 4 \times 10^9$ sec^{-1} and $h_c = 36$ in is $I_{res} \approx 335.98$. Thus the energy using the slot inductance (9) and stripline load conductance $G_L = 1/$ (12.5 ohms) is

$$W_{rec} \approx \frac{G_L}{2\pi\beta} \left(\frac{E_0 L_{slot} h}{2\pi b_o \mu_0} \right)^2 |1.471 - i0.822|^2 \, I_{res} \approx 33.1 \text{ nJ} \tag{126}$$

This energy is about half the bound result (21). This indicates that there will not be a significant (much less than the factor of 8.6^2 times the bound result discussed in the report) energy enhancement from the first resonance.

We now briefly discuss the bounding of the transmission line impedance loading the aperture which determines how much energy can be received from the resonant modes. Again we consider a stripline close to the aperture so it forms a center load, except now the load impedance is incorporated (instead of using the open circuit voltage). The transmission line current is

$$I_0 = V/Z_W \tag{127}$$

where the impedance is

$$Z_W = Z_W^+ + Z_W^- \tag{128}$$

and the impedances $Z_W^{\pm}$ are the input impedances to the transmission lines looking in the $\pm z$ directions. The energy absorbed in the transmission line is

$$W_{rec} = \frac{1}{2\pi}\int_{-\infty}^{\infty} \mathrm{Re}\left(|V|^2/Z_W\right) d\omega = \frac{1}{2\pi}\mathrm{Re}\left[\int_{-\infty}^{\infty} V(-\omega)V(\omega)/Z_W(\omega)d\omega\right] \tag{129}$$

The only poles in the upper half of the ω plane are from $V(-\omega)$ and are located at $\omega = -is_n$, $\omega = -is_n^*$, and $\omega = i\beta$ because $I_0(\omega) = V(\omega)/Z_W(\omega)$ is causal and passive. Thus the residues will involve the evaluation of the impedance at these frequencies $Z_W(-is_n)$, $Z_W(-is_n^*)$, and $Z_W(i\beta)$. Because these complex frequencies have fairly large imaginary parts, it should be possible to set a lower limit on Z_W, for example, how much lower it can be than the characteristic impedance Z_c.

Suppose, as an example, the impedance Z_W is that of two quarter wave transmission lines in series terminated in open circuits

$$Z_W(-is_1) = 2Z_i(-is_1) = i2Z_c\cot(-is_1\ell/c) \tag{130}$$

Choose the transmission line length ℓ_t such that, say, $\mathrm{Re}(-is_1\ell_t/c) = \pi/2$, $\mathrm{Im}(-is_1\ell_t/c) = 0.2662$

$$Z_W(-is_1) = i2Z_c\cot\left\{\frac{\pi}{2} + i\mathrm{Im}(-is_1\ell_t/c)\right\} = 2Z_c\frac{\sinh\{2\mathrm{Im}(-is_1\ell_t/c)\}}{\cosh\{2\mathrm{Im}(-is_1\ell_t/c)\}+1} = 0.5201\,Z_c \tag{131}$$

Thus a reduction of nearly a factor of four in impedance (from $2Z_c$ to $0.52\,Z_c$) can be achieved at the natural resonance frequency. On the other hand if the two transmission lines are terminated in their characteristic impedances we have

$$Z_W = 2Z_c \tag{132}$$

Alternatively if two open circuited quarter wave sections are used we have at the frequency $i\beta$

$$Z_W(i\beta) = 2Z_c\coth(\beta\ell/c) \sim 2Z_c\,,\ \beta\ell/c >> 1 \tag{133}$$

9 NUMERICAL ANALYSIS USING PATCH CODE

The existing frequency domain surface integral equation code PATCH was used for detailed numerical modeling of the fixture configurations. The frequency domain results were Fourier transformed to obtain the desired time responses. Numerical leakage problems associated with the modeling of conducting structures limits the shielding effectiveness that can be directly modeled in the original version of the code (which was used in this project). A two step process was therefore used to overcome this limitation. The exterior problem was modeled and the surface drive fields at the POEs were determined. The exterior grid, that was used to determine both short circuit base current and base impedance, for the monopole fixture is shown in Figure 31a.

The second step for the monopole fixture was to drive an interior model shown in Figure 31b with the Thévenin source consisting of the exterior impedance plus sleeve capacitance and open circuit monopole voltage (short circuit monopole current times monopole impedance). Only the 50 ohm load was modeled. Both the exterior problem and interior problem used equivalent strips to model the cylindrical conductors of radius a. The equivalent strip width (for uniform strip current density) was taken as $w/e^{3/2} = a$ [20].

Figure 32a shows the load voltage frequency spectrum. Figure 32b shows the time domain voltage appearing across 50 ohm load measurement system (the load current times 50 ohms) resulting from the incident wave (2) with 0.4 nsec rise time parameters and amplitude -64.64 kV/m. This result can thus be compared to the test results in Figure 27a. Figure 32c shows the integral of the

square of the voltage from Figure 32b which can be compared to the test results in Figure 27b. The agreement between the test results and the PATCH model is quite good up to 25 nsec after the initial pulse arrival (the agreement ends after this time as a result of the second pulse in the facility).

The remaining conductor geometries and loads for each of the test fixtures can also be modeled with the same procedures as carried out here. This limited selection of only the monopole fixture was consistent with funding constraints, but nevertheless allowed a check on the experimental data.

10 SUMMARY AND CONCLUSIONS

The first part of the Model Validation Project (MVP) devoted to electromagnetic pulse (EMP) energy bounds was carried out. The motivation for the work was based on previously developed EMP energy bounds [4], [5], [7] and port of entry (POE) models [12], [13], [14], [17]. Objectives and more detailed plans for the current project were discussed in the previously published proposal [8] and test plan [9].

The basic objective was to validate previously developed energy bound results by constructing and testing canonical test objects that incorporate key features of actual weapon systems in a controlled and known manner but are somewhat worse in coupling levels than the actual weapon geometries. The key features that were selected included: the severity of the EMP incident wave, external aspect ratios to induce resonant enhancement of the surface drive fields for the POEs, joint and connector POEs, interior cable geometries and characteristic impedances, and interior cable load impedances.

Three types of cylindrical test fixtures were constructed: a test fixture with a single slot POE, a test fixture with a bolted joint POE, and a test fixture with a monopole (crudely simulating a connector) POE. Each test fixture made use of cylindrical interior cables and stripline cables (except the monopole fixture) and various loads (matched, low and high impedance, compared to the cable characteristic impedance). The tests were carried out in the Electromagnetic Environments Simulator (EMES) which provided EMP pulses exceeding typical threat levels.

Canonical waveforms of the double exponential and inverse exponential type (which are typically used to describe the EMP threat requirements) were fit to the test waveforms so analytical and numerical modeling could proceed from simply described excitations representative of the test facility waveforms.

Analytical results for EMP energy bounds were applied to the slot and monopole POEs. These results are quite small compared to typical electroexplosive device (EED) pin-to-pin initiation energies and older electronics damage thresholds. Exterior resonant enhancement of the surface fields driving the POEs was discussed. The EMP energy bounds can be applied to these enhanced fields by increasing the amplitude of the incident wave driving the POEs in these formulas.

EMP energy bounds were developed for the bolted joint POE. The per slot worst case energy of the bolted joint was determined by assuming a symmetric exciting field. The maximum total energy is thus the sum of the individual per slot energies. This sum can then be weighted by the actual behavior of the drive field over the slot array (symmetric resonant drives, shadowed high frequency drives, or low frequency sinusoidally varying drives). A key finding in the analysis of multiple slot joint apertures is that because the inductive reactance of the joint is quite low, the worst case energy reception can only be attained by a low impedance cable configuration as can be accomplished by a stripline near the wall of the weapon system; however this means that only one bolted joint slot will efficiently drive the nearby cable. The penetrant magnetic flux of the other slots does not effectively link such a cable configuration. Furthermore, because the inductance of the slot is typically larger or equal to that of a bolt, the slot inductances isolate the cable load from

the adjacent slot drive currents. An interesting additional source of coupled energy, if the bolts have a nonzero resistive component and the incident wave fall time is sufficiently long, was briefly discussed.

More detailed models for coupled energy were also applied. These formulas incorporated cable geometries and loads in addition to the POE geometry. The stripline cables were treated as slot center loads, and the cylindrical cables were treated by modeling a wire behind the apertures. The magnetic flux per slot on the joint POE is additive in the case of a recessed wire; thus, unlike the maximum case, the total energy is the square of the number of apertures (if they are driven uniformly and the wire is centered) times the single slot energy. The recessed wire coupling yields very small energies compared to the stripline coupling.

Formulas and estimates for the peak voltage were also given. Tapered (dielectric gap) stripline transformers (for the slot and joint fixtures) were also constructed to obtain what is thought to be near worst case voltage responses in a weapon-like geometry. Estimates for these transformed voltages were based on gradual impedance transformations with little reflection. The peak voltage estimates were well below levels that would be of concern for pin-to-case failure of EEDs.

An estimate of the parallel parasitic capacitance associated with the point load termination (resulting from the generation of higher order coaxial modes) of the coaxial geometry was given. Its value was small enough to be ignored in most instances.

Detailed comparisons of the test results were made with the analytical bound predictions. Because of reflections in the test facility, only received energy results from a limited window of time can be compared with predictions based on the typical EMP waveform requirements. Thus two received energy values were used: one value from early time (before external resonant enhancements of the POE drive fields play a significant role), and the second value from an intermediate time of 25 nsec (just prior to the arrival of a significant test facility feed reflection which deviates from the typical EMP requirement).

The matched stripline cases for the slot fixture and bolted joint fixture gave early time energies below the analytical energy bound, but intermediate energies slightly above the energy bound (which was initially based on the POE in a ground plane, without resonant enhancement of the POE drive fields). These values were below 100 nJ. Thus, the resonant enhancement appeared to be present, but did not result in significantly increased energies over the ground plane predictions. The low impedance load stripline cases resulted in lower energies than the matched cases or the energy bounds.

The centered and eccentrically located cylindrical wire cases for the slot and bolted joint fixtures resulted in very small energies compared to the POE energy bound predictions. The detailed models for these cases predicted the correct order of the reduction in energy (from the POE energy bound), but were often somewhat exceeded by the test results (particularly for the bolted joint fixture). The exterior resonance may have been partly responsible for this increase over the detailed model predictions (which were based on ground plane arguments).

The energy bound for the monopole fixture (in the matched case) was also somewhat exceeded by the intermediate time test results (and here it was obviously the result of the exterior resonance). These values were several μJ. The more detailed model which included the cable characteristic impedance mismatch was considerably below the test result (again as a result of the exterior resonant enhancement of the surface drive field). Actual recessed pin connectors would obviously have a much smaller effective height (and thus greatly reduced energy bounds and open circuit voltages) relative to this canonical monopole POE. Geometries where the entire connector is insulated with respect to case would have similar effective heights to the canonical monopole POE but slightly larger capacitances.

The peak voltage predictions were in relatively good agreement with the test results for all

three test fixtures. The voltages for stripline cables were in the several tens of volts range. The voltages for the monopole fixture were in the several hundreds volts range. There were slight inaccuracies in the small voltages associated with the cylindrical wire cases in the slot and bolted joint fixtures. The matched tapered stripline peak voltages (in the slot and bolted joint fixtures) were also accurately predicted. These values were slightly greater than 100 volts.

The high impedance loads on the tapered stripline cases (in the slot and bolted joint fixtures) yielded several times the matched voltages. This was later shown to be a result of an unexpected parasitic shunt capacitance inherent in the 1000 ohm load resistors which rendered the voltage divider extrapolation (which was used to interpret the data) invalid. Network analyzer measurements were used to estimate this parasitic element; the modified voltage divider extrapolation, incorporating this parasitic element, then yielded voltages only sightly exceeding the matched voltages.

The stainless steel bolts of the bolted joint fixture were replaced by ferrous steel bolts (in the case of the tapered stripline with high impedance load). Similar voltages were recorded; thus the bolt material did not have any significant effect (this was anticipated since the external inductance dominates the conductor surface impedance at the high frequencies associated with fast rise time EMP).

A more rigorous means of dealing with the exterior resonant enhancement of the POE drive field was investigated. The slot POE drive current on a cylindrical object subjected to a double exponential EMP waveform was expanded in a damped sinusoid series (singularity expansion in the frequency domain). The energy bound for the POE was carried out with this drive field (limiting consideration to the leading term or first length resonance). It was shown that the contribution from the first resonance was several tens of nJ; which explains the increase of the intermediate time test results to values slightly above the POE energy bound on a ground plane. This increase is not significant for typical POEs.

The second important finding, resulting from the use of the singularity expansion bounding procedure, is the limitations on the transforming properties of transmission line cables. Without considering dissipation, cable transmission lines ordinarily have the ability to impedance transform a load to a matched value at the POE. But because the external resonances occur at complex frequencies with relatively large imaginary parts (low effective quality factors), the transformation properties of these transmission lines are quite limited (to a band surrounding the characteristic impedance of the cable, which is relatively large compared to the inductive reactance of typical bolted joint or slot POEs). Thus impedance matching of bolted joint or slot POEs is usually not possible.

Detailed numerical modeling of the monopole test configuration was also carried out using the existing surface integral equation code PATCH. This is a frequency domain code and thus the code results were Fourier transformed. Because of numerical leakage problems associated with the original version of the code (and the fact that the shielding provided by the canonical test objects is relatively good), a two-step process was used. The exterior problem was modeled and the exterior POE drive circuit was determined. The interior problem was then modeled with the drive circuit impressed by sources and loads and the interior voltages and currents were determined. The results obtained by the numerical models corroborated the test results. (The same procedure can be used for the other fixtures; this limited selection was made as a result of funding constraints.)

The predicted and measured induced voltages are considerably below the pin-to-case threshold of EEDs. The predicted and measured energies are considerably below pin-to-pin EED thresholds and below damage thresholds of older electronics. The voltages and energies are large enough that electronic upset cannot be ruled out (at least at the level of POE bounding without any major interior mismatches included).

References

[1] K. S. H. Lee (editor), *EMP Interaction: Principles, Techniques, and Reference Data*, New York: Hemisphere Press, 1986.

[2] L. K. Warne and T. E. Koontz, "Comparison of Energies Delivered to a Simple Tubular Dipole Antenna With Low Impedance Load by EMR and EMP," Sandia National Laboratories internal memorandum, to T. S. Edrington, July 10, 1987, pp1-52.

[3] L. K. Warne and K. C. Chen, "A bound on EMP coupling," AFWL Interaction Note 466, June 1988, pp. 1-29.

[4] L. K. Warne and K. C. Chen, "A Bound on EMP Coupling," IEEE Transactions on Electromagnetic Compatibility, Vol. 32, No. 3, August 1990, pp. 217-221.

[5] L. K. Warne and K. C. Chen, "A Bound on Aperture Coupling from Realistic EMP," IEEE Transactions on Electromagnetic Compatibility, Vol. 36, No. 2, May 1994, pp. 149-154.

[6] D. E. Merewether, J. A. Cooper, and R. L. Parker (editors), *Electromagnetic Pulse Handbook For Missiles And Aircraft In Flight*, Prepared by Sandia Laboratories, Albuquerque, NM, for the Air Force Weapons Laboratories, SC-M-710346, September 1972, pp. 17, 23, 24.

[7] L. K. Warne, T. E. Koontz, and K. C. Chen, "EM Penetration Bounds," Sandia National Laboratories internal memorandum, to T. S. Edrington, August 5, 1988, pp. 1-43.

[8] M. E. Morris and J. G. Lewis, "Validation of EMR/EMP Bounds," Sandia National Laboratories internal memorandum, March 1995.

[9] M. E. Morris, L. K. Warne, K. O. Merewether, K. C. Chen, J. E. Solberg, and J. G. Lewis, "Validation of EMP Bound Test Plan," Sandia National Laboratories internal memorandum, June 1995.

[10] S. Ramo, J. R. Whinnery, T. Van Duzer, *Fields and Waves in Communication Electronics*, New York: John Wiley & Sons, 1965, pp. 445-448.

[11] W. R. Smythe, *Static and Dynamic Electricity*, New York: Hemisphere Pub. Co., 1989, pp. 76-78.

[12] L. K. Warne and K. C. Chen, "A Simple Transmission Line Model for Narrow Slot Apertures Having Depth and Losses," IEEE Transactions on Electromagnetic Compatibility, Vol. 34, No. 3, August 1992, pp. 173-182.

[13] L. K. Warne, "Low Frequency Magnetic Field Penetration of Narrow Slot Apertures Having Depth," Sandia National Laboratories internal memorandum, to M. E. Morris, March 12, 1990, pp. 1-16.

[14] L. K. Warne and K. C. Chen, "Effective Impedance of Bolt Loads on Narrow Slot Apertures Having Depth," Journal of Electromagnetic Waves and Applications, Vol. 6, No. 7, 1992, pp. 891-910.

[15] F. Gardiol, *Microstrip Circuits*, New York: John Wiley & Sons, Inc., 1994, pp. 42-46.

[16] R. W. P. King, *The Theory of Linear Antennas*, Cambridge Massachusetts: Harvard U. Press, 1956, p. 184.

[17] L. K. Warne, T. E. Koontz, and K. C. Chen, "Equivalent Polarizabilities of Apertures with Depth," AFWL Interaction Note 474, March 1989, pp. 1-99.

[18] L. K. Warne, "Low Frequency Capacitance of a Tubular Dipole," Sandia National Laboratories internal memorandum, to R. H. Bonn, December 14, 1990.

[19] L. K. Warne, K. O. Merewether, K. C. Chen, M. E. Morris, J. E. Solberg, and J. G. Lewis, "Validation of EMP Bounds, volume 2: test data, " Sandia National Laboratories internal report, Sept. 29, 1995.

[20] L. K. Warne and K. O. Merewether, "Equivalent Radius of Strip Conductors Carrying Uniformly Distributed Current," Sandia National Laboratories internal memorandum, to W. A. Johnson, December 1995.

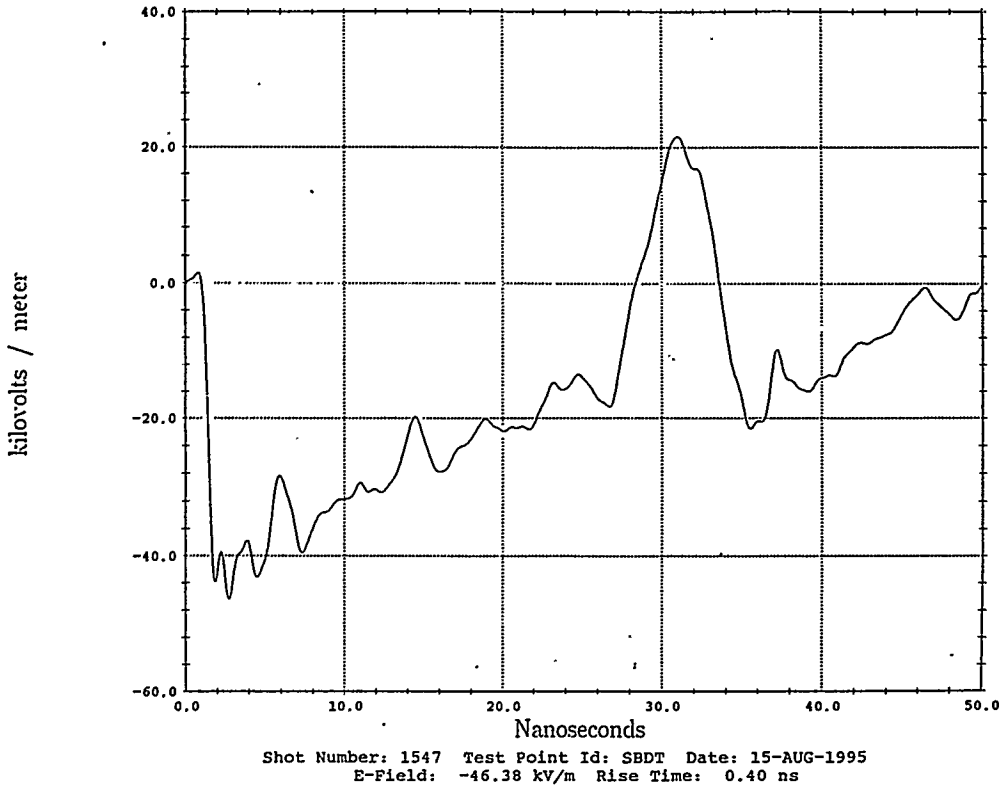

Figure 1. Typical Electromagnetic Enironments Simulator (EMES) incident electric field waveform.

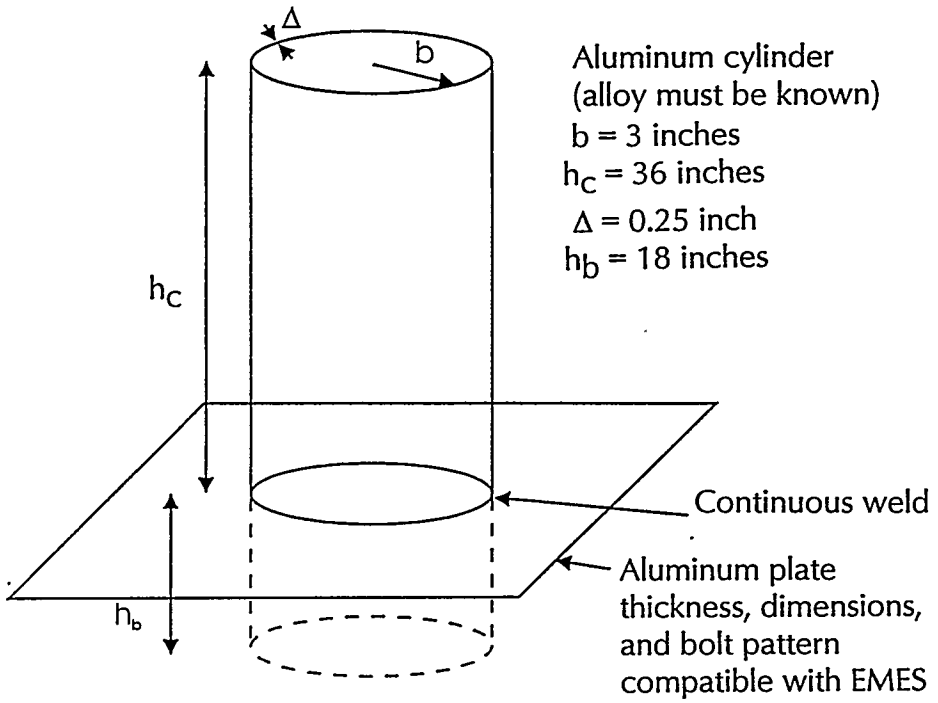

(a) fixtures consist of cylinder welded on to square plate, which forms part of the ground plane in EMES facility

Figure 2. Conceptual drawings of canonical test fixtures.

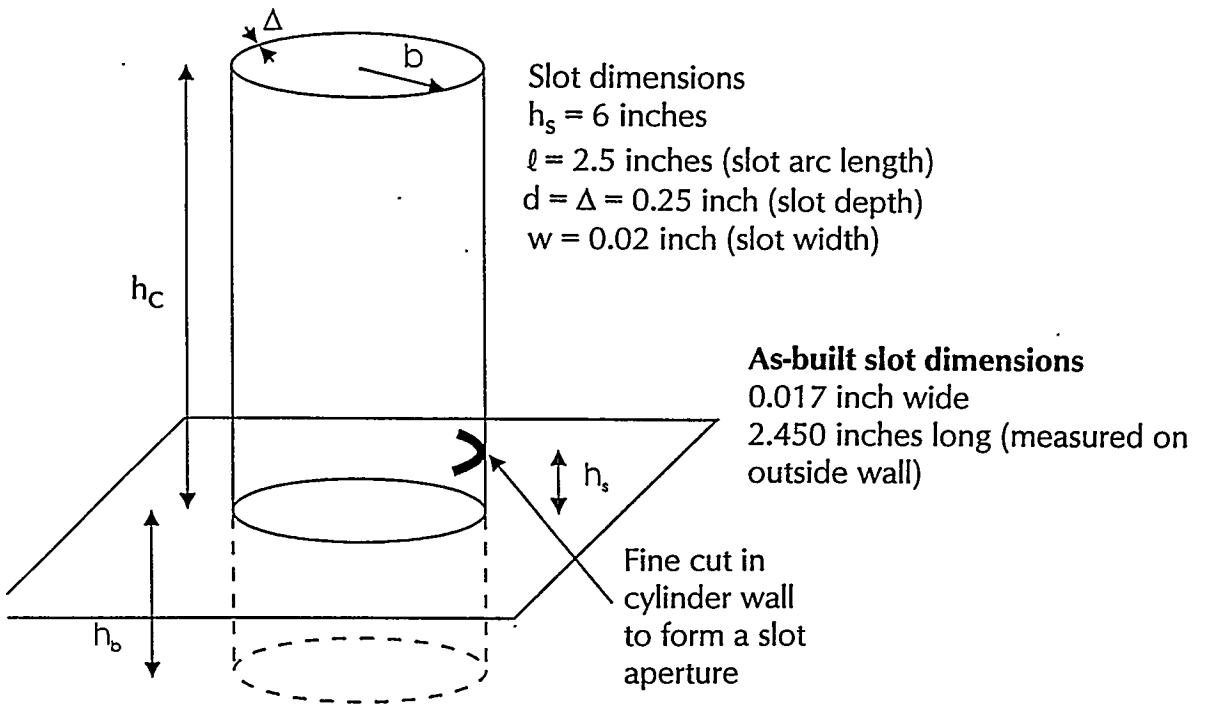

(b) slot test fixture

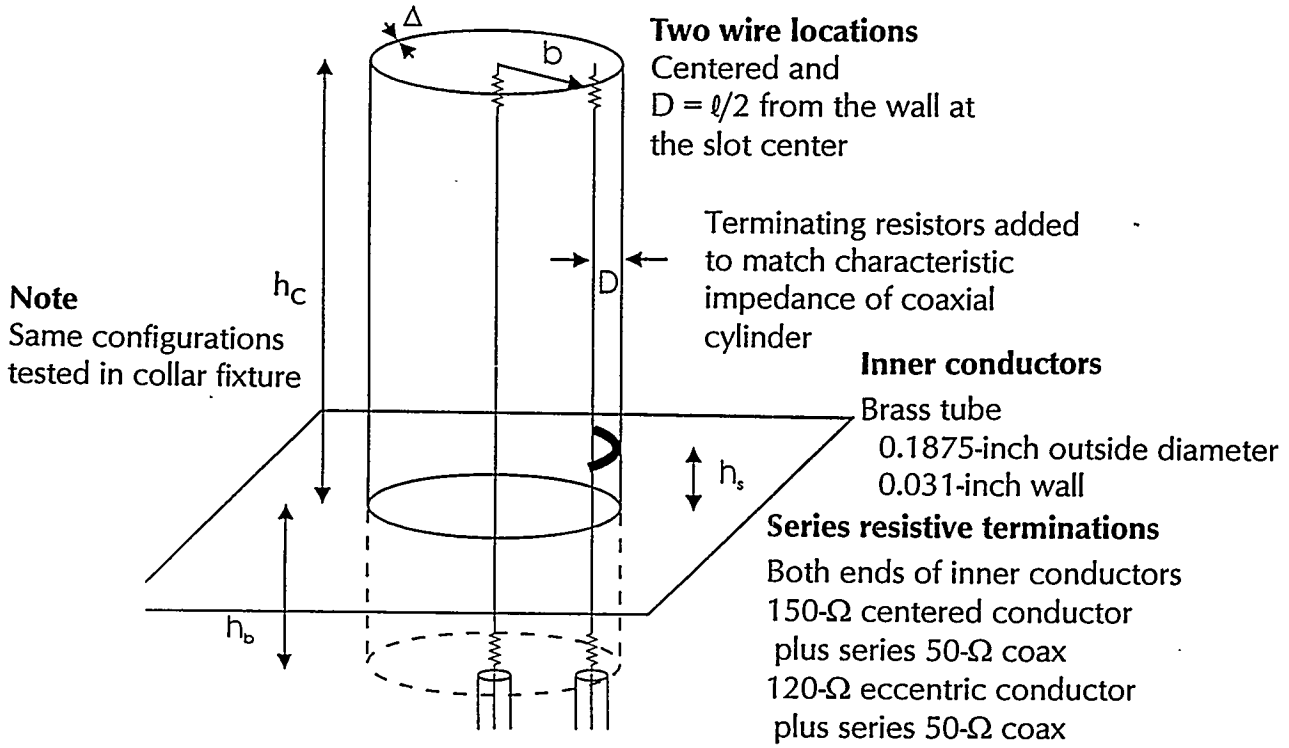

(c) slot test fixture showing two alternate wire load arrangements (centered wire and eccentric wire)

Figure 2. Conceptual drawings of canonical test fixtures (continued).

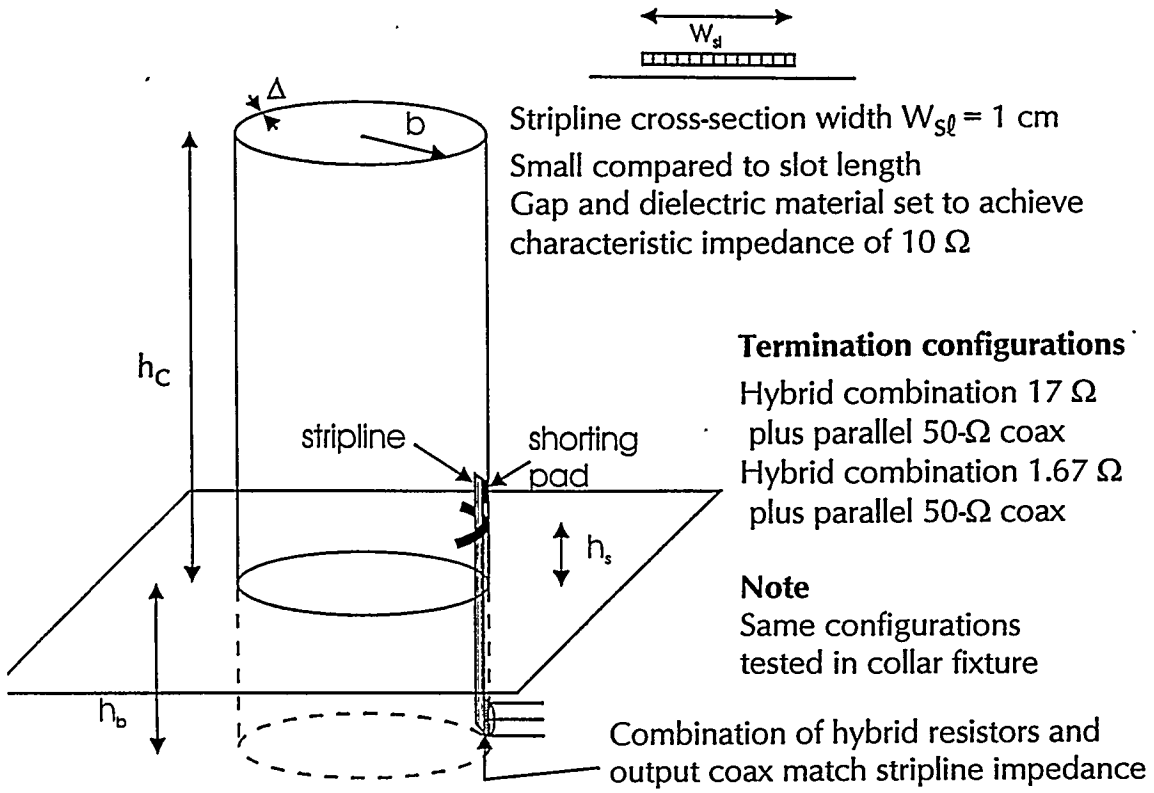

(d) slot test fixture showing stripline cable

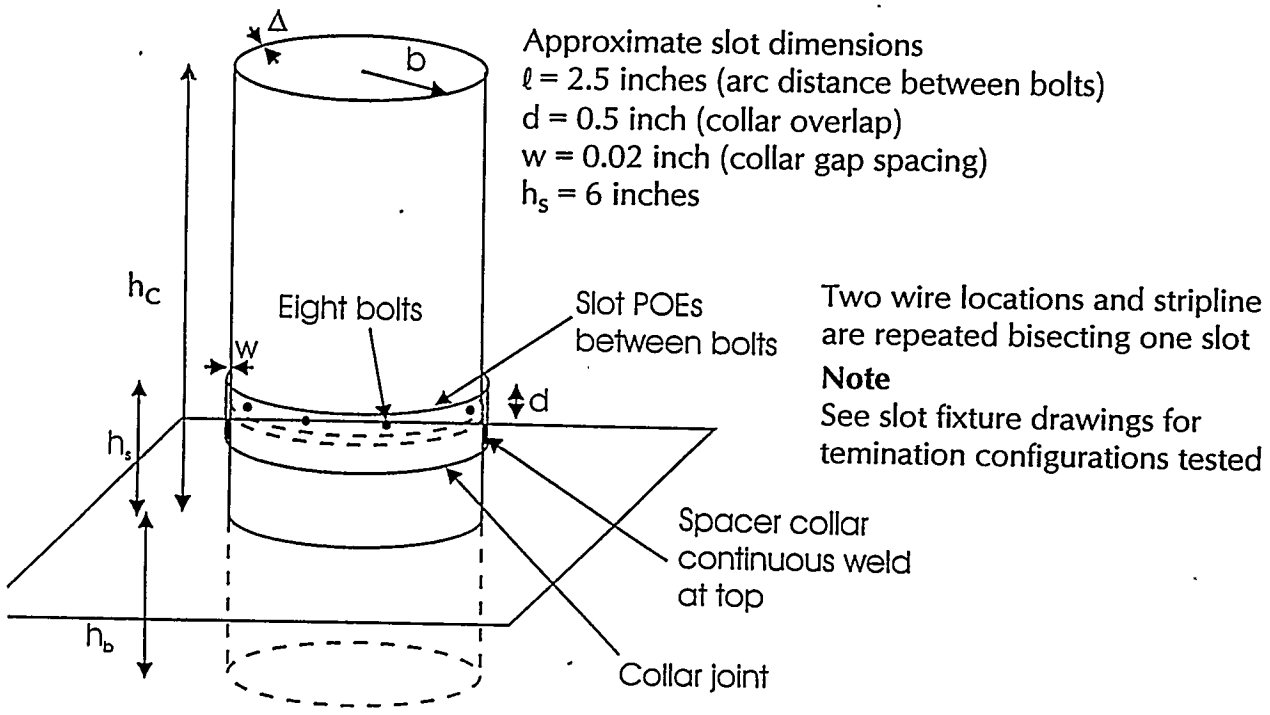

(e) bolted collar joint test fixture

Figure 2. Conceptual drawings of canonical test fixtures (continued).

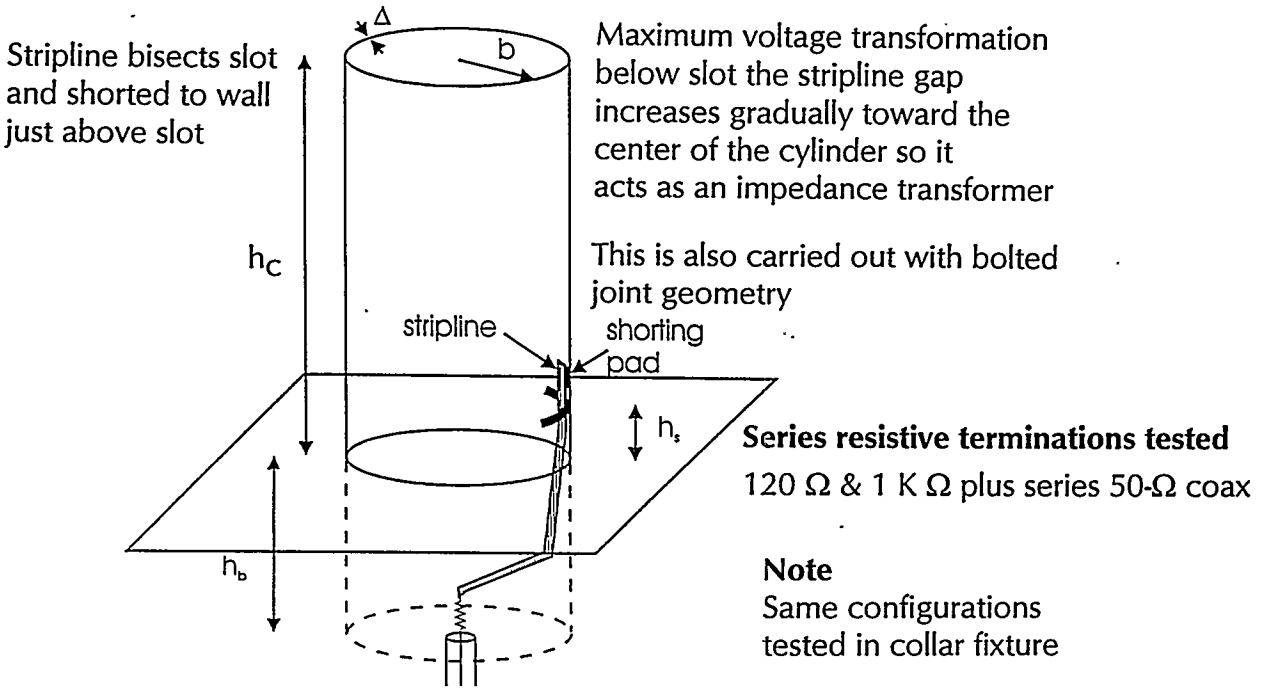

(f) slot test fixture with tapered stripline cable

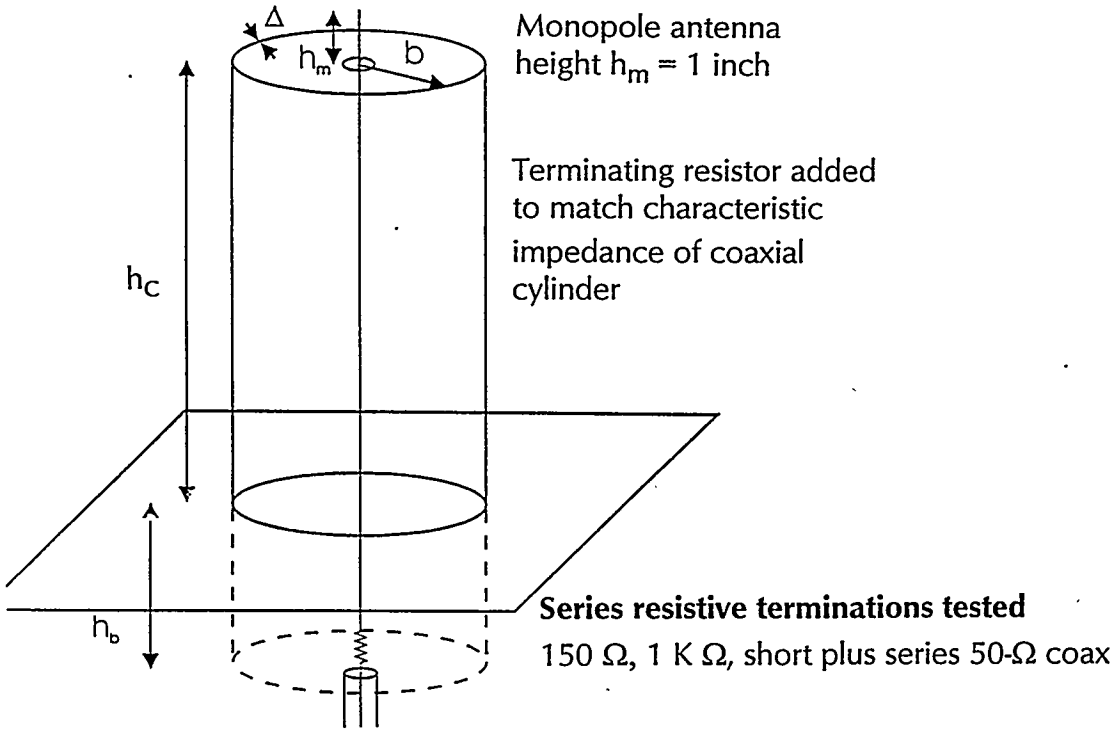

(g) monopole test fixture with centered cable

Figure 2. Conceptual drawings of canonical test fixtures (continued).

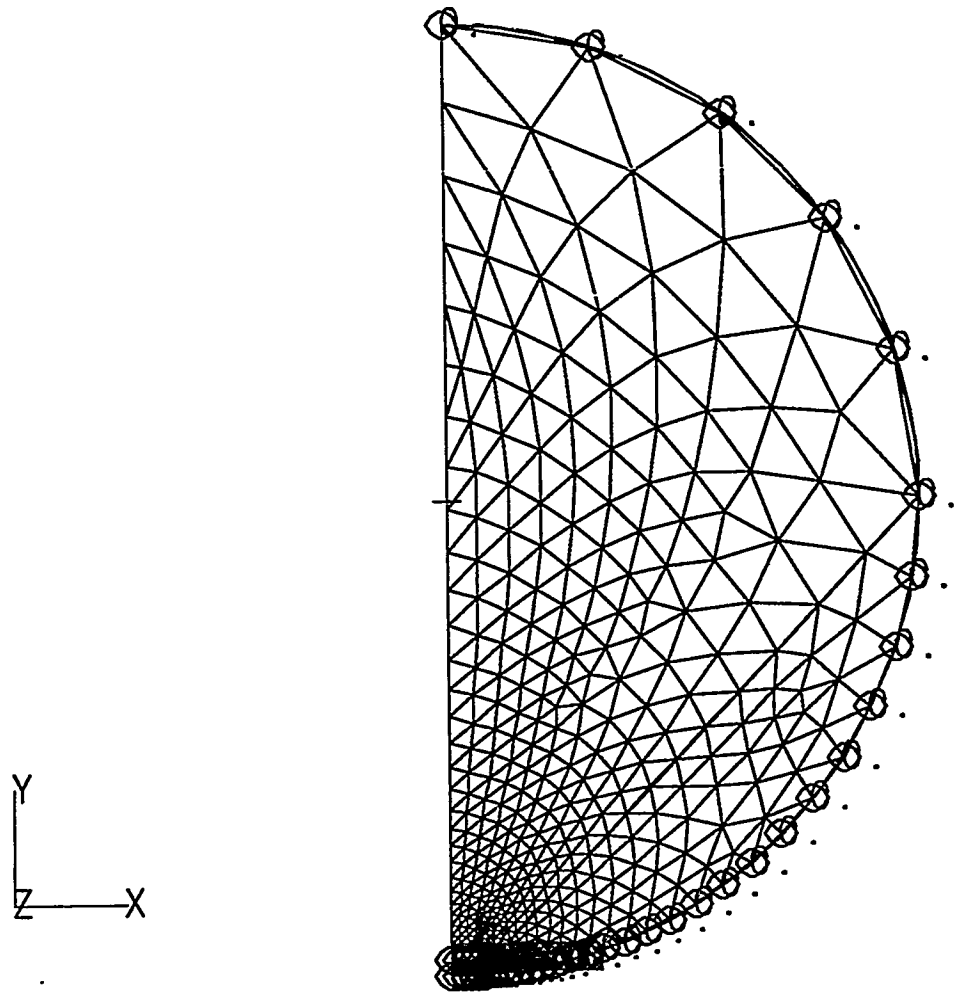

(a) two-dimensional finite element grid used to predict the characteristic impedance of the uniform stripline (end height of tapered stripline) cable with respect to the cylinder

Figure 3. Numerical grid model used in checking design electrical parameters.

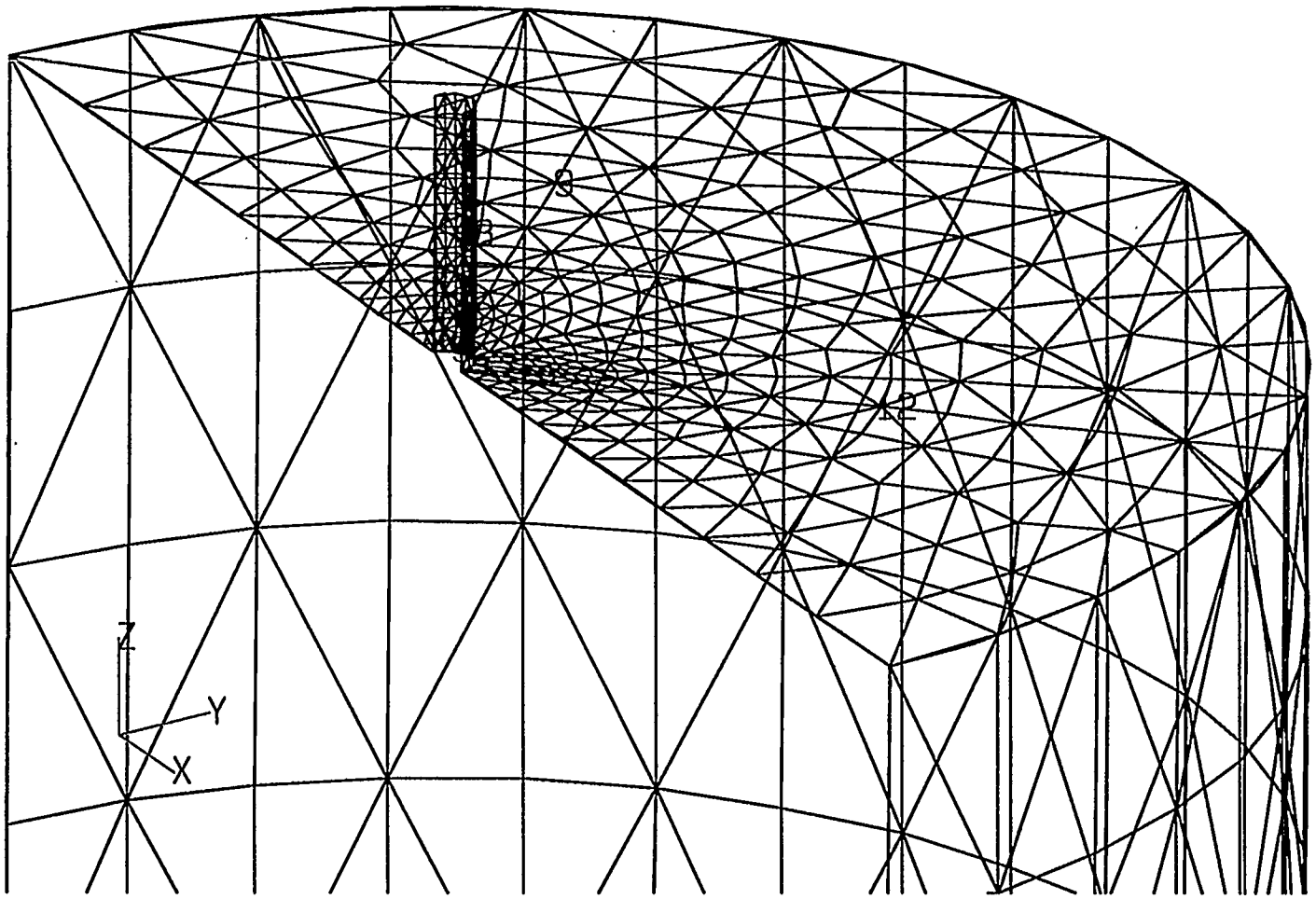

(b) surface integral equation code PATCH three-dimensional surface grid to determine the monopole capacitance with respect to the cylinder (only half the problem is modeled by use of a symmetry plane).

Figure 3. Numerical grid model used in checking design electrical parameters (continued).

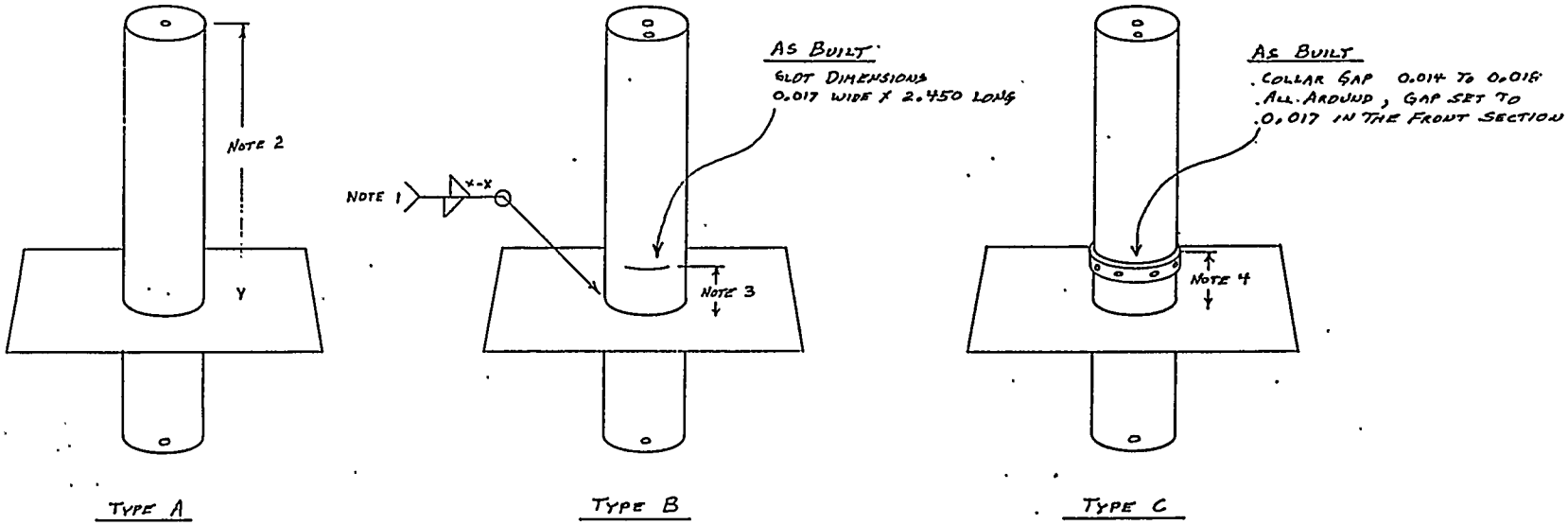

NOTES

1. TUBE IS ALIGNED PERPENDICULAR TO MOUNTING PLATE ON ALL FIXTURES. WELD TUBE TO MOUNTING PLATE WITH A CONTINUOUS FILLET WELD TOP SURFACE, INTERMITTENT FILLET WELD (LENGTH AND PITCH DETERMINED BY FABRICATOR) BOTTOM SURFACE.
2. 36" FROM MOUNTING PLATE TO TOP OF FIXTURE WITH COVER PLATE INSTALLED.
3. THE SLOT IN THE TUBE TO BE 6" FROM THE MOUNTING PLATE AND CENTERED ON THE CENTERLINE OF THE PLATE.
4. THE EDGE OF THE COLLAR TO BE 6" FROM THE MOUNTING PLATE WITH THE COLLAR BOLTS EQUALLY SPACED FROM THE CENTERLINE OF THE PLATE.

Test Fixtures
Scale - None
Sheet 1 of 9

Figure 4. Detailed mechanical drawings of test fixture and cable hardware.

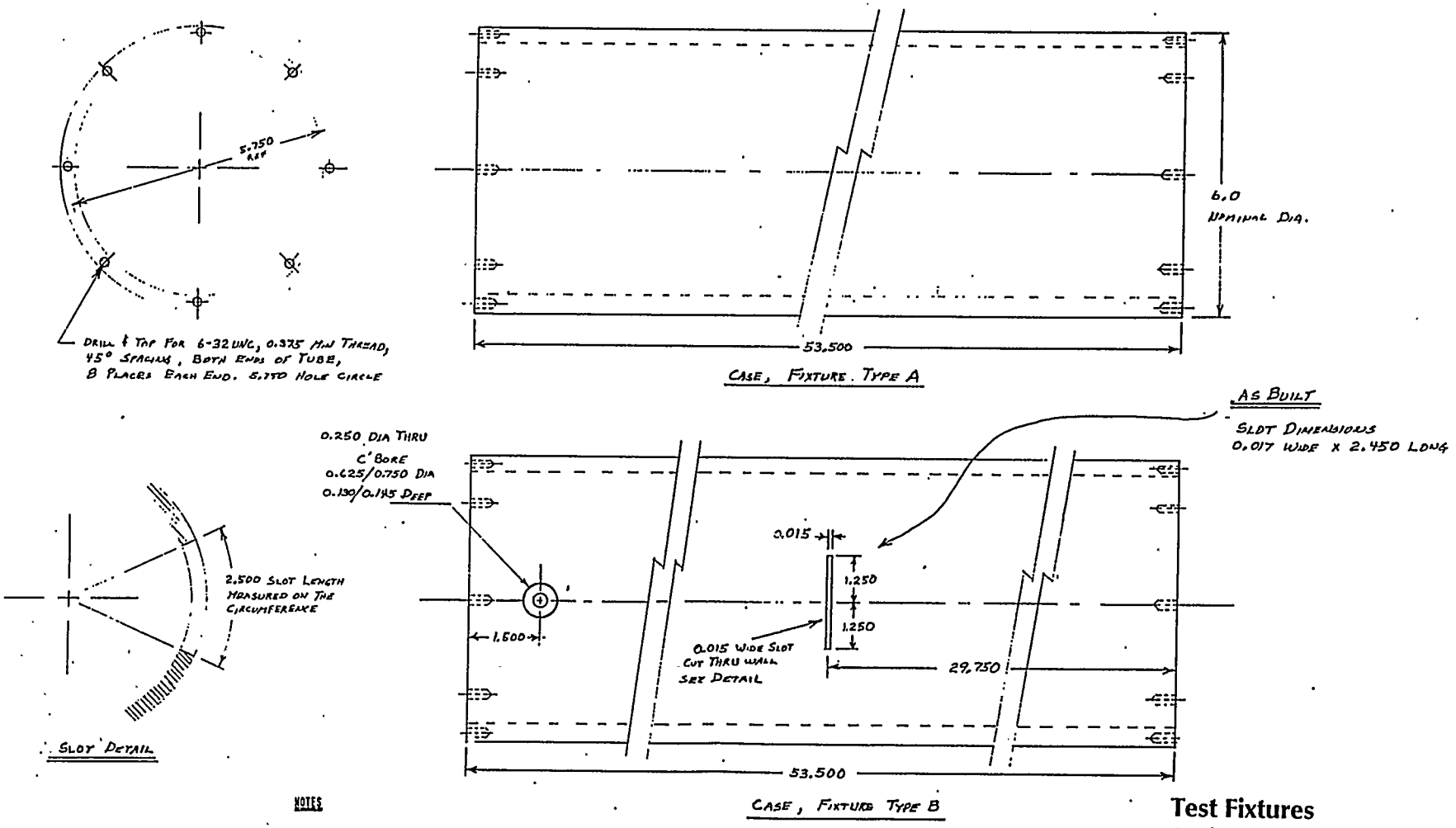

Figure 4. Detailed mechanical drawings of test fixture and cable hardware (Continued).

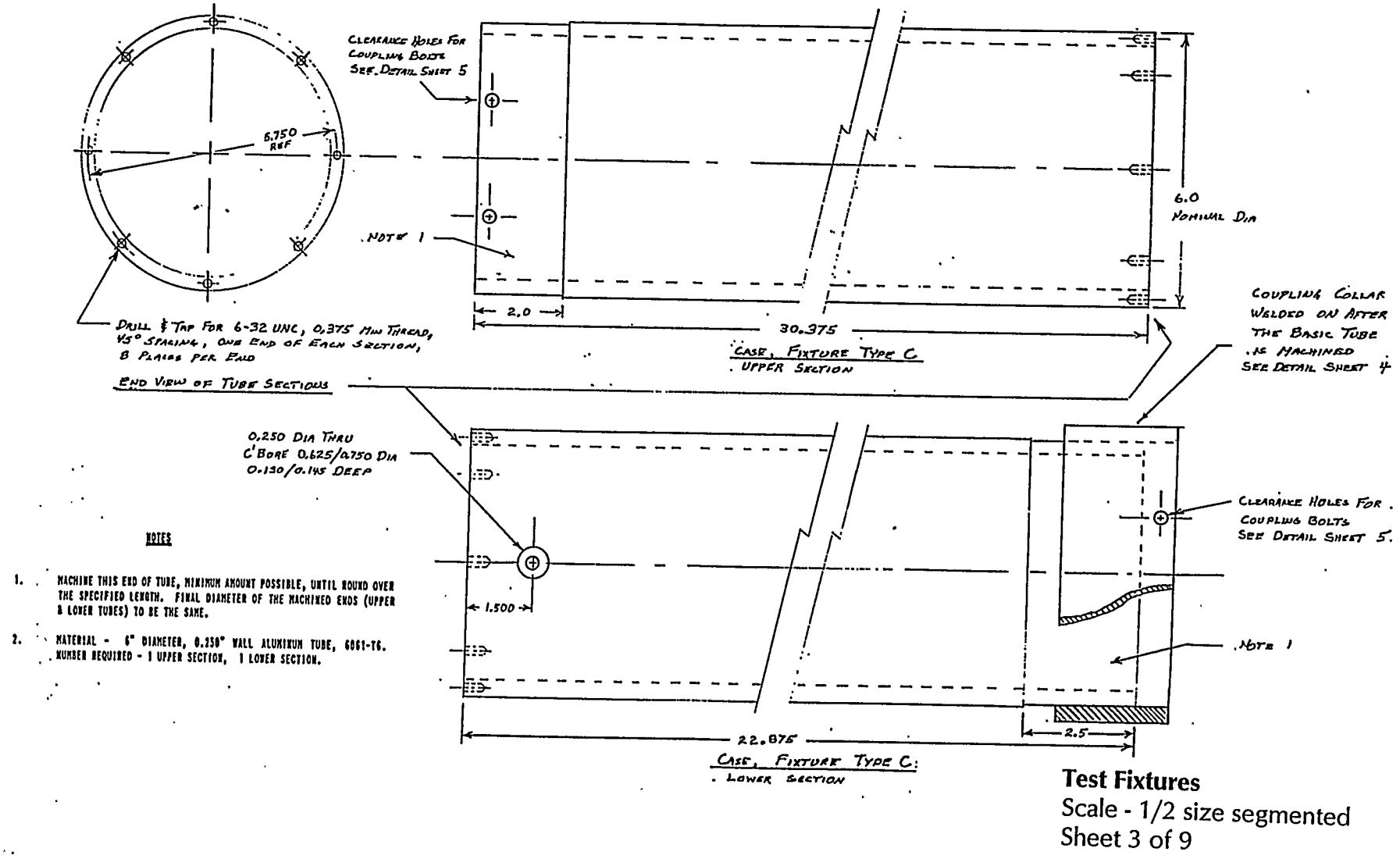

Figure 4. Detailed mechanical drawings of test fixture and cable hardware (Continued).

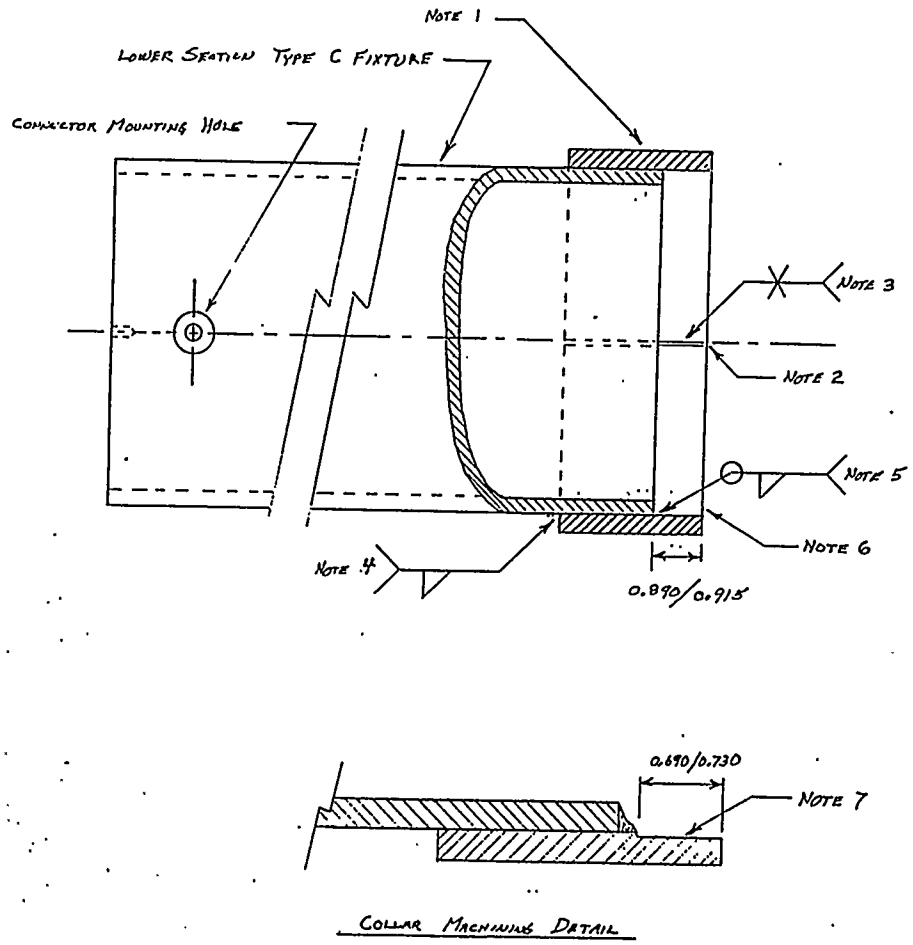

NOTES

1. THE COLLAR TO BE FABRICATED FROM 0.25" THICK X 2.5" WIDE X REQUIRED LENGTH ALUMINUM PLATE, 6061-T6, ROLLED AND CUT TO FIT THE CIRCUMFERENCE OF THE TUBE. GAP OF THE BUTT JOINT DETERMINED BY THE FABRICATOR.
2. BUTT JOINT TO BE LOCATED ON THE DIAMETRICALLY OPPOSITE SIDE OF THE TUBE FROM THE CONNECTOR MOUNTING HOLE IN THE OTHER END OF TUBE.
3. WELDING OF THE COLLAR BUTT JOINT. EXPOSED PORTION, WELD BOTH SIDES; LAPPED PORTION, CLOSE THE JOINT, FULL PENETRATION NOT REQUIRED.
4. INTERMITTENT FILLET WELD. WELD LENGTH AND PITCH AT THE DISCRETION OF THE FABRICATOR.
5. FILLET WELD, ALL AROUND, BEAD AS SMALL AS POSSIBLE. JOINT MUST BE "RF" TIGHT.
6. MACHINE END FACE OF COLLAR, MINIMUM POSSIBLE, UNTIL TRUE.
7. MACHINE INNER SURFACE OF COLLAR TO A DIAMETER Approx 0.030" LARGER THAN THE MACHINED END OF THE UPPER TUBE. DESIRED FINAL CONDITION; 0.015 SPACE BETWEEN COLLAR AND UPPER TUBE, ALL AROUND, AFTER ASSEMBLY.

Test Fixtures
Scale - 1/2 size segmented
Sheet 4 of 9

Figure 4. Detailed mechanical drawings of test fixture and cable hardware (Continued).

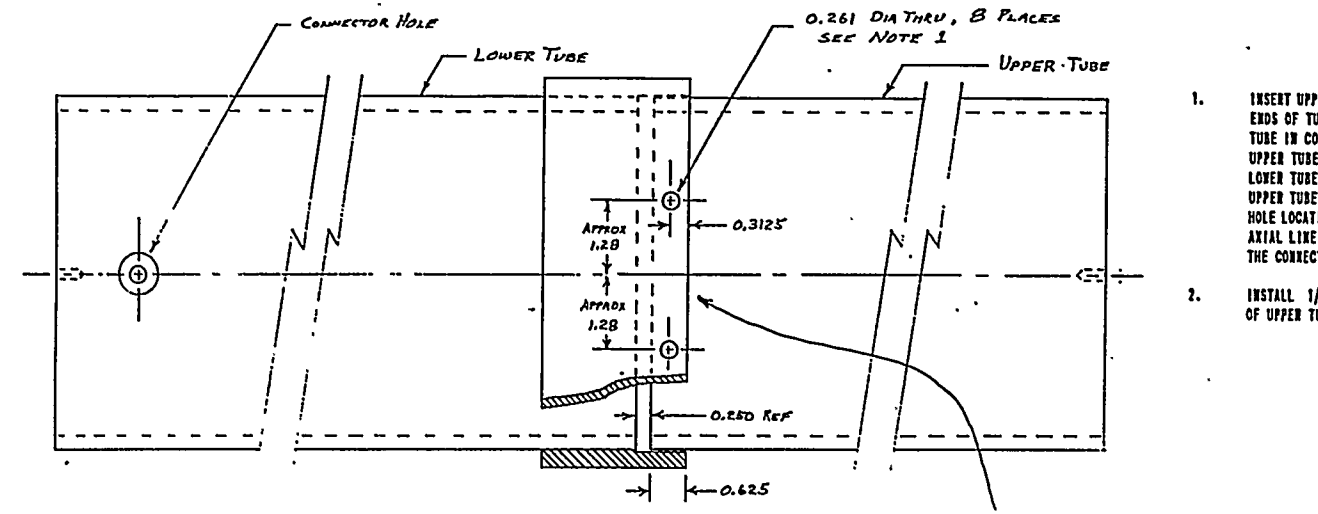

NOTES

1. INSERT UPPER TUBE INTO COLLAR 0.625" (APPROX 0.250" GAP BETWEEN ENDS OF TUBES, IGNORING THE WELD). SHIM, AS REQUIRED, TO CENTER TUBE IN COLLAR WITH ONE OF THE 6-32 TAPPED HOLES IN THE END OF THE UPPER TUBE AXIALLY ALIGNED WITH THE CONNECTOR MOUNTING HOLE IN THE LOWER TUBE. MATCH DRILL 8 HOLES, LETTER 0 DRILL, THRU COLLAR AND UPPER TUBE, EQUALLY SPACED AROUND THE CIRCUMFERENCE OF THE COLLAR. HOLE LOCATION TO BE SUCH THAT THE HOLES ARE EQUALLY SPACED FROM THE AXIAL LINE BETWEEN THE TAPPED HOLE IN THE END OF THE UPPER TUBE AND THE CONNECTOR HOLE IN THE LOWER TUBE.

2. INSTALL 1/4 - 28 FLOATING NUT PLATES, 8 PLACES, ON INSIDE SURFACE OF UPPER TUBE WITH #2 X 1/4" DRIVE SCREWS.

AS BUILT
COLLAR GAP 0.014 TO 0.018
ALL AROUND, GAP SET TO
0.017 IN THE FRONT SECTION

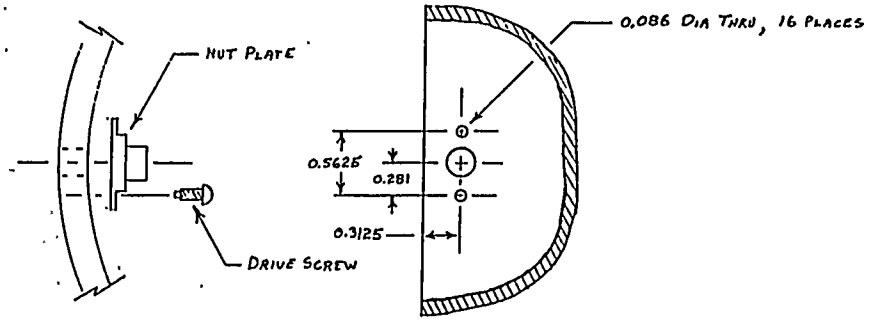

DETAIL, NUT PLATE INSTALLATION
DRAWN FULL SIZE - SEE NOTE 2

Test Fixtures
Scale - 1/2 size segmented
Sheet 5 of 9

Figure 4. Detailed mechanical drawings of test fixture and cable hardware (Continued).

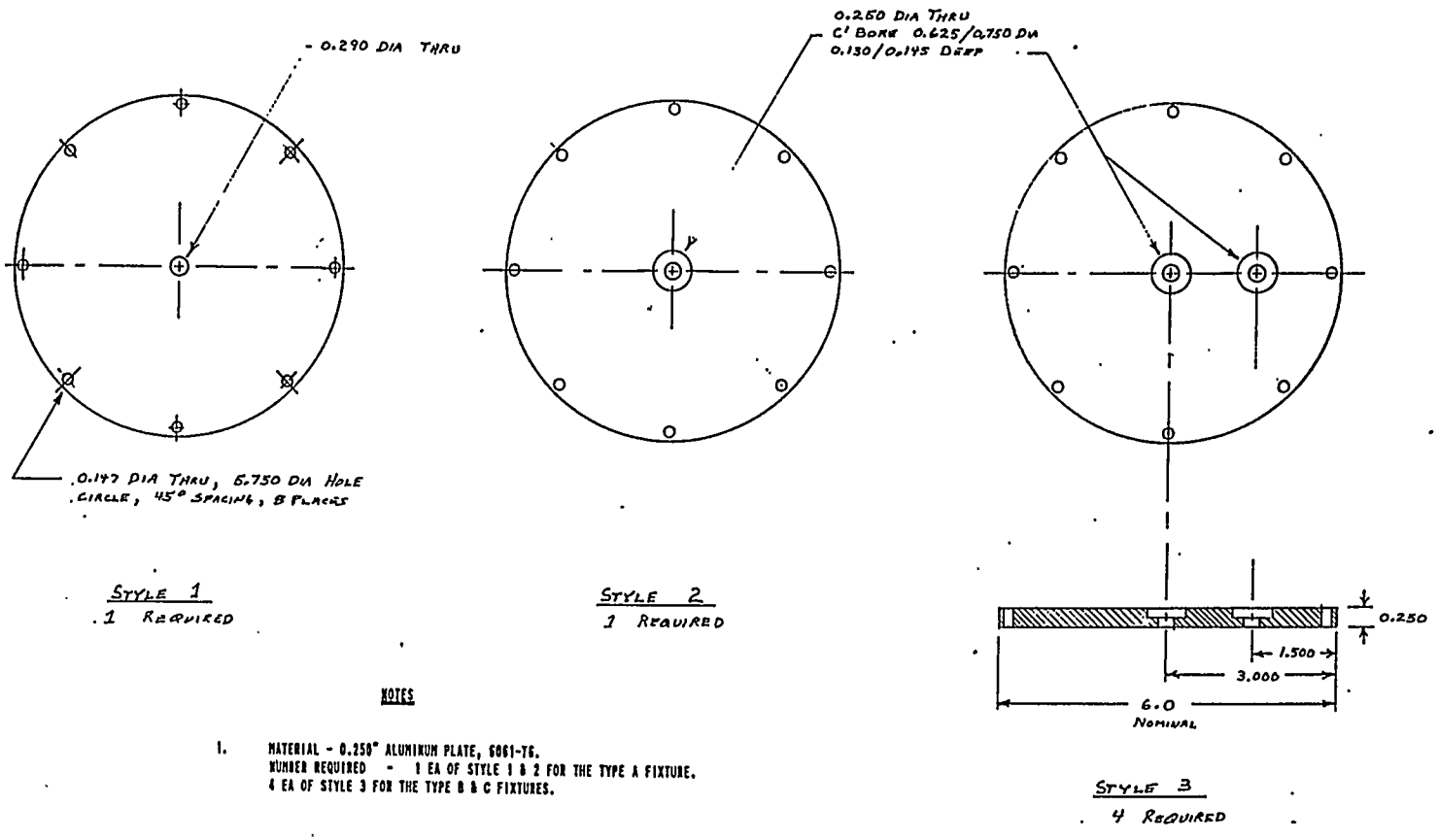

NOTES

1. MATERIAL - 0.250" ALUMINUM PLATE, 6061-T6.
   NUMBER REQUIRED - 1 EA OF STYLE 1 & 2 FOR THE TYPE A FIXTURE.
   4 EA OF STYLE 3 FOR THE TYPE B & C FIXTURES.

Test Fixtures
Scale - 1/2 size segmented
Sheet 6 of 9

Figure 4. Detailed mechanical drawings of test fixture and cable hardware (Continued).

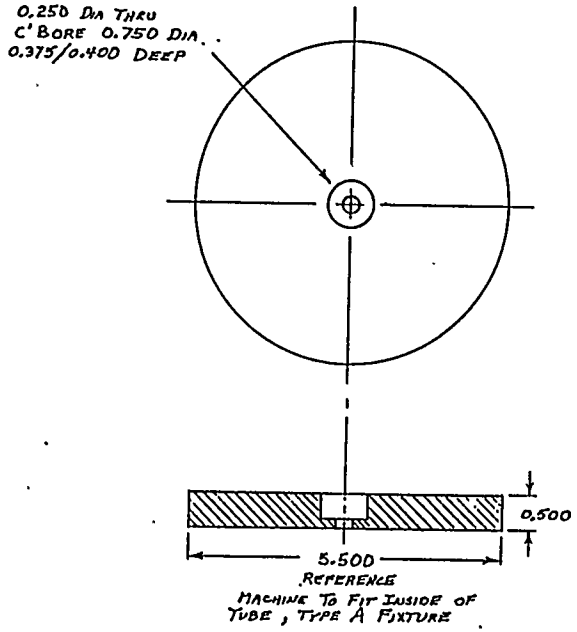

NOTES

1. MATERIAL - 0.500" ALUMINUM PLATE, 6061-T6.
   NUMBER REQUIRED -. 1 FOR THE TYPE A FIXTURE.

Plug Plate
Scale - 1/2 size
Sheet 7 of 9

Figure 4. Detailed mechanical drawings of test fixture and cable hardware (Continued).

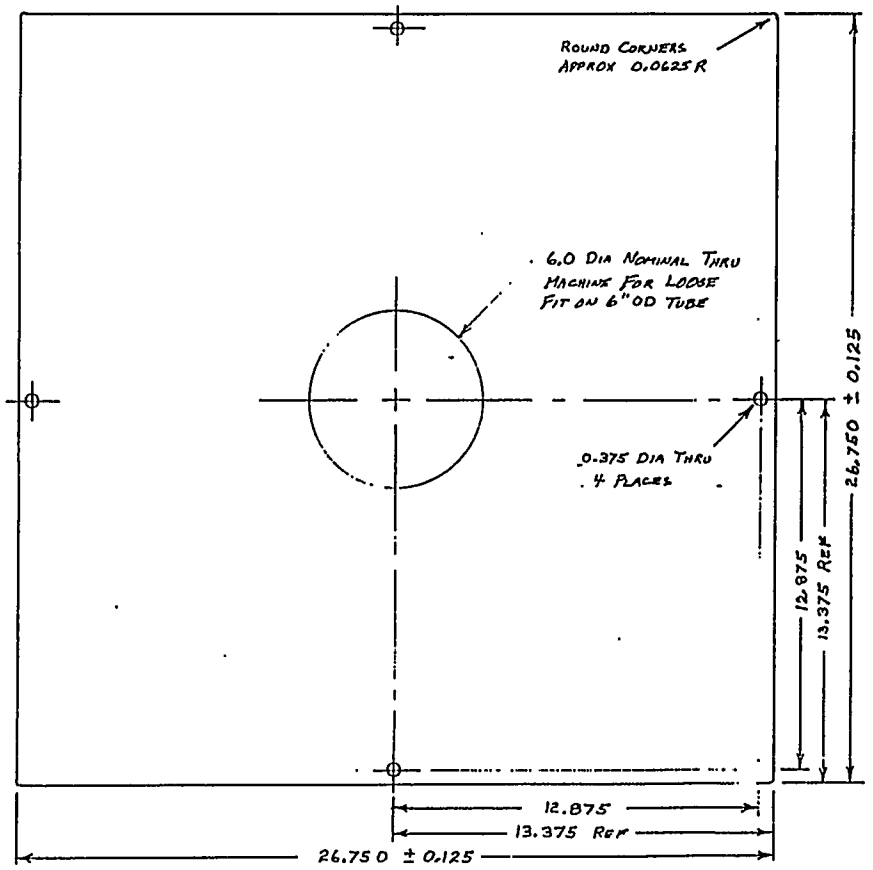

NOTES

1. MATERIAL - 0.250" ALUMINUM PLATE, 6061-T6.
   NUMBER REQUIRED - 3, ONE FOR EACH TYPE FIXTURE.

Mounting Plate
Scale - 1/4 size
Sheet 8 of 9

Figure 4. Detailed mechanical drawings of test fixture and cable hardware (Continued).

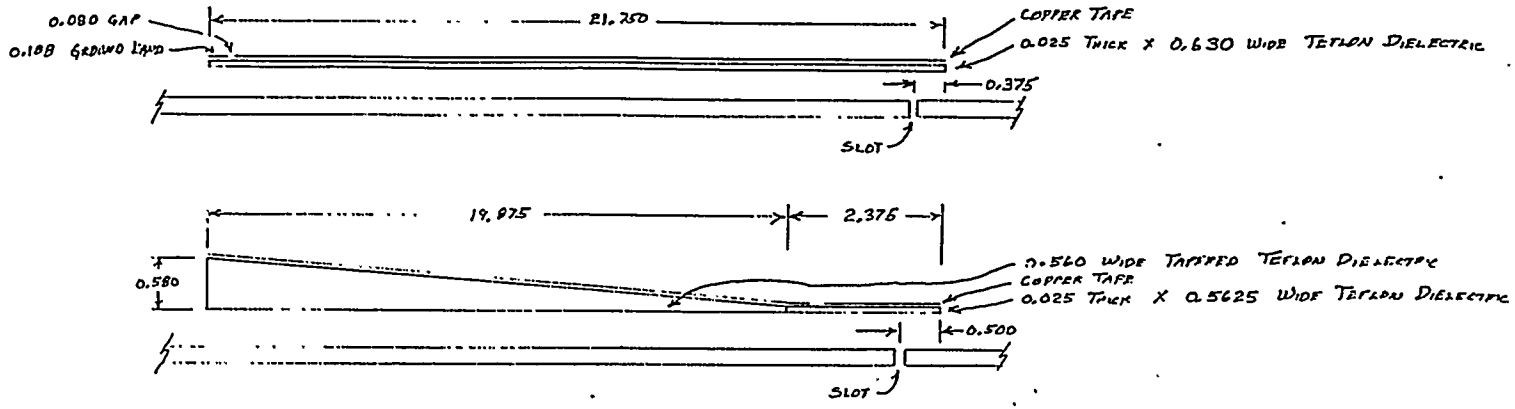

STRIP LINES, SLOT (TYPE B) FIXTURE

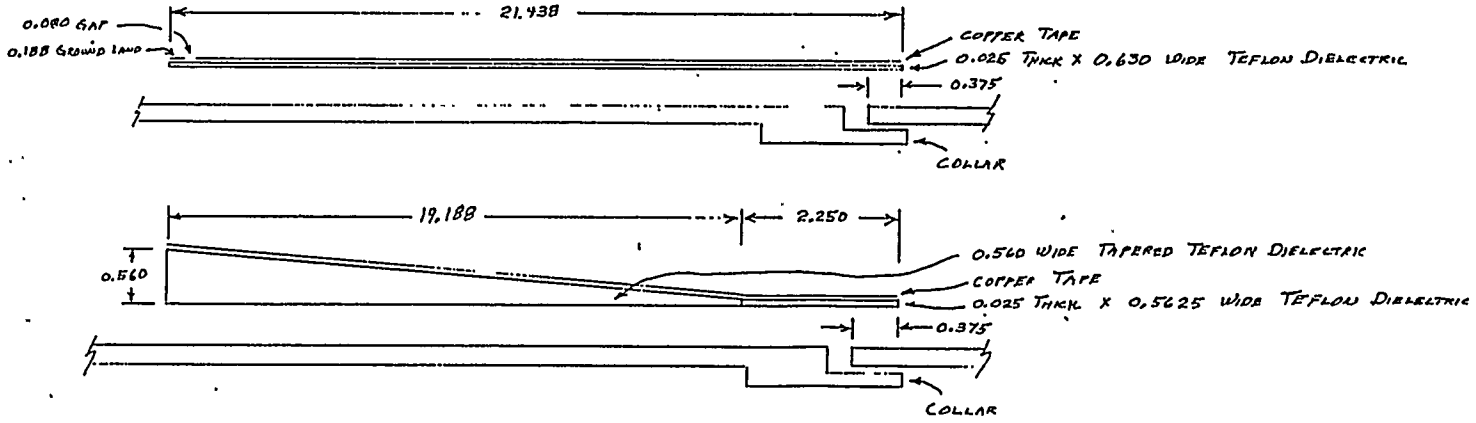

STRIP LINES, COLLAR (TYPE C) FIXTURE

Strip Lines, Type B & C Fixtures
Scale - None
Sheet 9 of 9

Figure 4. Detailed mechanical drawings of test fixture and cable hardware (Continued).

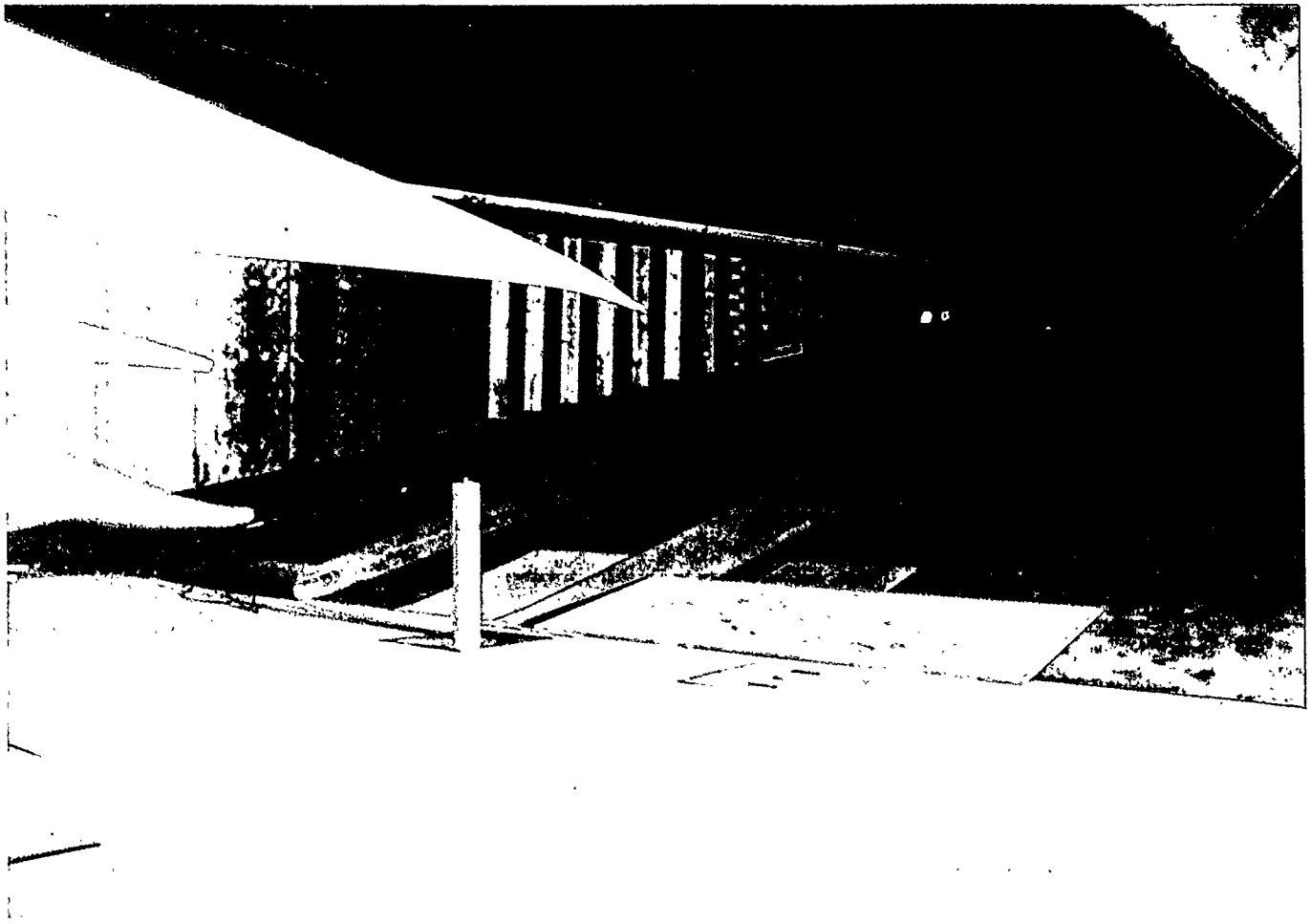

Monopole fixture in EMES

Figure 5. Photographs of monopole, slot and bolted joint fixtures with accompanying cable, load, and bolt hardware.

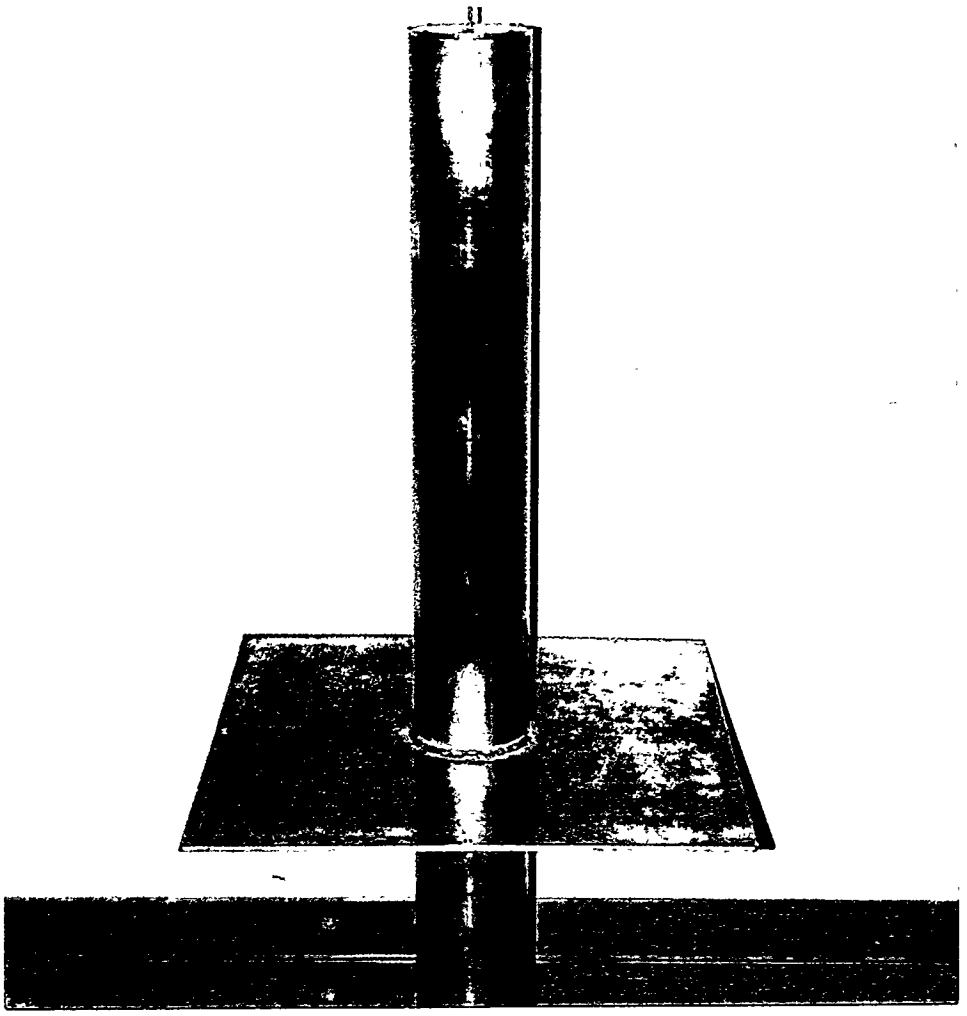

Monopole fixture

Figure 5. Photographs of monopole, slot, and bolted joint fixtures with accompanying cable, load, and bolt hardware (continued).

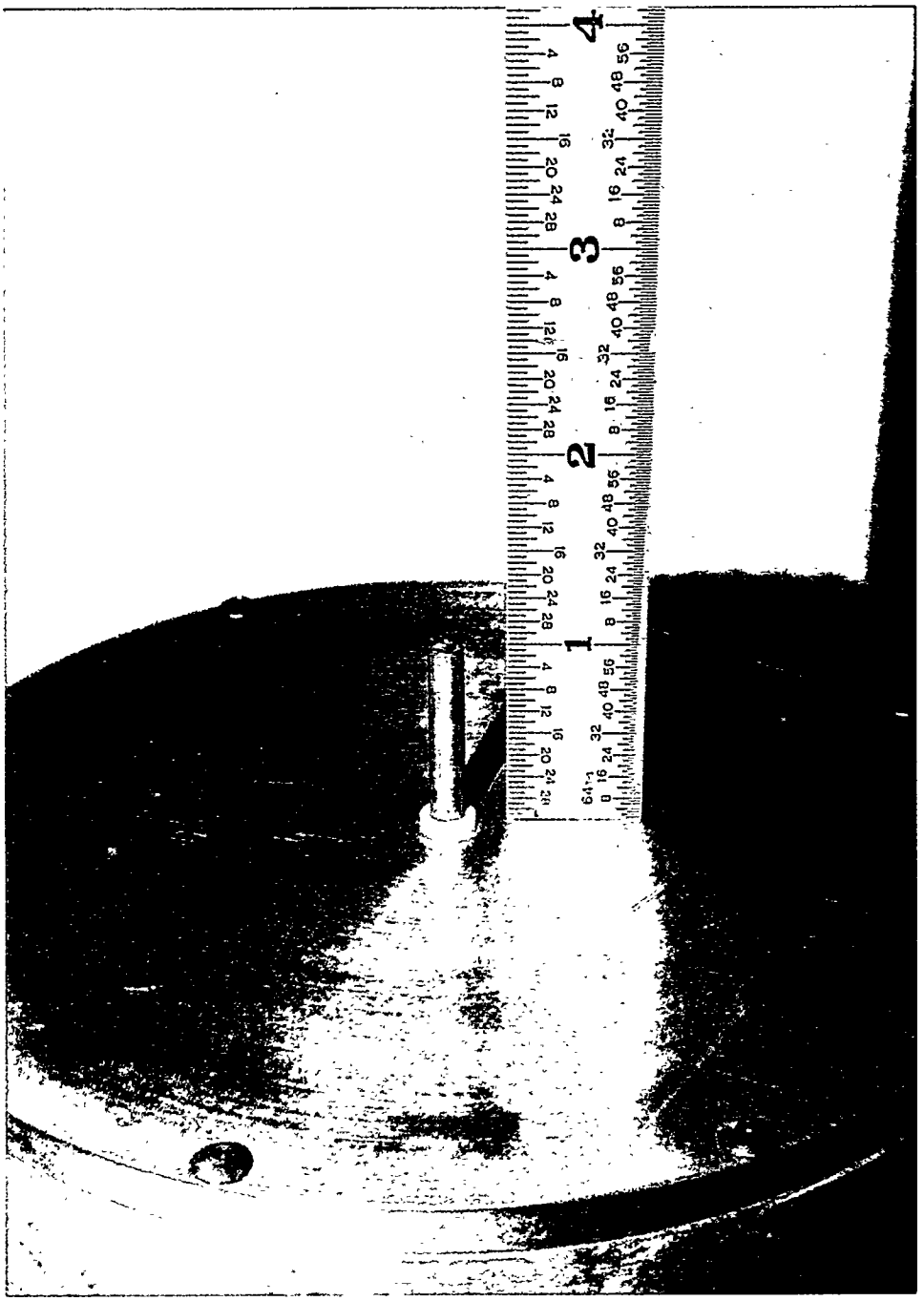

Monopole and dielectric sleeve

Figure 5. Photographs of monopole, slot, and bolted joint fixtures with accompanying cable, load, and bolt hardware (continued).

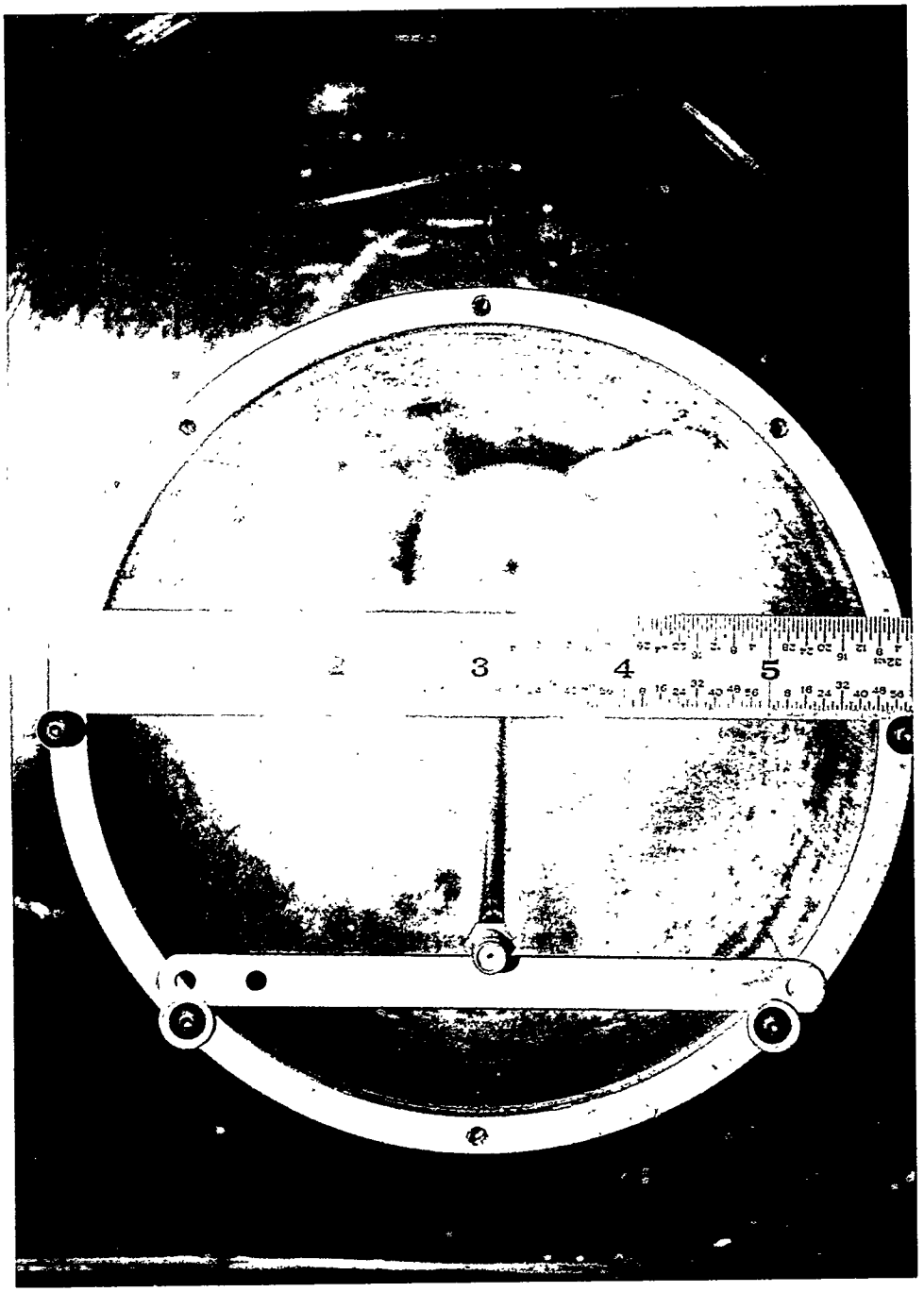

Cylindrical conductor in monopole fixture

Figure 5. Photographs of monopole, slot, and bolted joint fixtures with accompanying cable, load, and bolt hardware (continued).

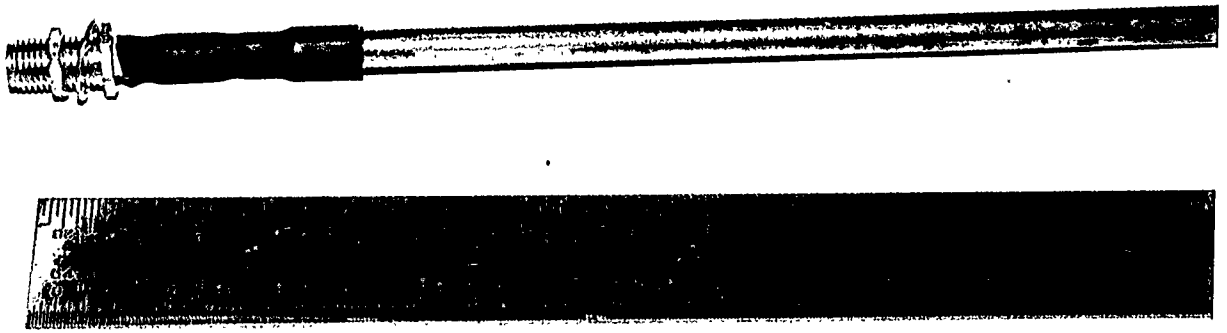

Cylindrical conductor and series resistive load near coax termination

Figure 5. Photographs of monopole, slot, and bolted joint fixtures with accompanying cable, load, and bolt hardware (continued).

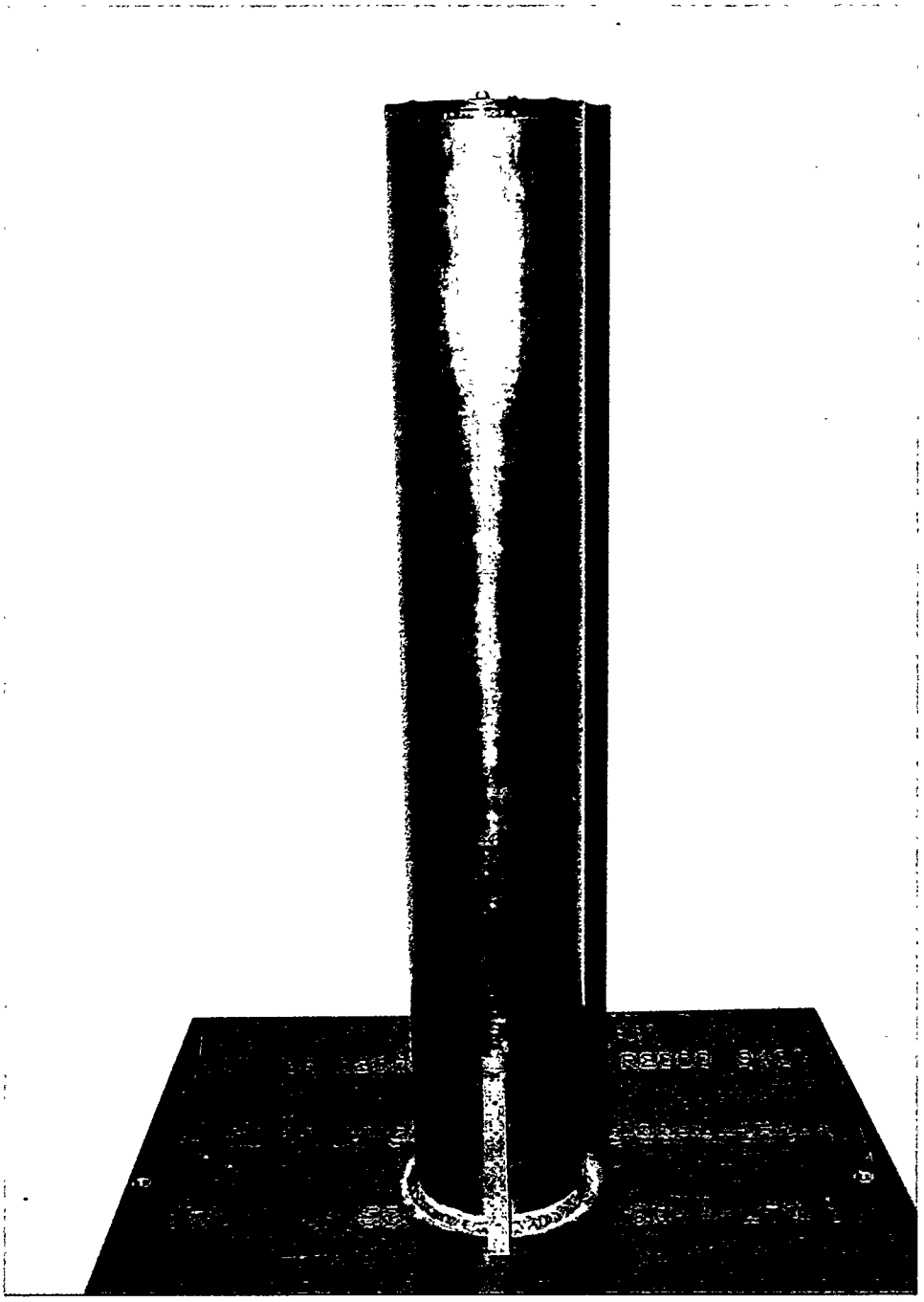

Slot fixture

Figure 5. Photographs of monopole, slot, and bolted joint fixtures with accompanying cable, load, and bolt hardware (continued).

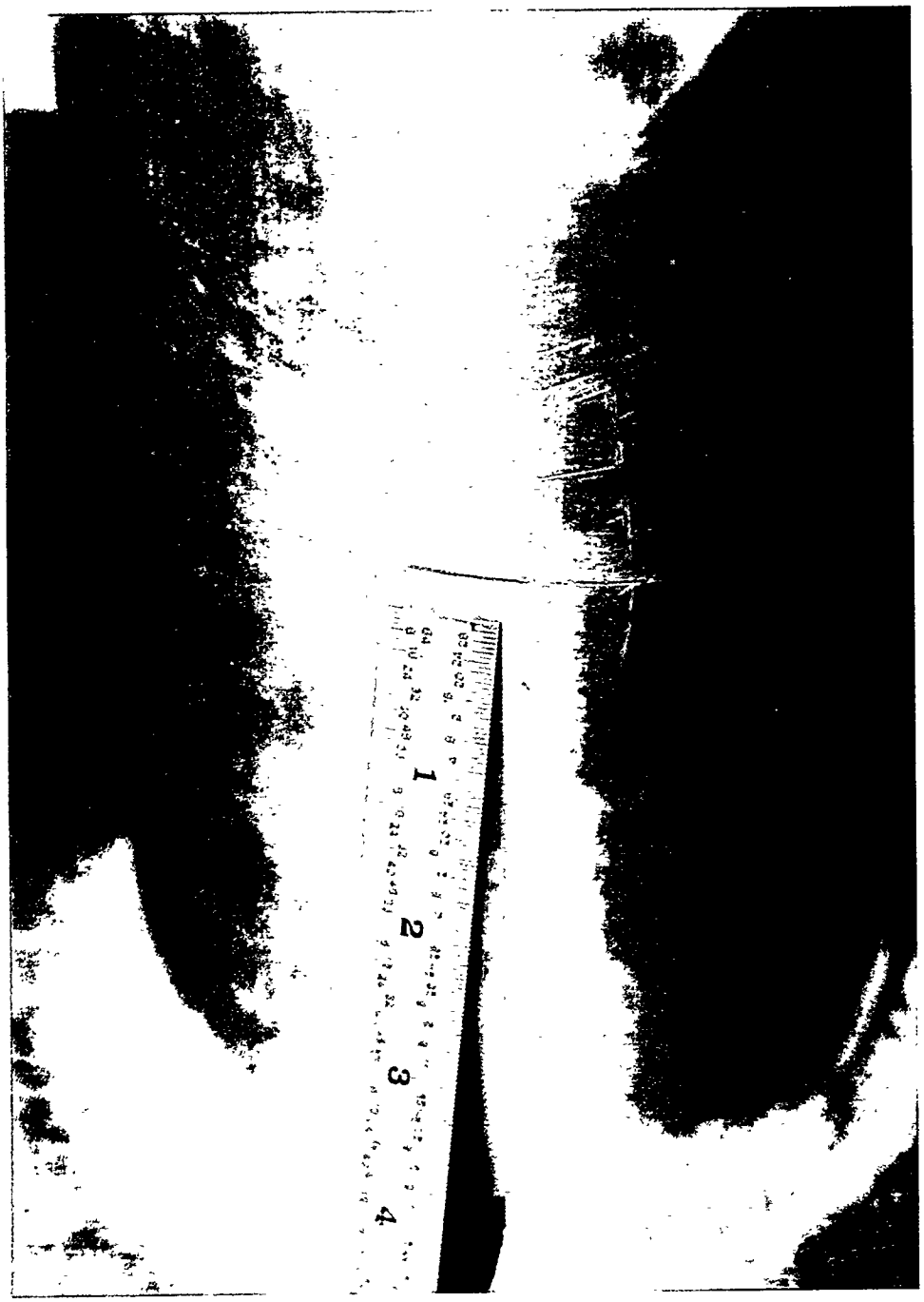

Slot

Figure 5. Photographs of monopole, slot, and bolted joint fixtures with accompanying cable, load, and bolt hardware (continued).

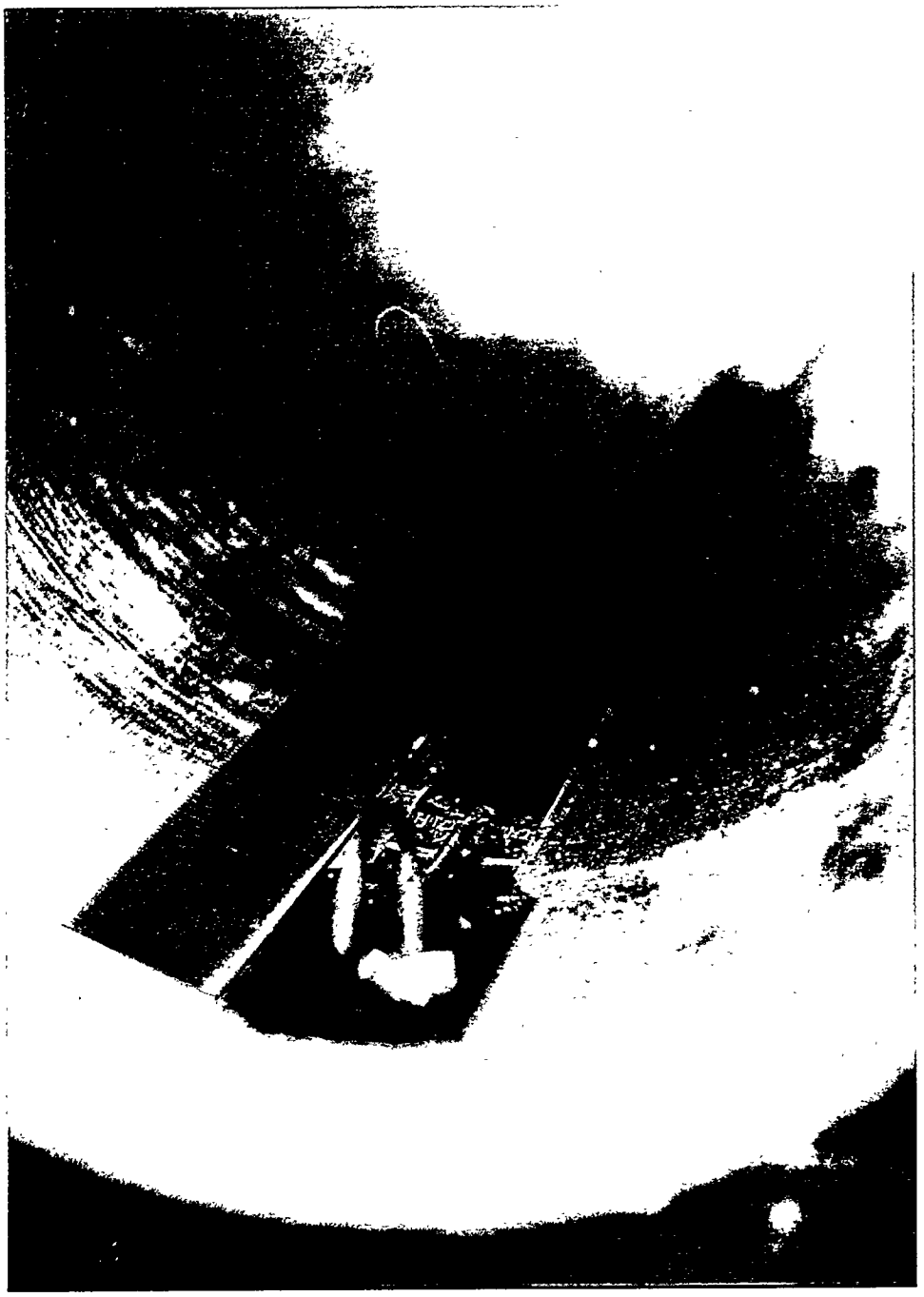

Hybrid resistor and coax load on stripline in slot fixture

Figure 5. Photographs of monopole, slot, and bolted joint fixtures with accompanying cable, load, and bolt hardware (continued).

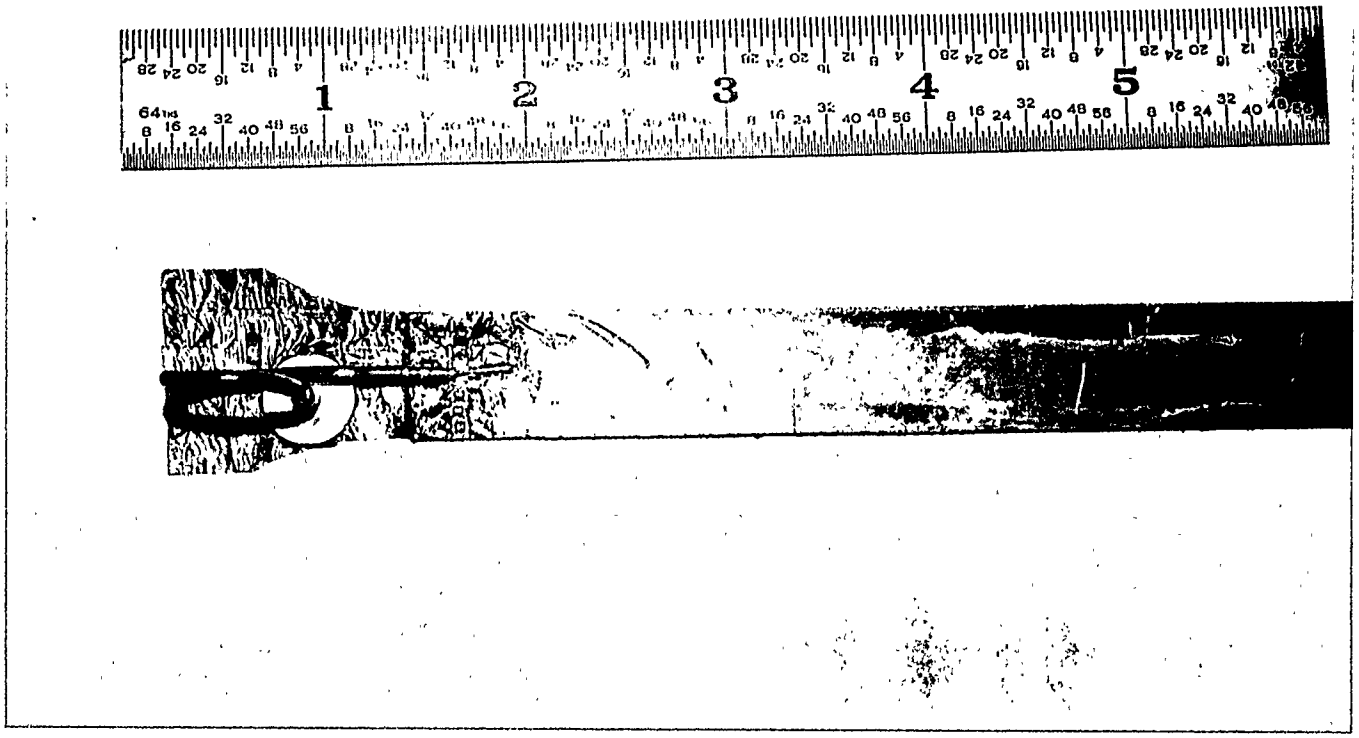

Hybrid resistor and coax load on stripline

Figure 5. Photographs of monopole, slot, and bolted joint fixtures with accompanying cable, load, and bolt hardware (continued).

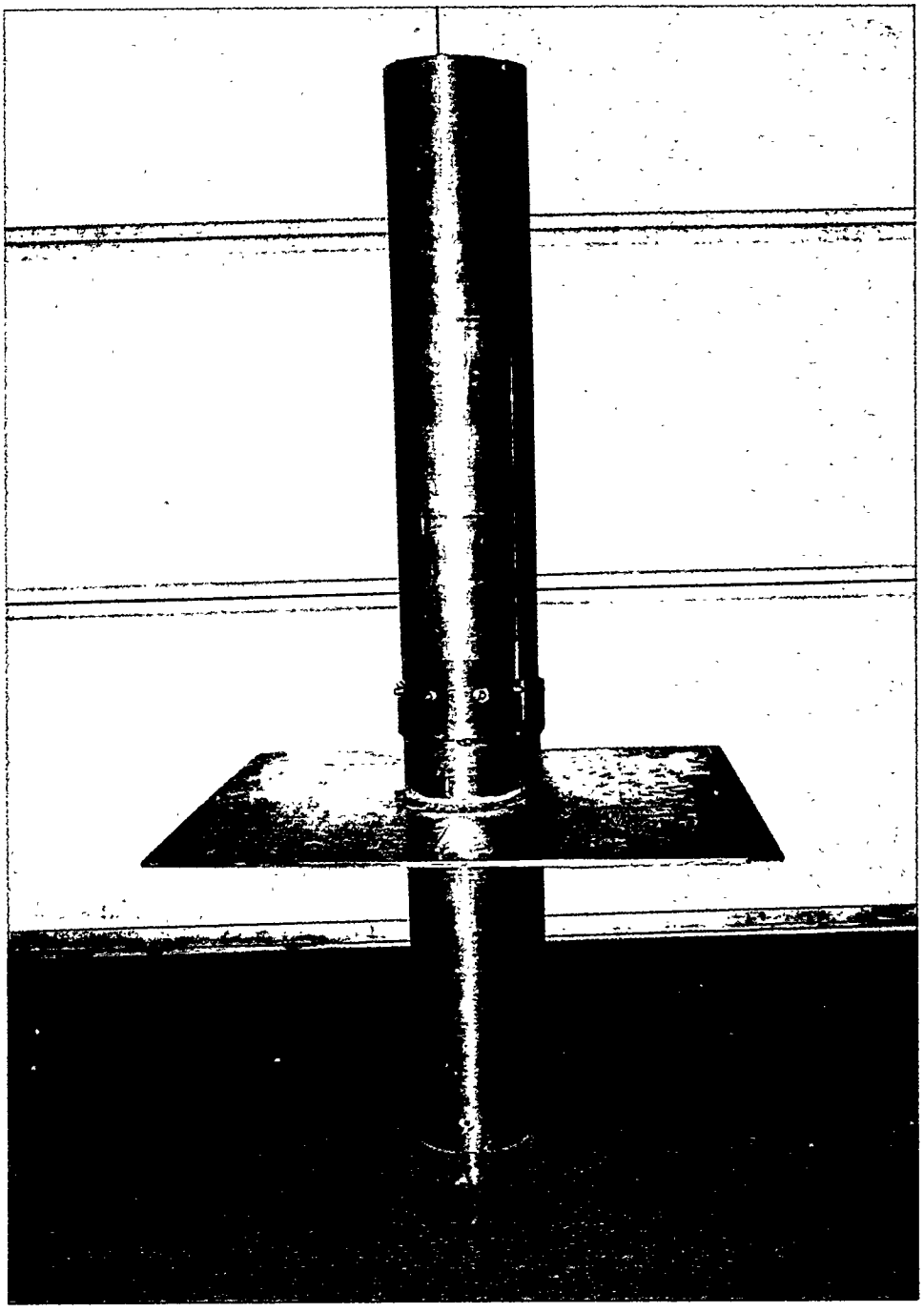

Bolted joint fixture

Figure 5. Photographs of monopole, slot, and bolted joint fixtures with accompanying cable, load, and bolt hardware (continued).

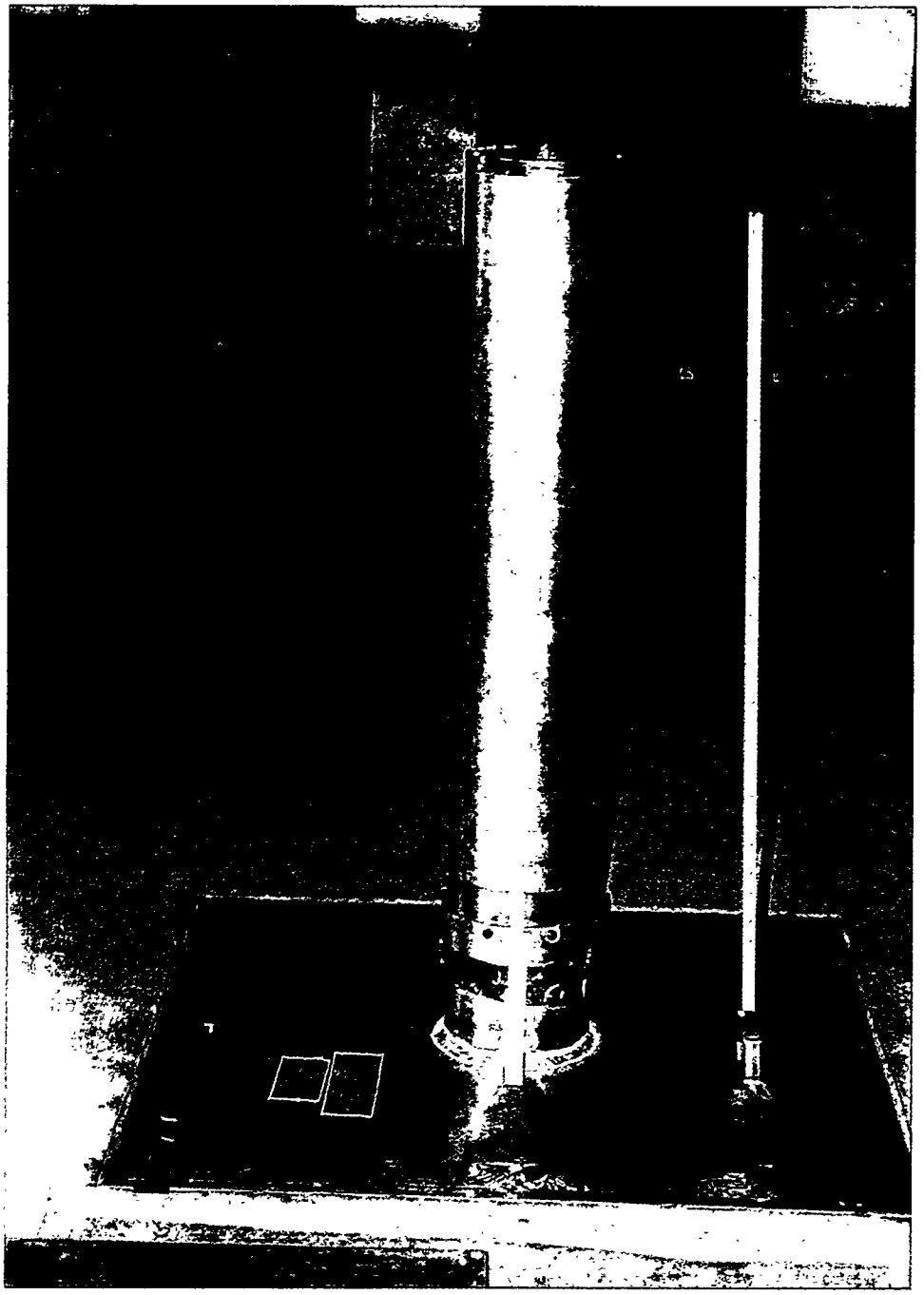

Bolted joint fixture in EMES

Figure 5. Photographs of monopole, slot, and bolted joint fixtures with accompanying cable, load, and bolt hardware (continued).

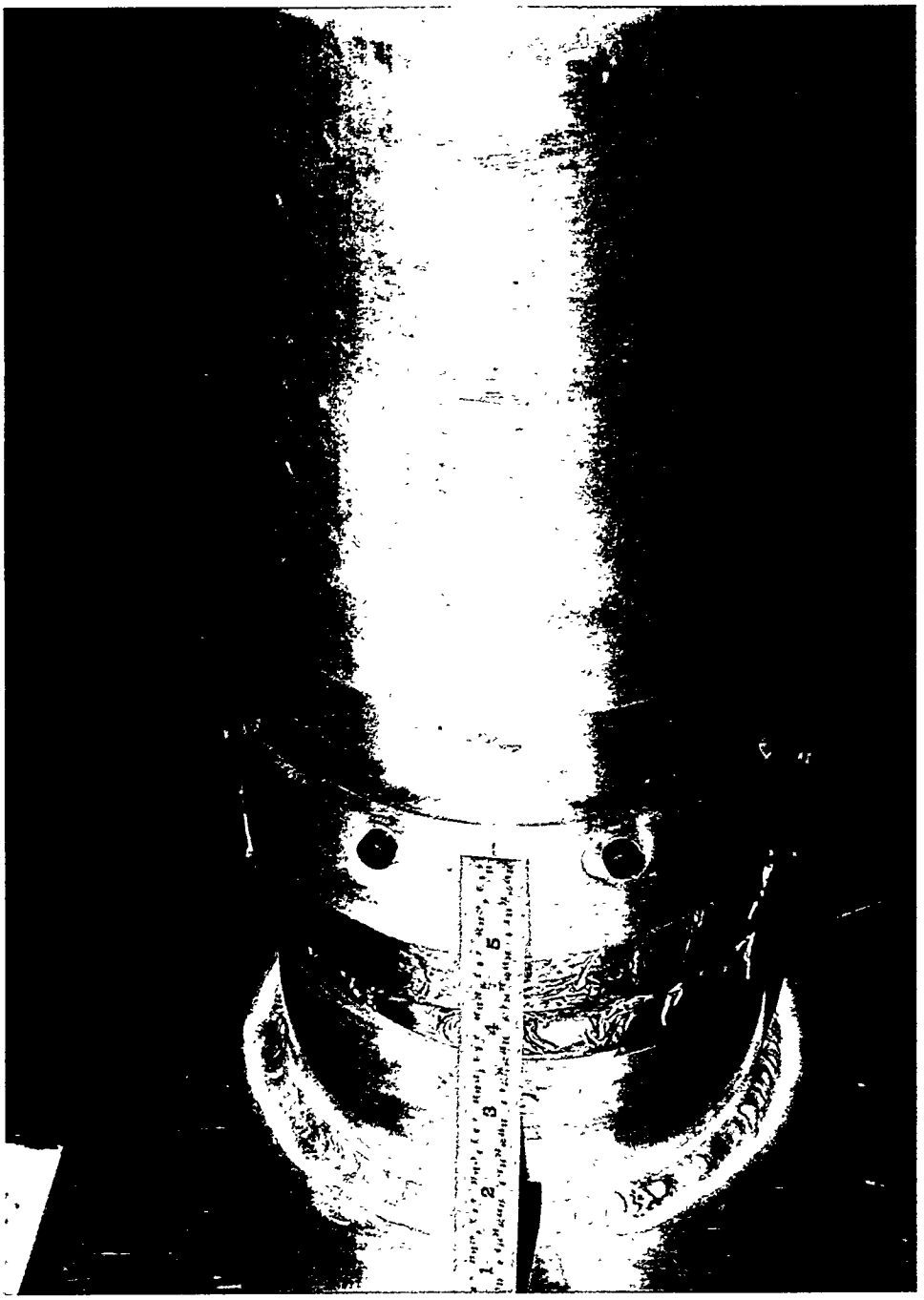

Bolted joint

Figure 5. Photographs of monopole, slot, and bolted joint fixtures with accompanying cable, load, and bolt hardware (continued).

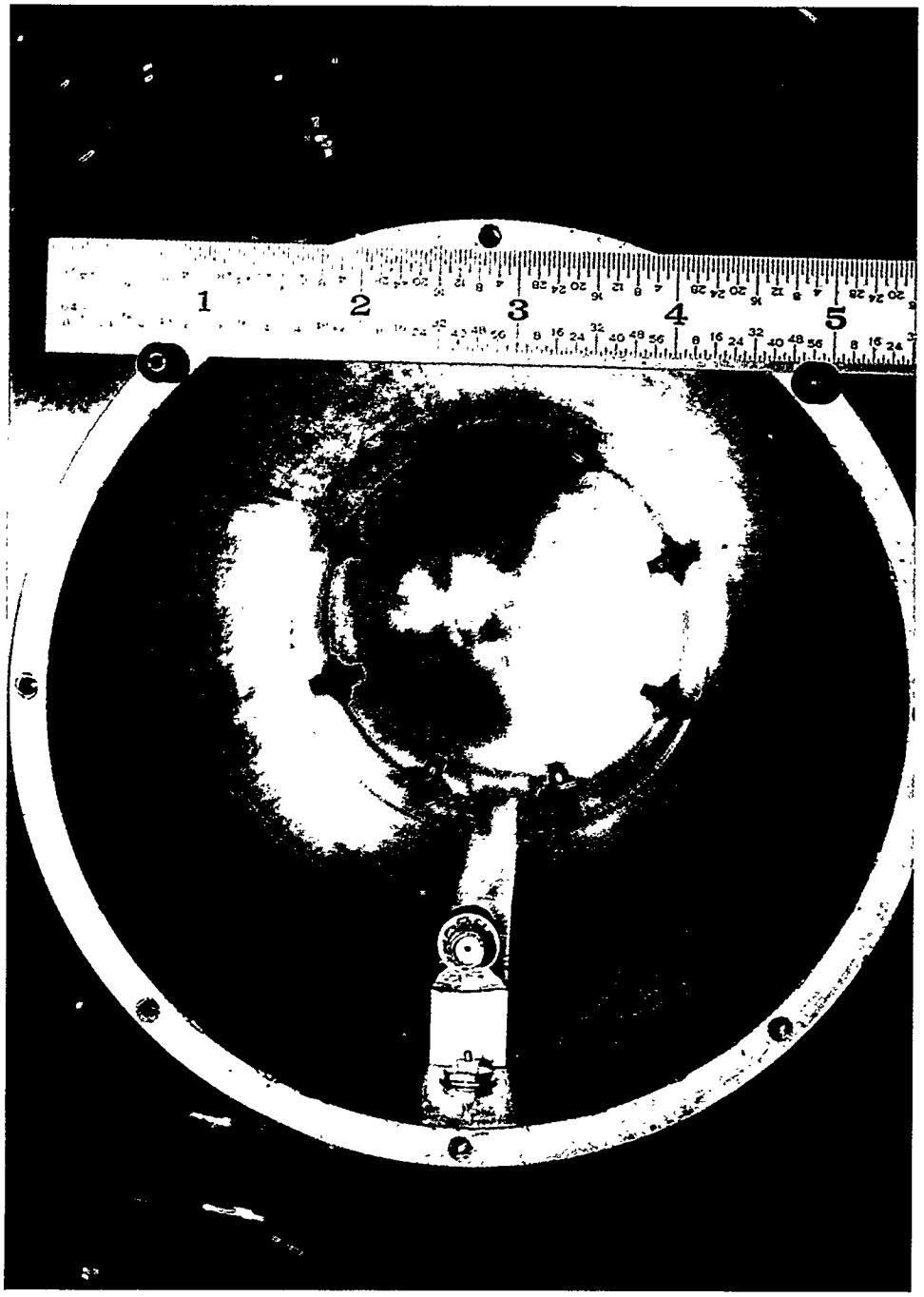

Tapered stripline in bolted joint fixture

Figure 5. Photographs of monopole, slot, and bolted joint fixtures with accompanying cable, load, and bolt hardware (continued).

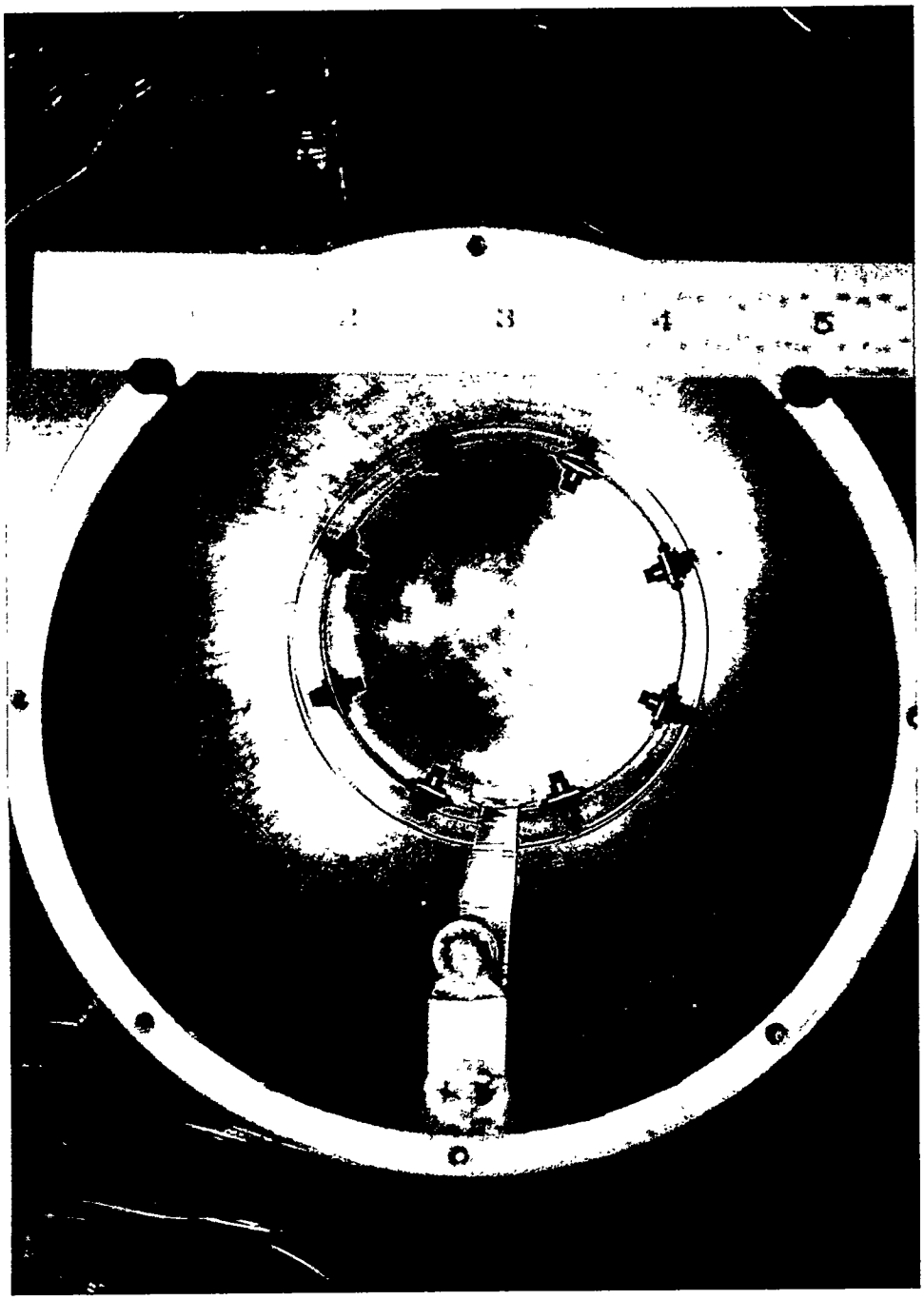

Tapered stripline in bolted joint fixture

Figure 5. Photographs of monopole, slot, and bolted joint fixtures with accompanying cable, load, and bolt hardware (continued).

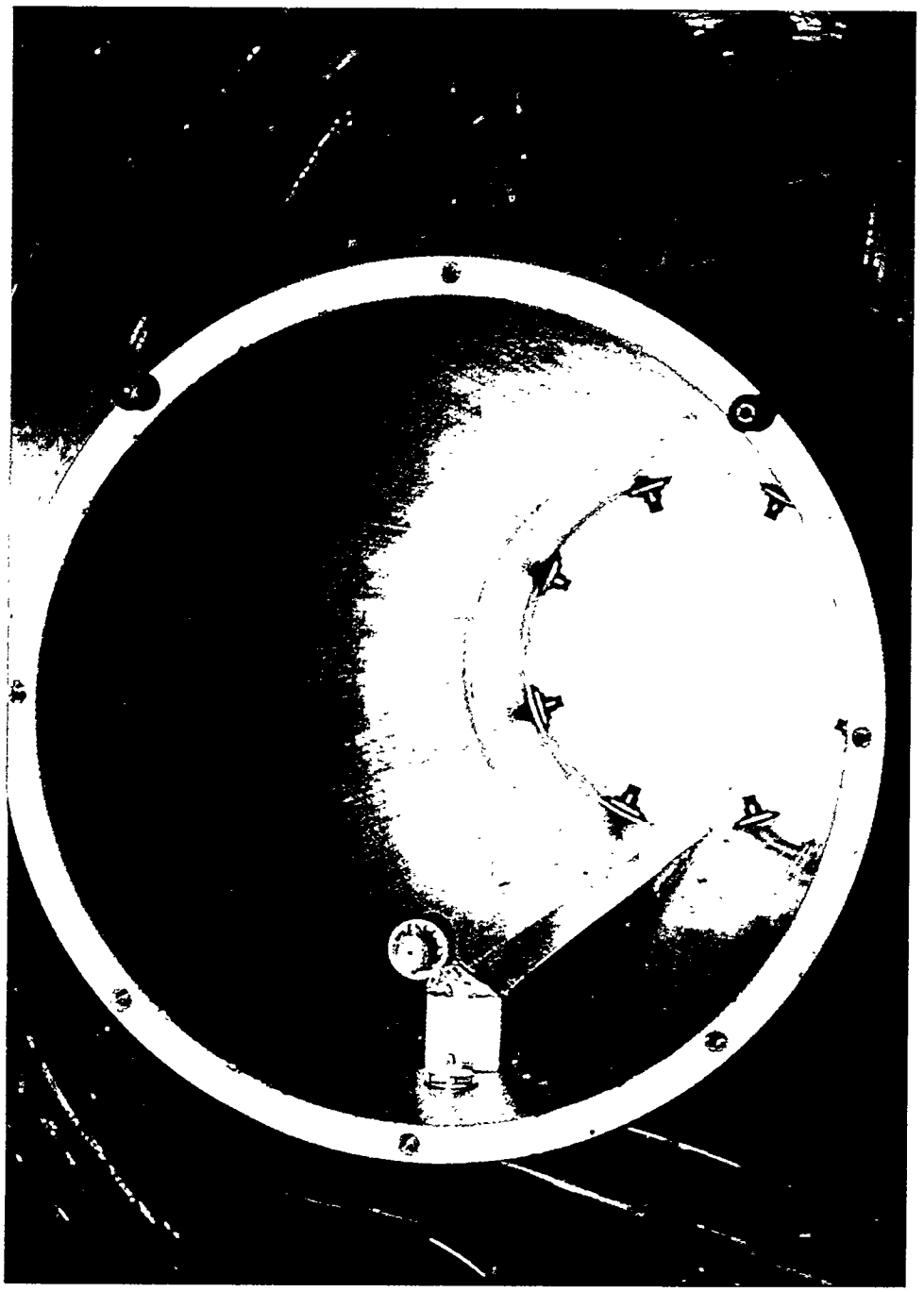

Tapered stripline in bolted joint fixture

Figure 5. Photographs of monopole, slot, and bolted joint fixtures with accompanying cable, load, and bolt hardware (continued).

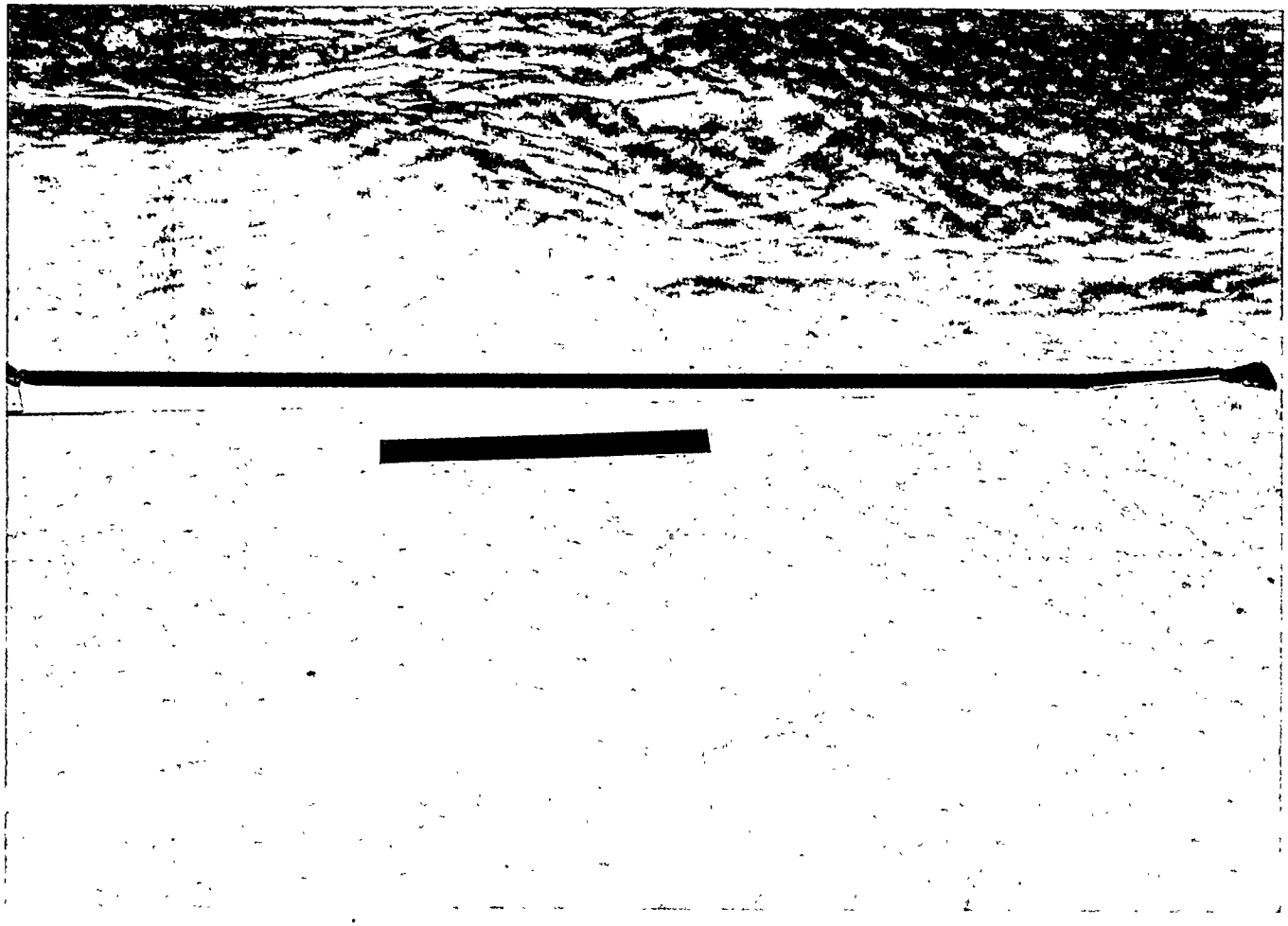

Tapered stripline

Figure 5. Photographs of monopole, slot, and bolted joint fixtures with accompanying cable, load, and bolt hardware (continued).

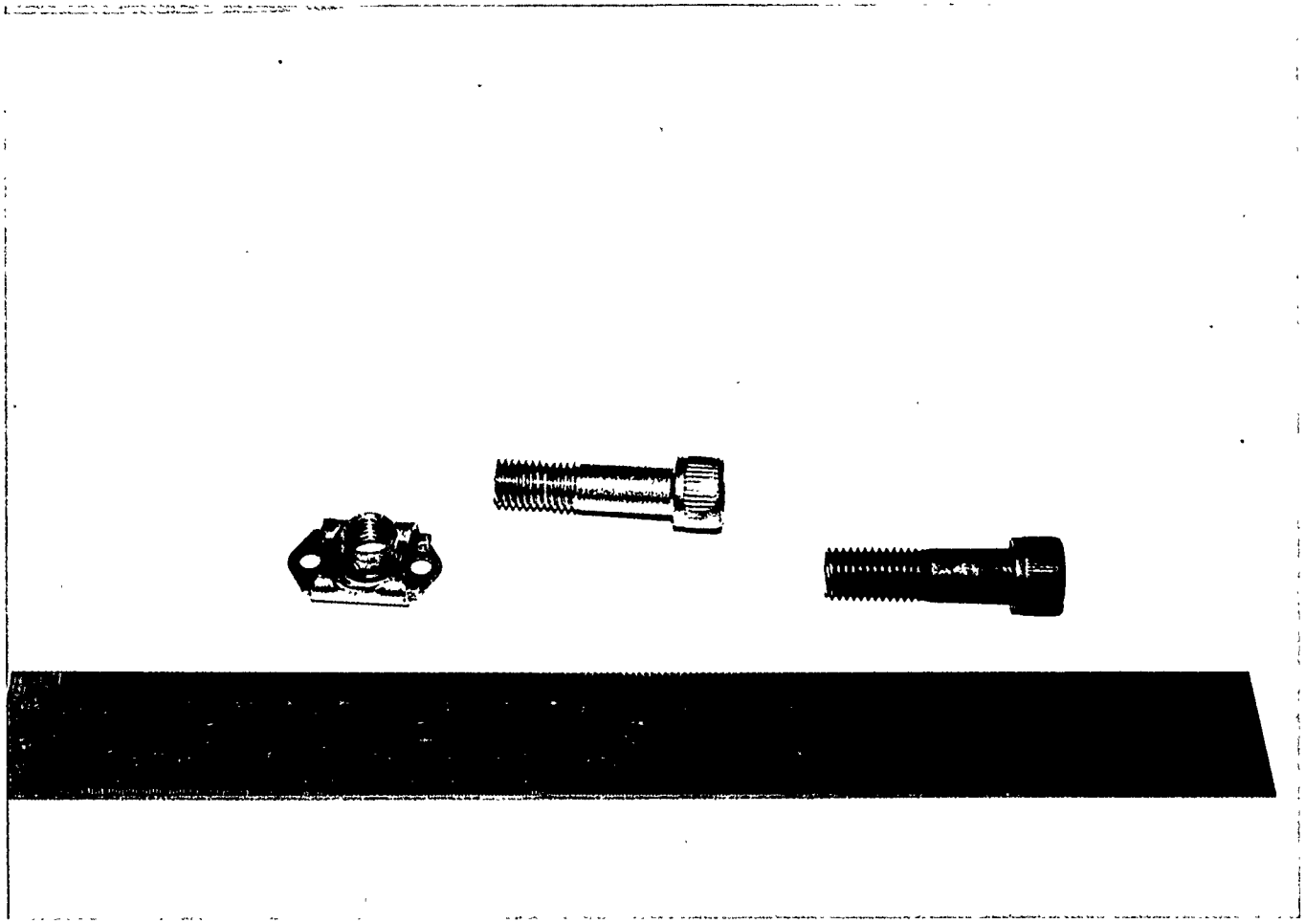

Stainless steel and ferrous steel bolts and nut plate

Figure 5. Photographs of monopole, slot, and bolted joint fixtures with accompanying cable, load, and bolt hardware (continued).

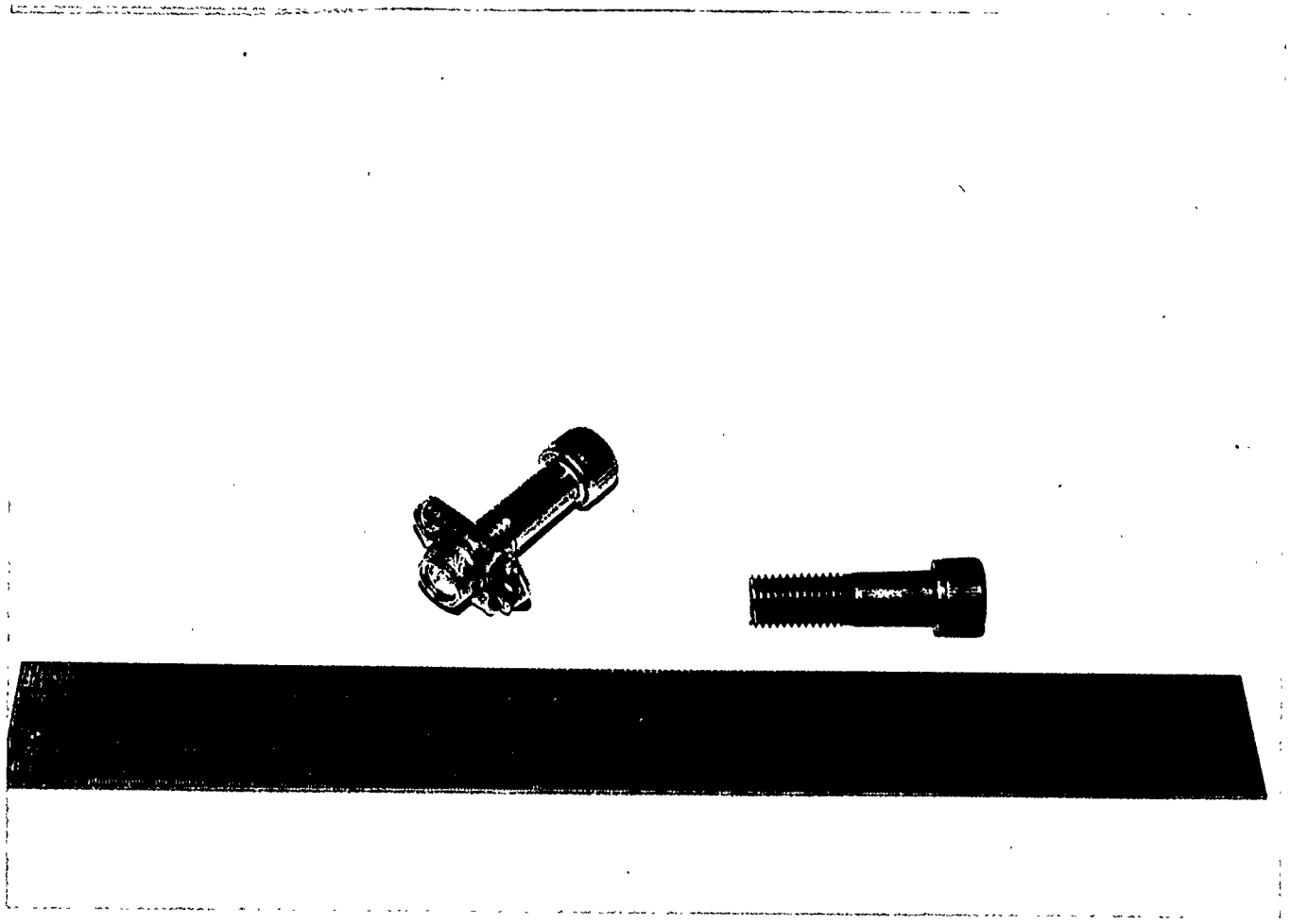

Stainless steel and ferrous steel bolts and nut plate

Figure 5. Photographs of monopole, slot, and bolted joint fixtures with accompanying cable, load, and bolt hardware (continued).

Cursor ..... 4.904 ft
Distance/Div..... 0.5 ft/div
Vertical Scale.... 500 mρ/div
Vp 0.78
Noise Filter..... 1 avg
Power..... ac

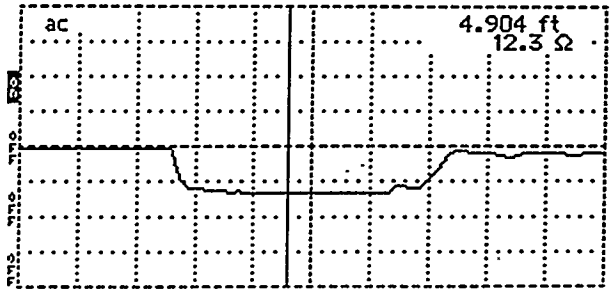

Tektronix 1502B TDR
Date Aug 24 1995
Cable COLLAR FIXTURE
Notes STRIP LINE NOT TERMINATED
Input Trace
Stored Trace
Difference Trace

(a)

Cursor ..... 4.904 ft
Distance/Div..... 0.5 ft/div
Vertical Scale.... 250 mρ/div
Vp 0.78
Noise Filter..... 16 avg
Power..... ac

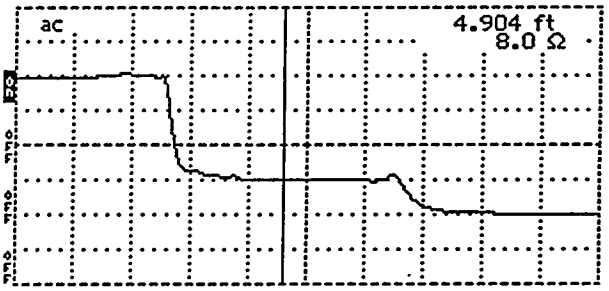

Tektronix 1502B TDR
Date Aug. 24, 1995
Cable COLLAR FIXTURE
Notes STRIP LINE TERMINATED
Input Trace
Stored Trace
Difference Trace

(b)

Cursor ..... 2.000 ftΔ
Distance/Div..... 0.5 ft/div
Vertical Scale.... 500 mρ/div
Vp 0.78
Noise Filter..... 16 avg
Power..... ac

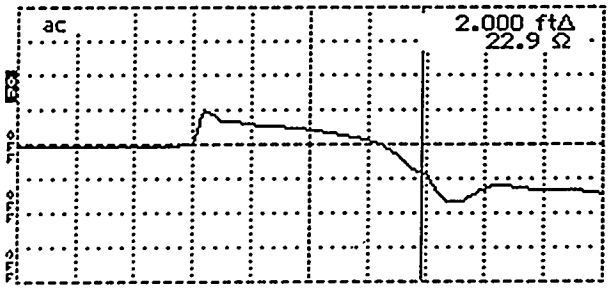

Tektronix 1502B TDR
Date 8/25/95
Cable SMT FIXTURE
Notes TAPERED STRIP LINE NO SERIES TERM RESISTOR
Input Trace
Stored Trace
Difference Trace

(c)

Figure 6. Time Domain Reflectometer (TDR) plots of stripline reflection coefficients (characteristic impedance at various locations along the cables is noted.

Cursor ..... 0.420 ftΔ
Distance/Div..... 0.5 ft/div
Vertical Scale.... 500 mΩ/div
VP 0.78
Noise Filter..... 16 avg
Power..... ac

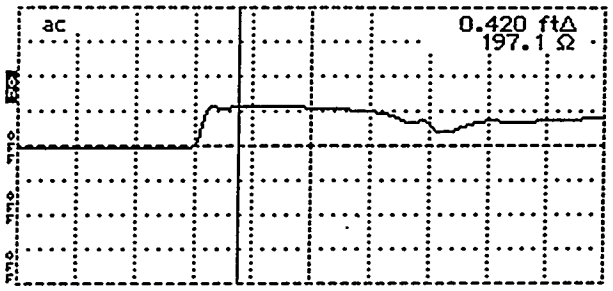

Tektronix 1502B TDR
Date 8/25/95
Cable SLOT FIXTURE
Notes TAPERED STRIP LINE
120Ω SERIES RESISTOR
(170Ω TERMINATION
Input Trace
Stored Trace
Difference Trace

(d)

Cursor ..... 5.020 ft
Distance/Div..... 0.5 ft/div
Vertical Scale.... 250 mΩ/div
VP 0.78
Noise Filter..... 16 avg
Power..... ac

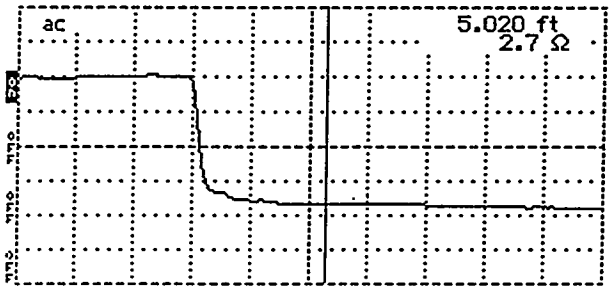

Tektronix 1502B TDR
Date 8/30/95
Cable COLLAR FIXTURE
Notes STRIP LINE, 0.625"
6 - 10Ω TERMINATION
(1.67Ω)
Input Trace
Stored Trace
Difference Trace

(e)

Cursor ..... 5.460 ft
Distance/Div..... 0.5 ft/div
Vertical Scale.... 250 mΩ/div
VP 0.78
Noise Filter..... 16 avg
Power..... ac

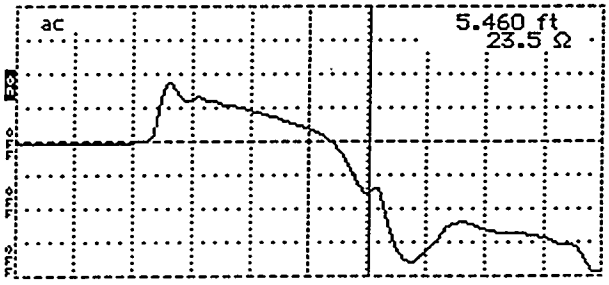

Tektronix 1502B TDR
Date SEPT 1 95
Cable COLLAR FIXTURE
Notes TAPERED STRIP
LINE - NO SERIES TERMINATION
Input Trace
Stored Trace
Difference Trace

(f)

Figure 6. Time Domain Reflectometer (TDR) plots of stripline reflection coefficients (characteristic impedance at various locations along the cables is noted (continued).

Cursor ..... 3.980 ft
Distance/Div..... 0.5 ft/div
Vertical Scale.... 250 mΩ/div
VP 0.78
Noise Filter..... 16 avg
Power..... ac

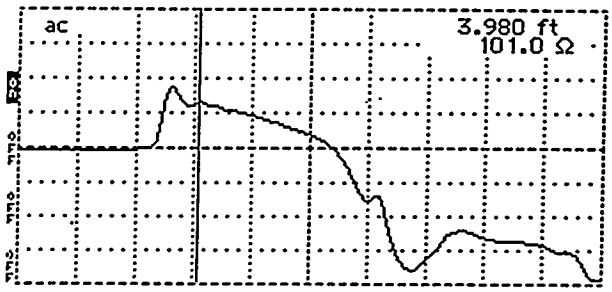

Tektronix 1502B TDR
Date SEPT 1 95
Cable COLLAR FIXTURE
Notes TAPERED STRIP LINE - NO SERIES TERMINATION
Input Trace
Stored Trace
Difference Trace

(g)

Cursor ..... 6.260 ft
Distance/Div..... 0.5 ft/div
Vertical Scale.... 486 mΩ/div
VP 0.78
Noise Filter..... 16 avg
Power..... ac

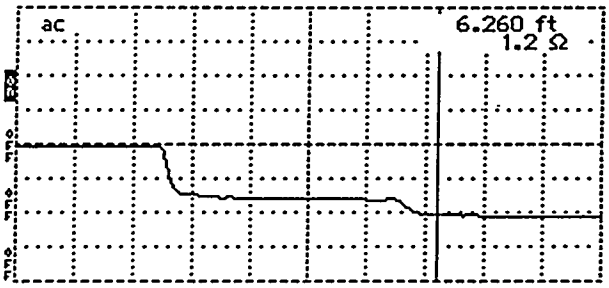

Tektronix 1502B TDR
Date SEPT 5 95
Cable SLOT FIXTURE
Notes STRIP LINE TERMINATION 12.5Ω
Input Trace
Stored Trace
Difference Trace

(h)

Cursor ..... 5.000 ft
Distance/Div..... 0.5 ft/div
Vertical Scale.... 486 mΩ/div
VP 0.78
Noise Filter..... 16 avg
Power..... ac

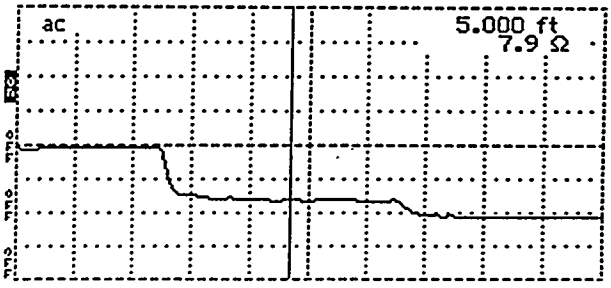

Tektronix 1502B TDR
Date SEPT 5 95
Cable SLOT FIXTURE
Notes STRIP LINE 12.5Ω TERMINATION
Input Trace
Stored Trace
Difference Trace

(i)

Figure 6. Time Domain Reflectometer (TDR) plots of stripline reflection coefficients (characteristic impedance at various locations along the cables is noted (continued).

Cursor ..... 4.880 ft
Distance/Div..... 0.5 ft/div
Vertical Scale.... 500 mΩ/div
Vp 0.78
Noise Filter..... 16 avg
Power..... ac

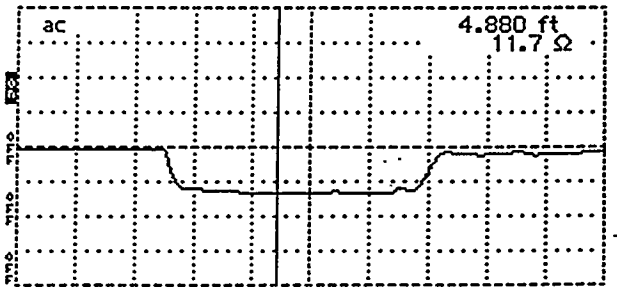

Tektronix 1502B TDR
Date SEPT 5, 95
Cable SLOT FIXTURE
Notes ~~LONG~~ STRIP LINE
NO TERMINATION
Input Trace
Stored Trace
Difference Trace

(j)

Cursor ..... 4.820 ft
Distance/Div..... 0.5 ft/div
Vertical Scale.... 500 mΩ/div
Vp 0.78
Noise Filter..... 16 avg
Power..... ac

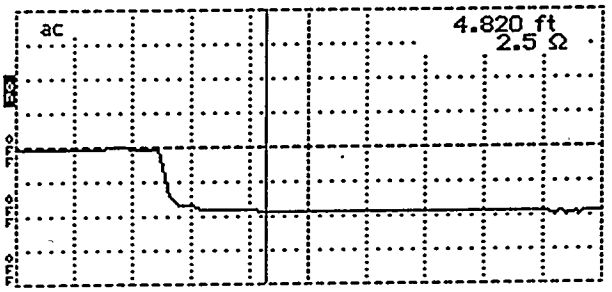

Tektronix 1502B TDR
Date SEPT 6 95
Cable SLOT FIXTURE
Notes STRIP LINE
162Ω TERMINATION
Input Trace
Stored Trace
Difference Trace

(k)

Figure 6. Time Domain Reflectometer (TDR) plots of stripline reflection coefficients (characteristic impedance at various locations along the cables is noted (continued).

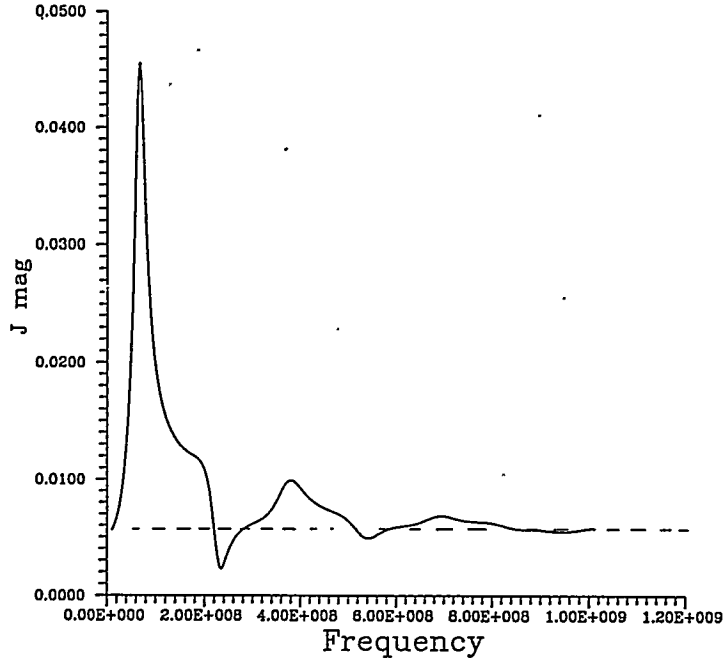

(a) total aximuthal surface magnetic field at the center of the cylinder, at the point facing the incoming plane wave direction (low and high frequency limits are twice the incident magnetic field)

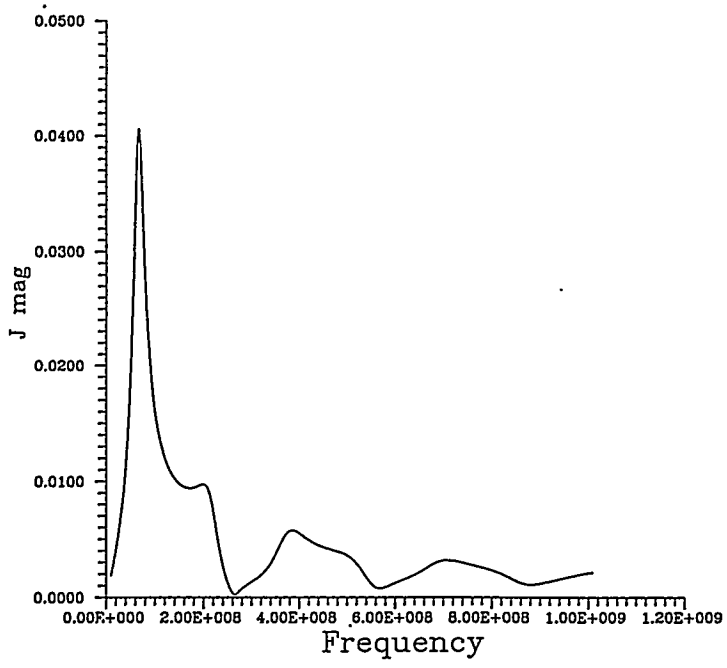

(b) the $n = 0$ symmetric surface current mode amplitude

Figure 7. Surface currents on a conducting cylinder with 6-inch diameter and 6-foot length (except d) excited by a unit amplitude (electric field) axially polarized incident wave.

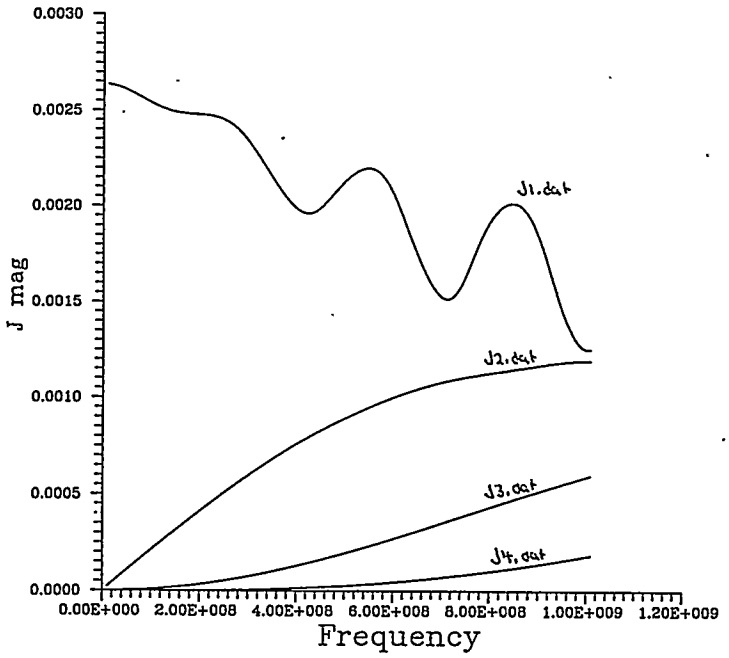

(c) $n = 1$ through $n = 4$ asymmetric surface current modal amplitudes

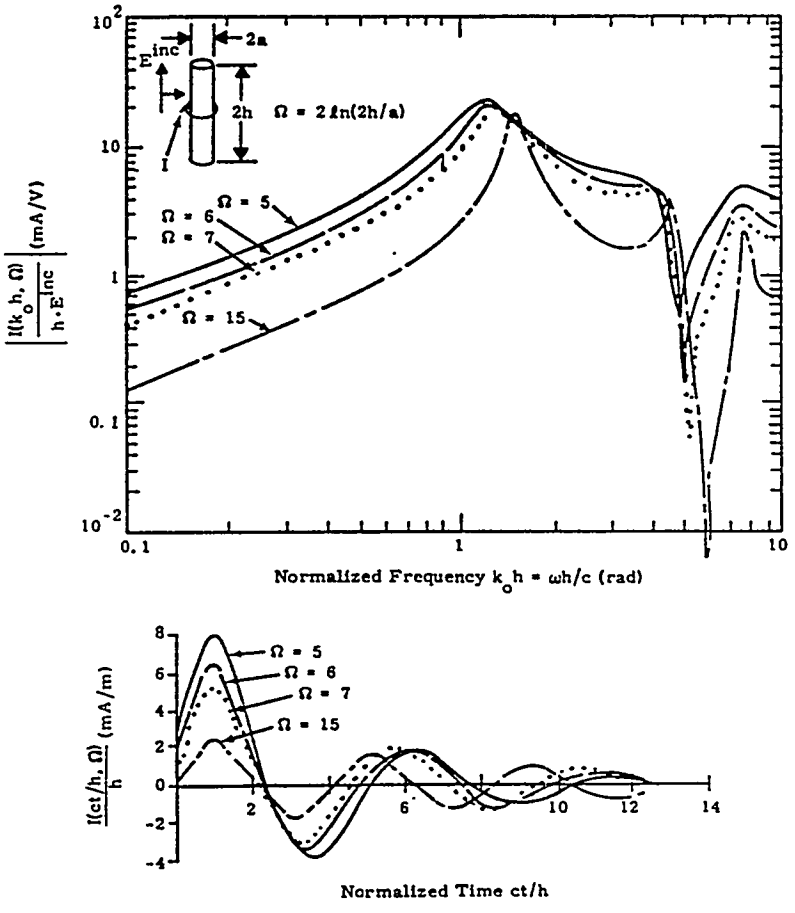

(d) total cylinder current in the frequency domain and the total current step function response (from [6])

Figure 7. Surface currents on a conducting cylinder with 6-inch diameter and 6-foot length (except d) excited by a unit amplitude (electric field) axially polarized incident wave (continued).

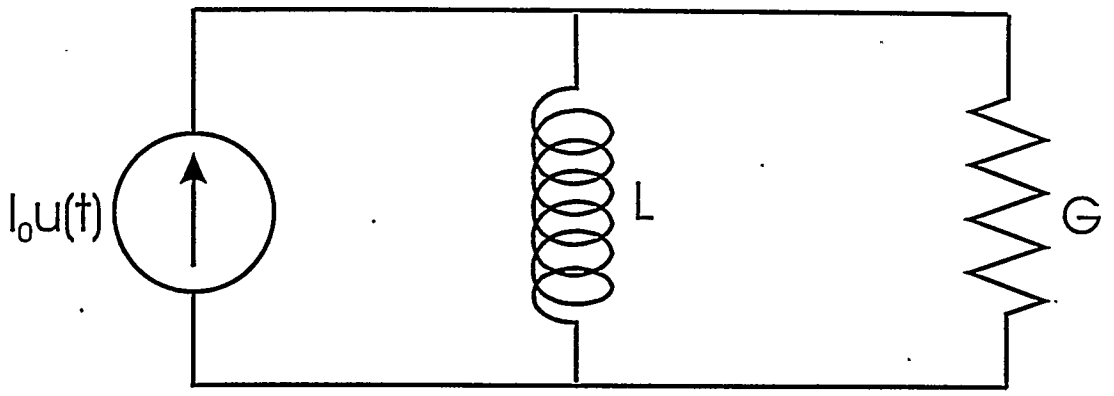

.Figure 8. Simple inductor-conductor circuit excited by step function current source.

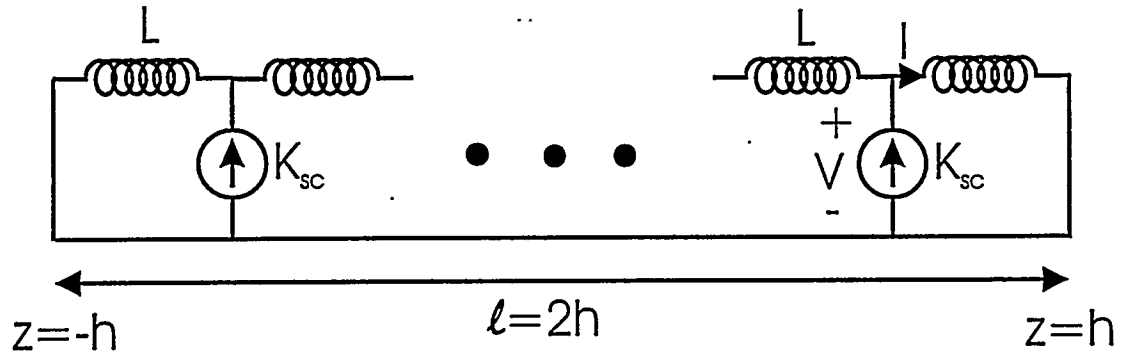

Figure 9. Low-frequency inductive transmission line model of slot aperture driven by distributed short circuit current sources.

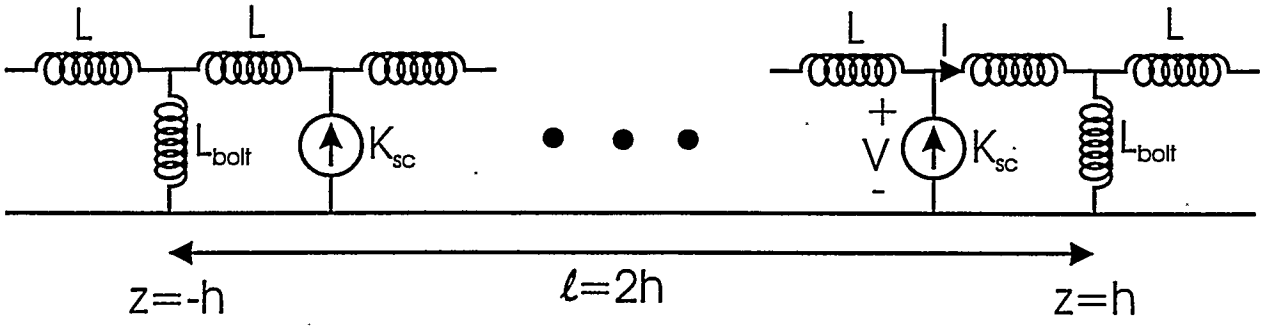

Figure 10. Low-frequency transmission line model of bolted joint aperture driven by short circuit current sources (if the current sources are symmetrical, symmetry planes can be introduced through the center of each bolt inductor to isolate a single bolted slot aperture).

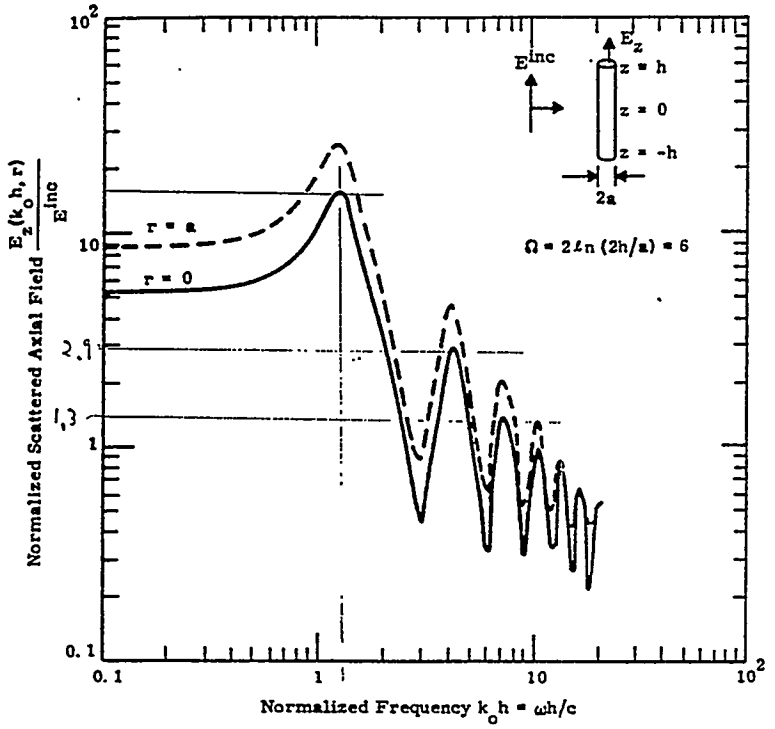

(a) normal electric field, in the frequency domain, for unit amplitude axially polarized incident plane wave

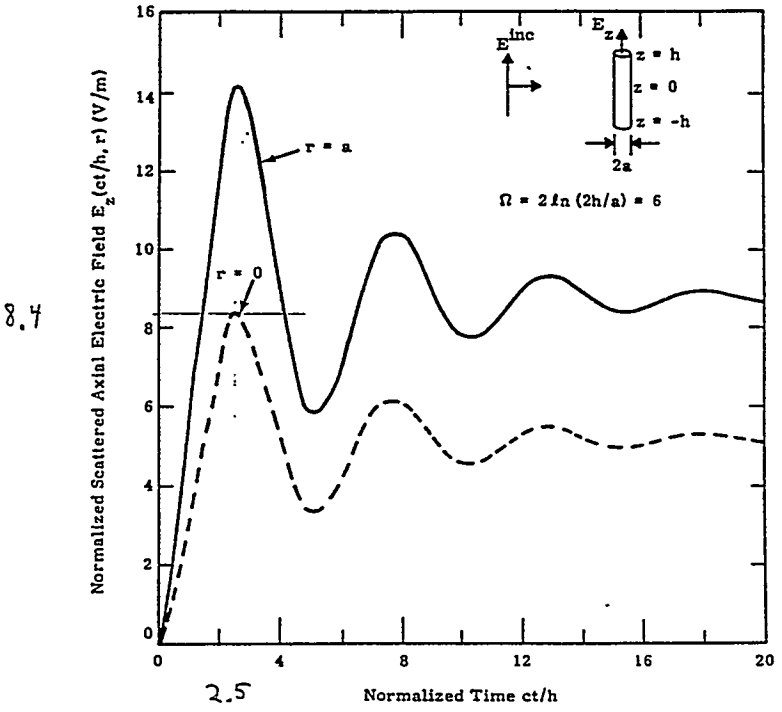

(b) normal electric field resulting from a unit step axially polarized incident plane wave

Figure 11. The normal surface electric field at the end of a conducting cylinder with ten-to-one aspect ratio (from [6]).

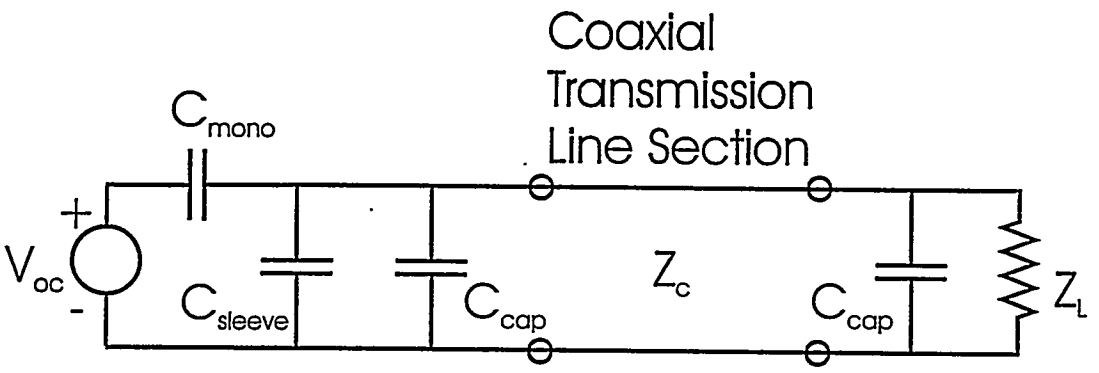

Figure 12. Low-frequency monopole fixture equivalent circuit model.

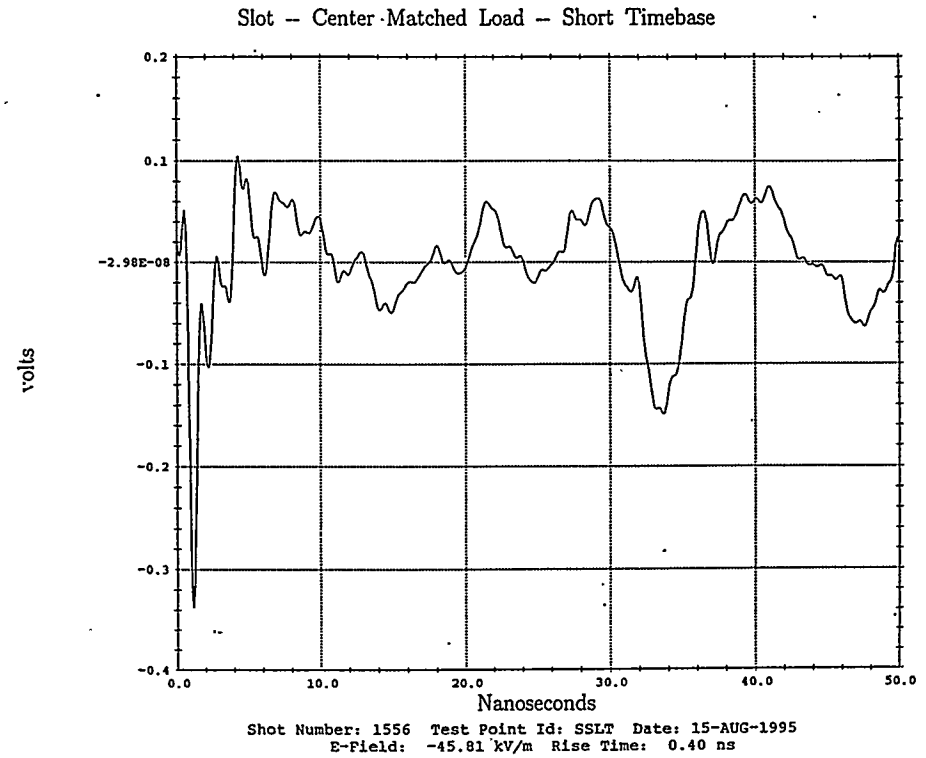

(a) voltage waveform into 50-ohm measurement system

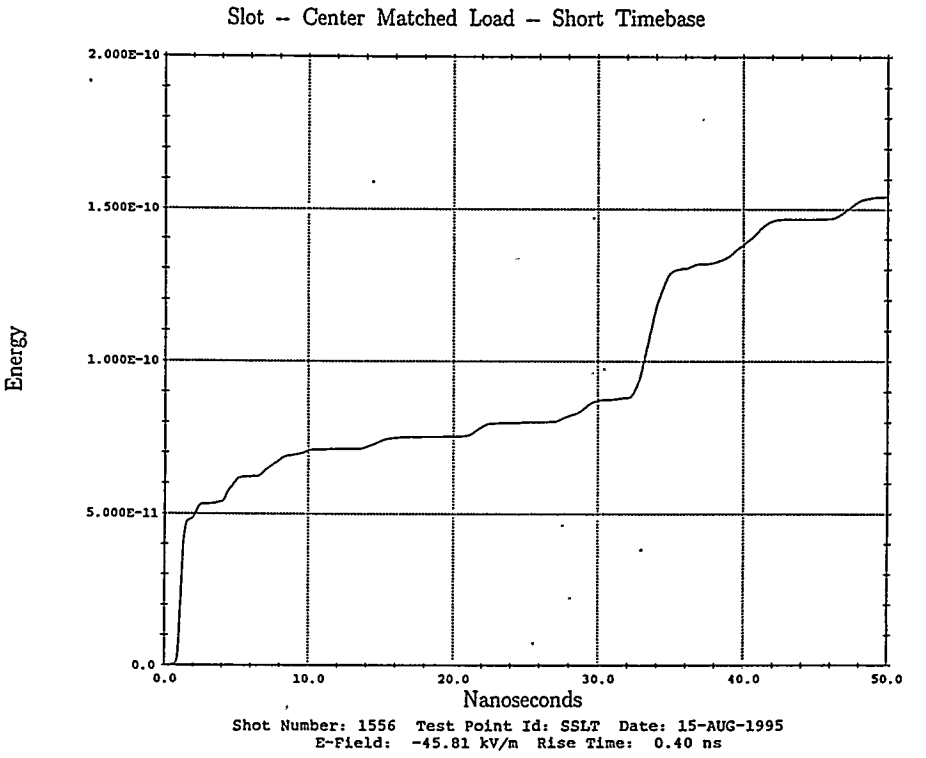

(b) integral of the square of the output voltage

Figure 13. Measured output for slot fixture with center wire and matched (200-ohm) load.

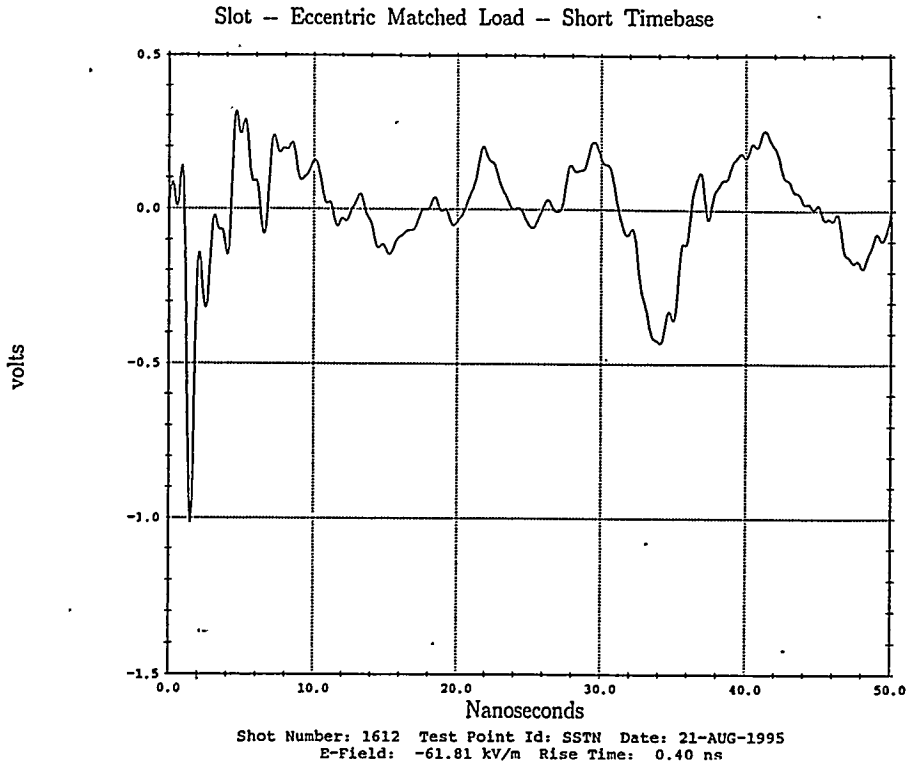

(a) voltage waveform into 50-ohm measurement system

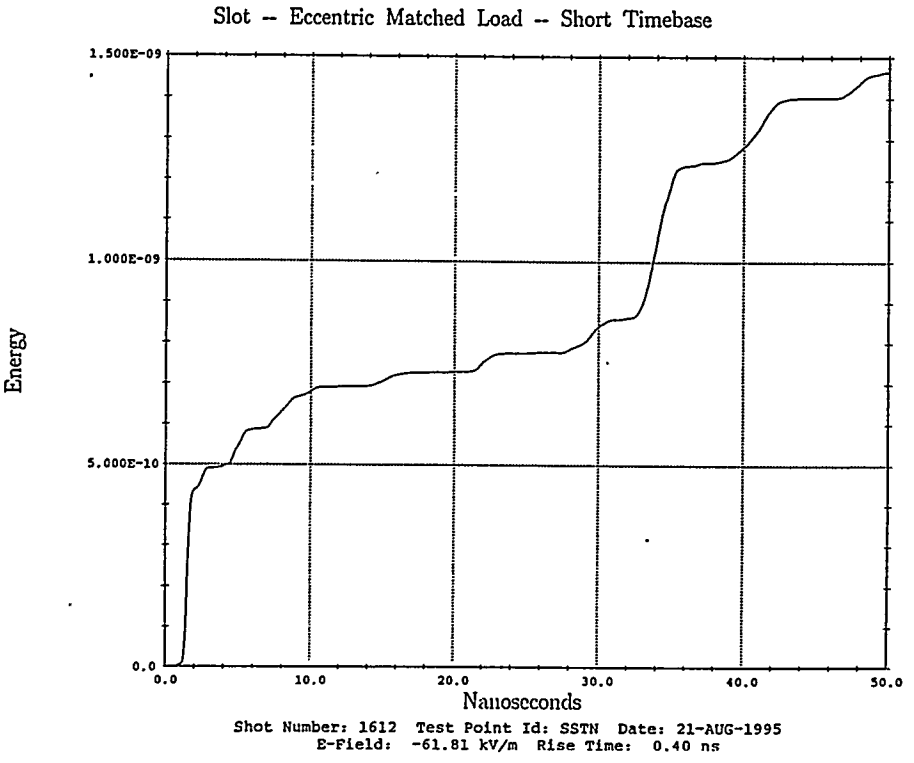

(b) integral of the square of the output voltage

Figure 14. Measured output for slot fixture with eccentric wire and matched (170 ohm) load.

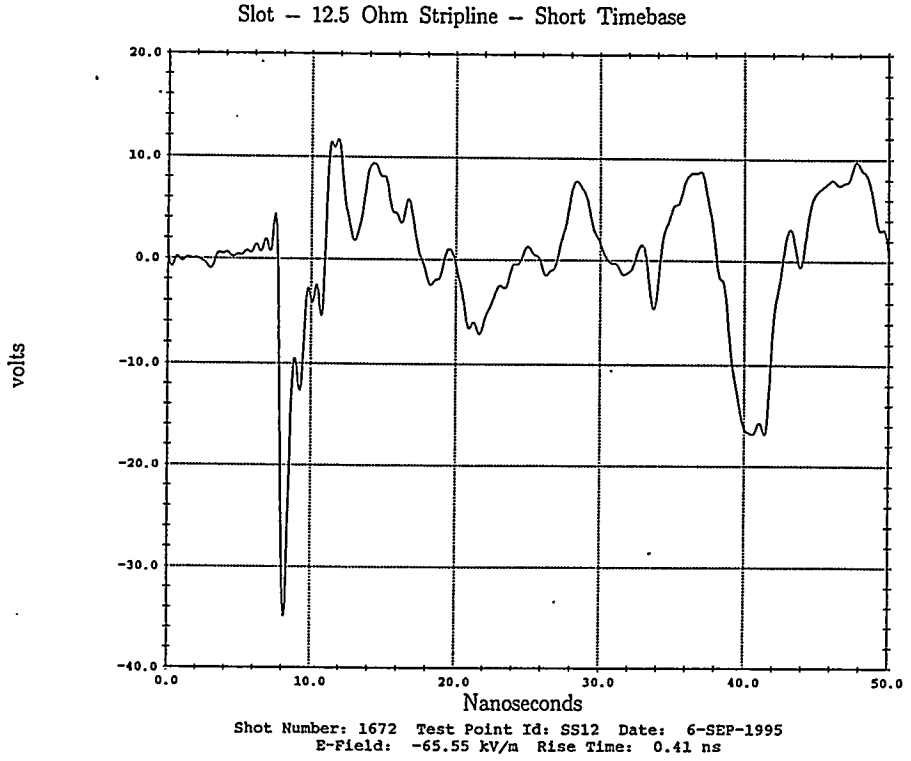

(a) voltage waveform

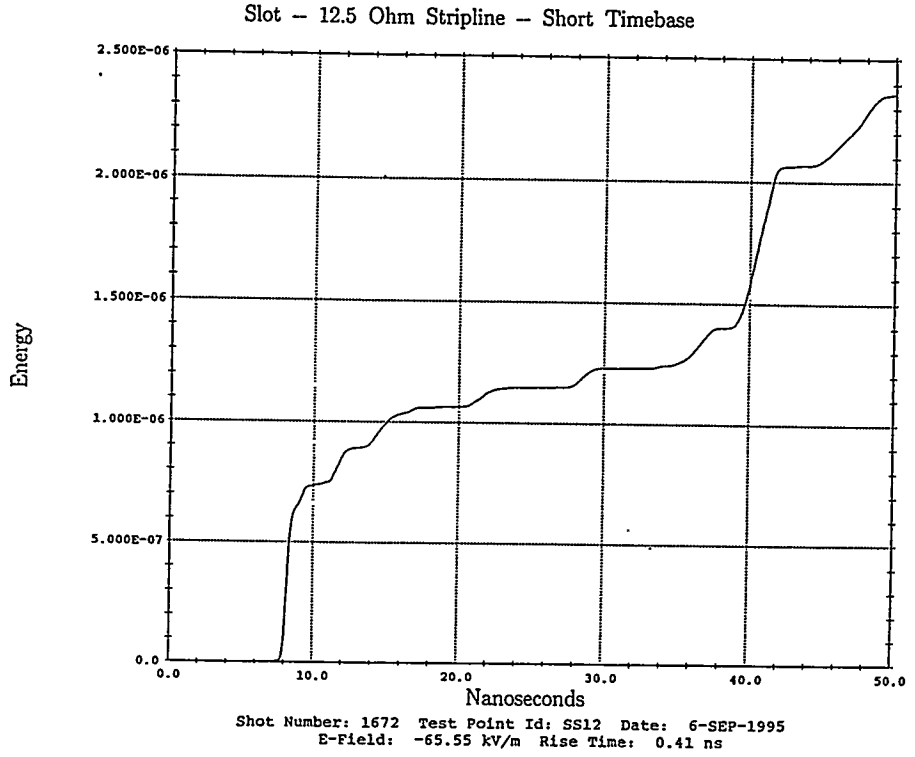

(b) integral of the square of the output voltage

Figure 15. Measured output for slot fixture with stripline cable and matched (12.5 ohm) load.

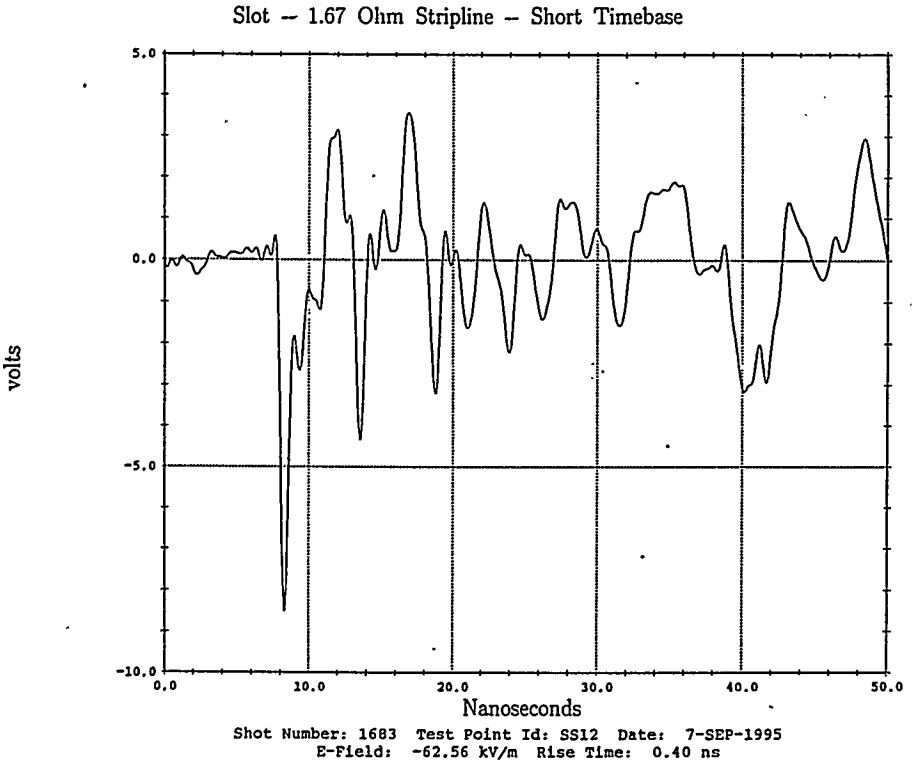

(a) voltage waveform

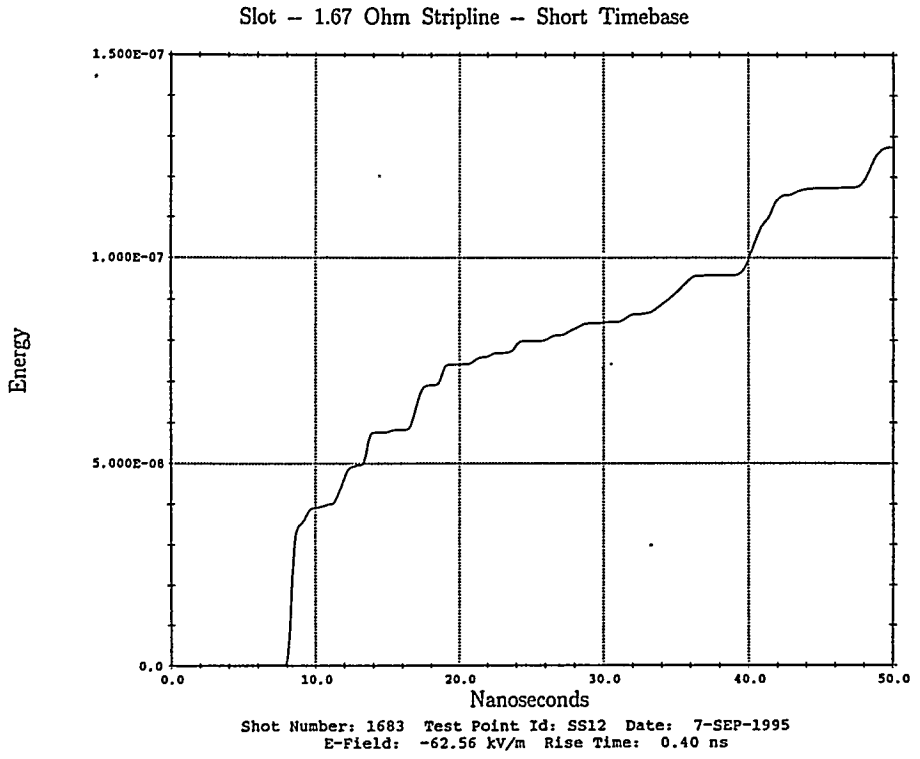

(b) integral of the square of the output voltage

Figure 16. Measured output for slot fixture with stripline cable and low impedance (1.67 ohm) load.

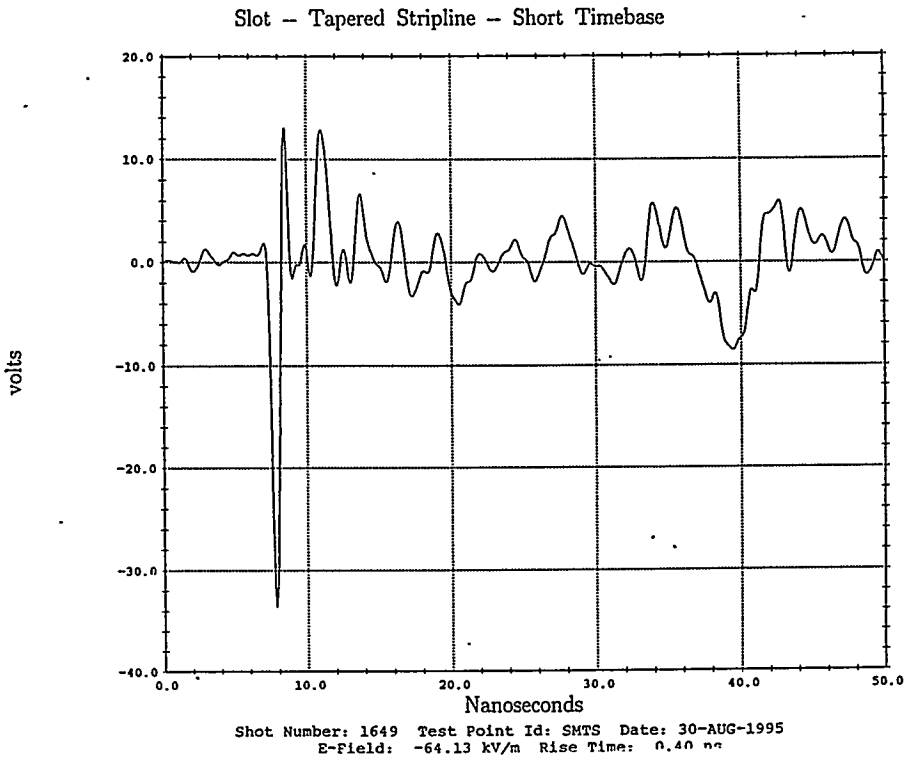

(a) voltage waveform

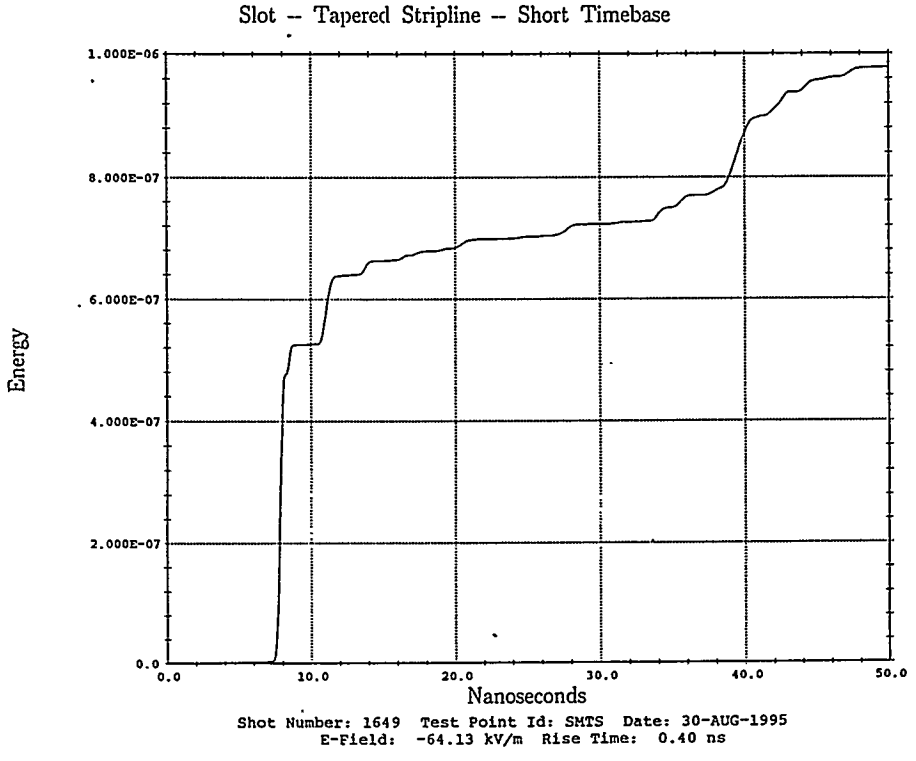

(b) integral of the square of the output voltage

Figure 17. Measured output for slot fixture with tapered stripline cable and matched (170 ohm) load.

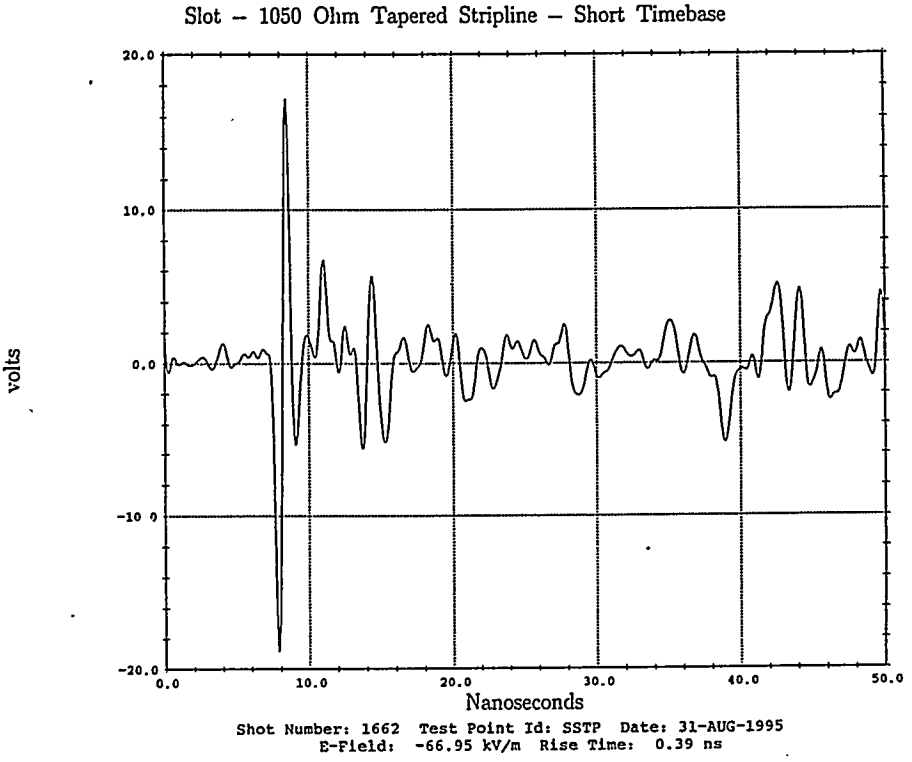

Figure 18. Measured output voltage (into 50-ohm measurement system) for slot fixture with high impedance load (nominal 1050 ohm, but parasitic capacitance lowers value).

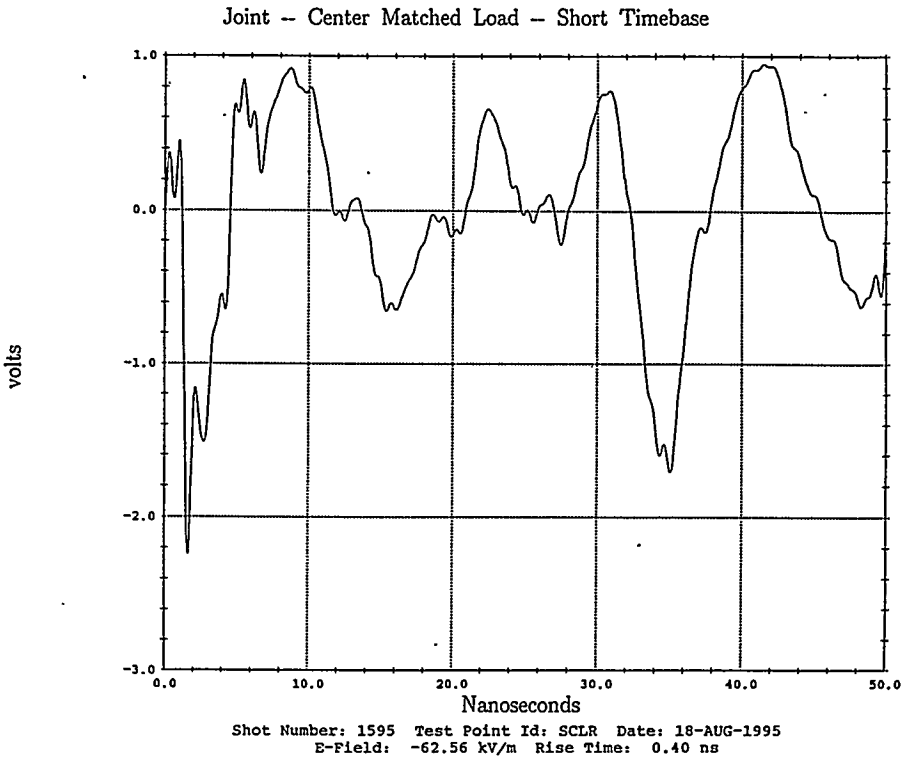

(a) voltage waveform into 50-ohm measurement system

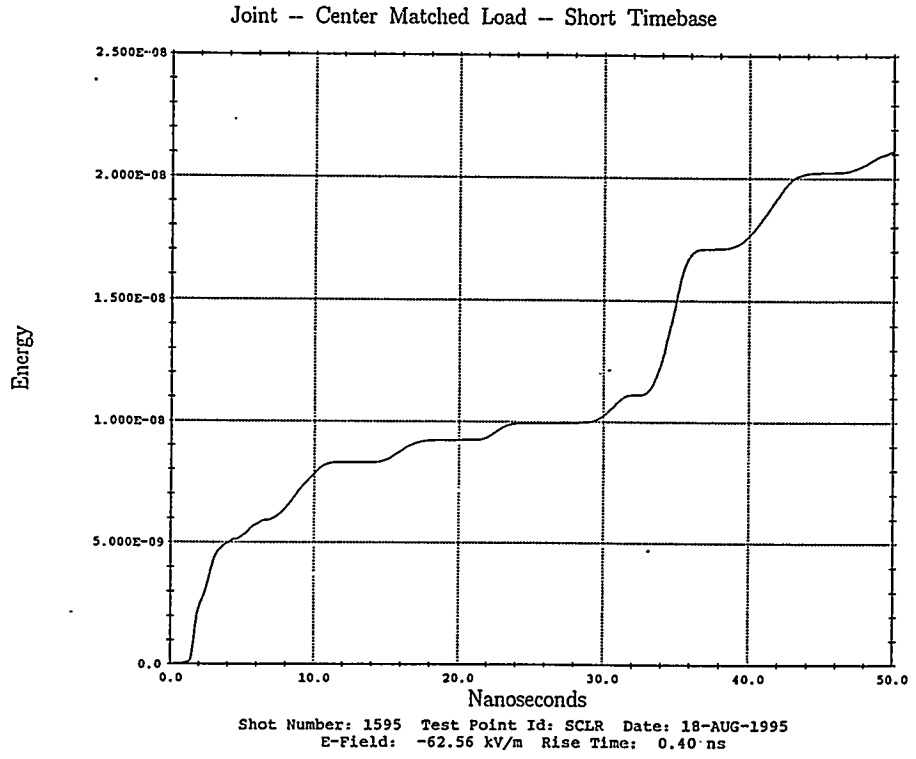

(b) integral of the square of the output voltage

Figure 19. Measured output for bolted joint fixture with center wire and matched (200 ohm) load.

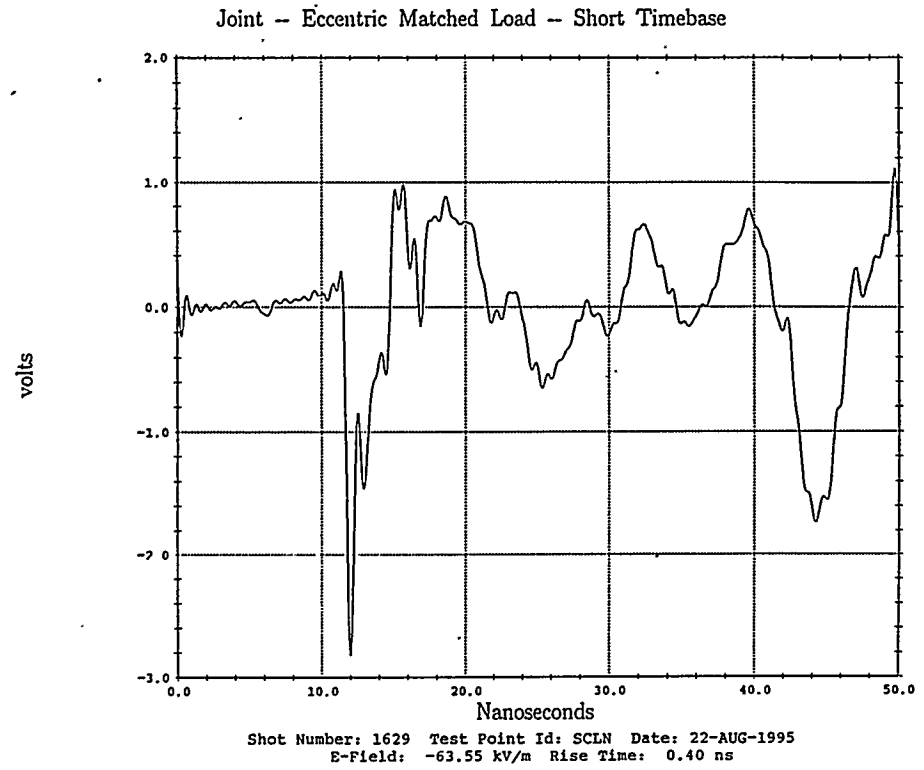

(a) voltage waveform into 50-ohm measurement system

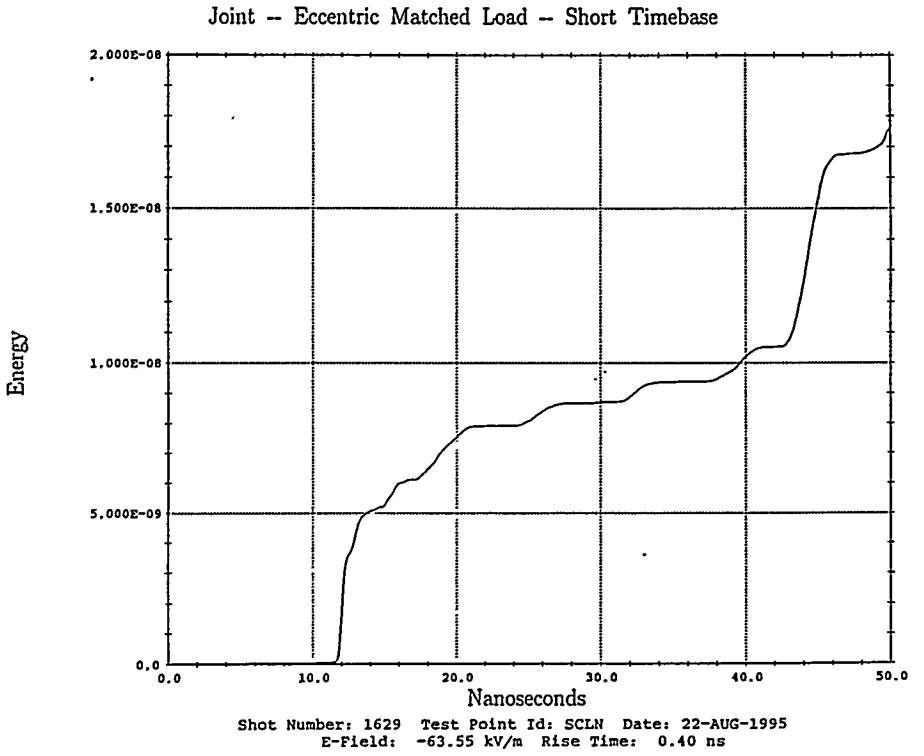

(b) integral of the square of the output voltage

Figure 20. Measured output for bolted joint fixture with eccentric wire and matched (170 ohm) load.

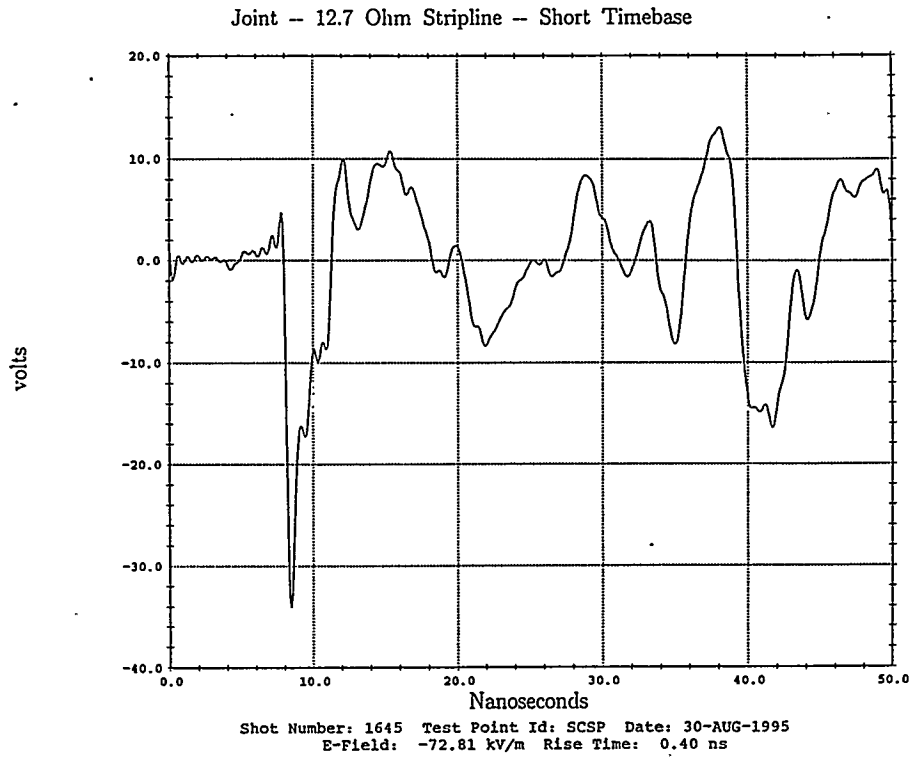

(a) voltage waveform

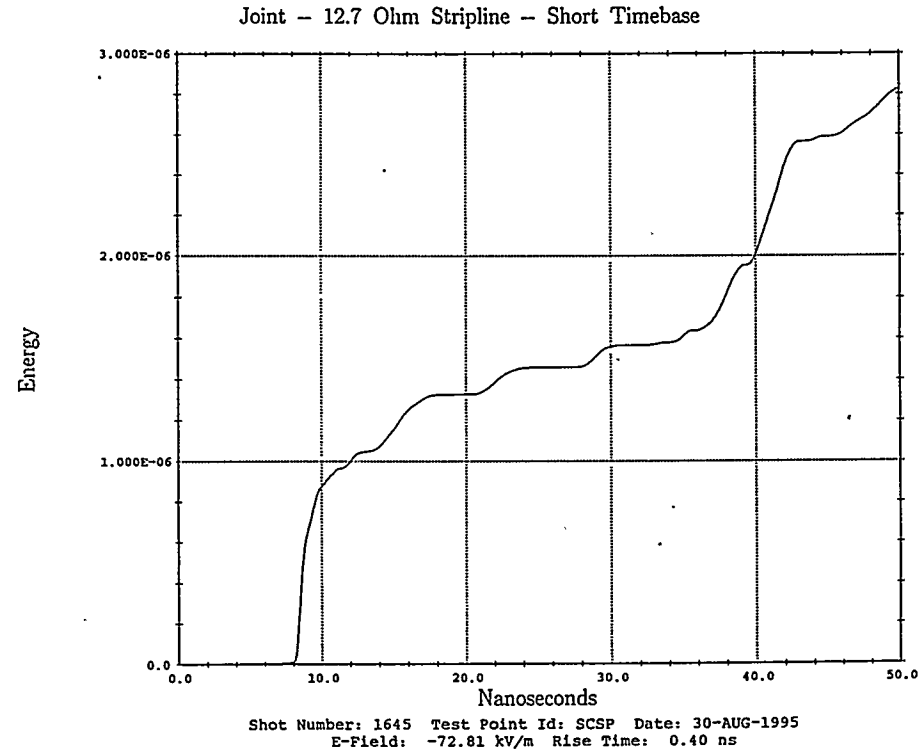

(b) integral of the square of the output voltage

Figure 21. Measured output for bolted joint fixture with stripline cable and matched (12.5 ohm) load.

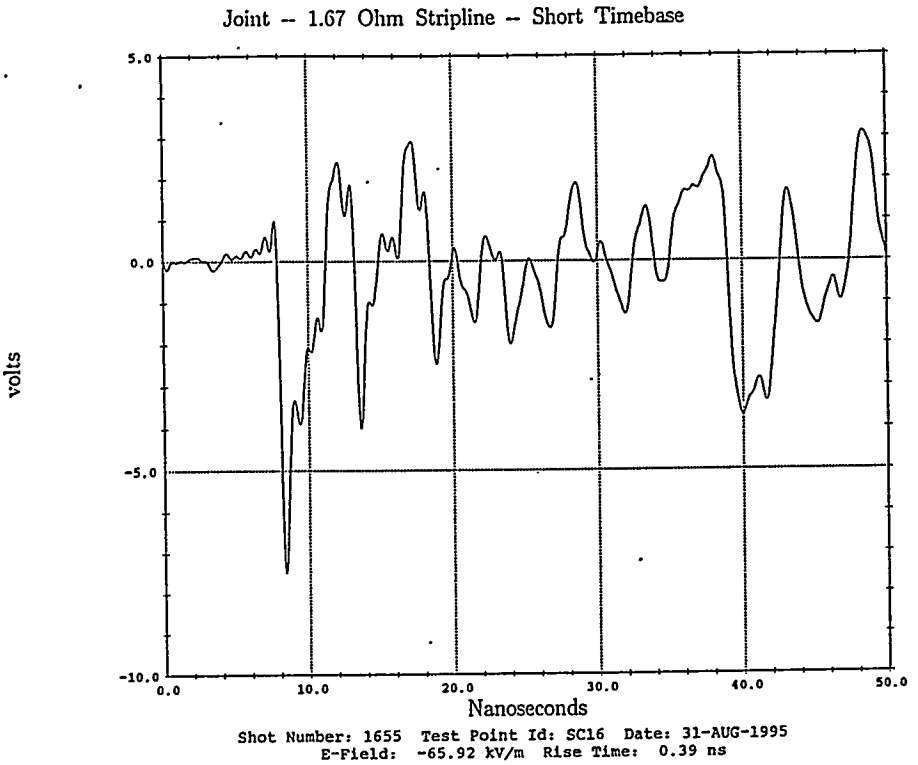

(a) voltage waveform

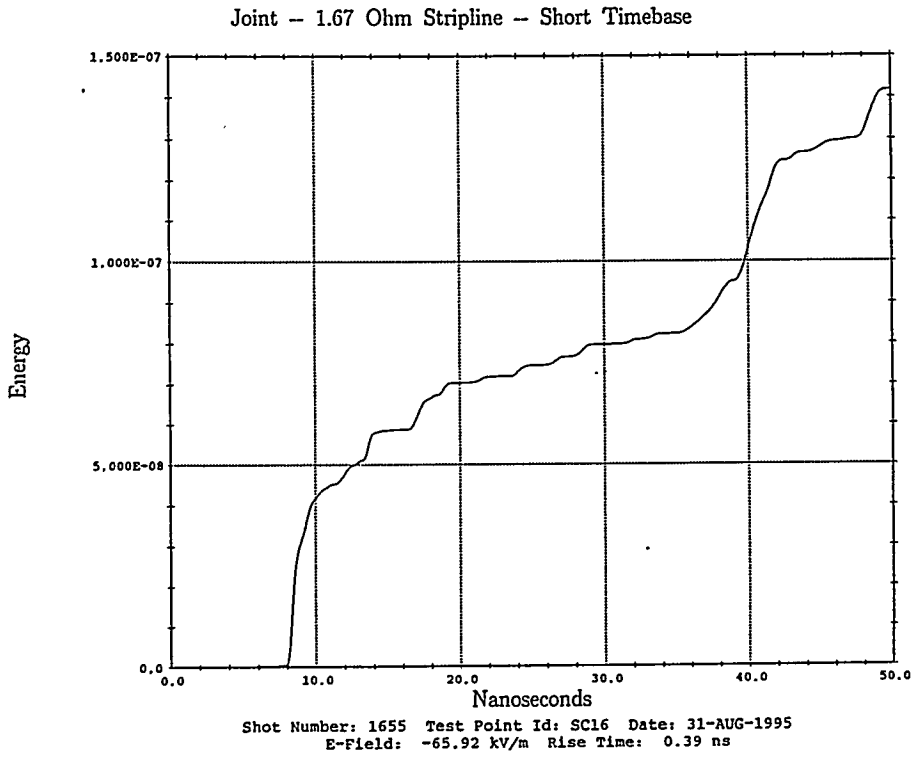

(b) integral of the square of the output voltage

Figure 22. Measure output for bolted joint fixture with stripling cable and low impedance (1.67 ohm) load.

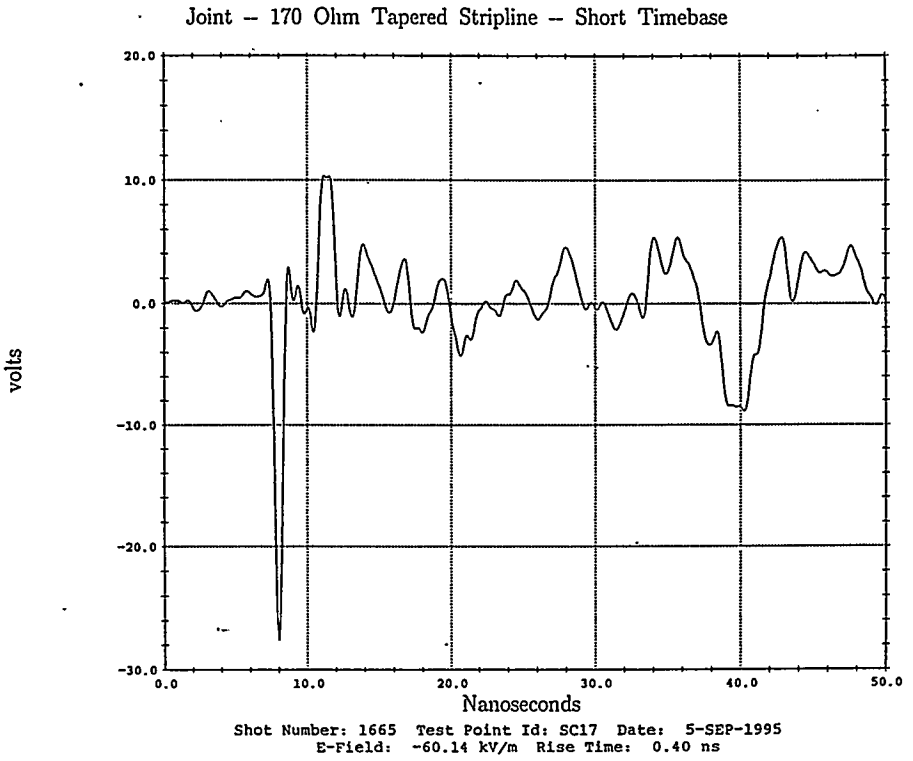

(a) voltage waveform

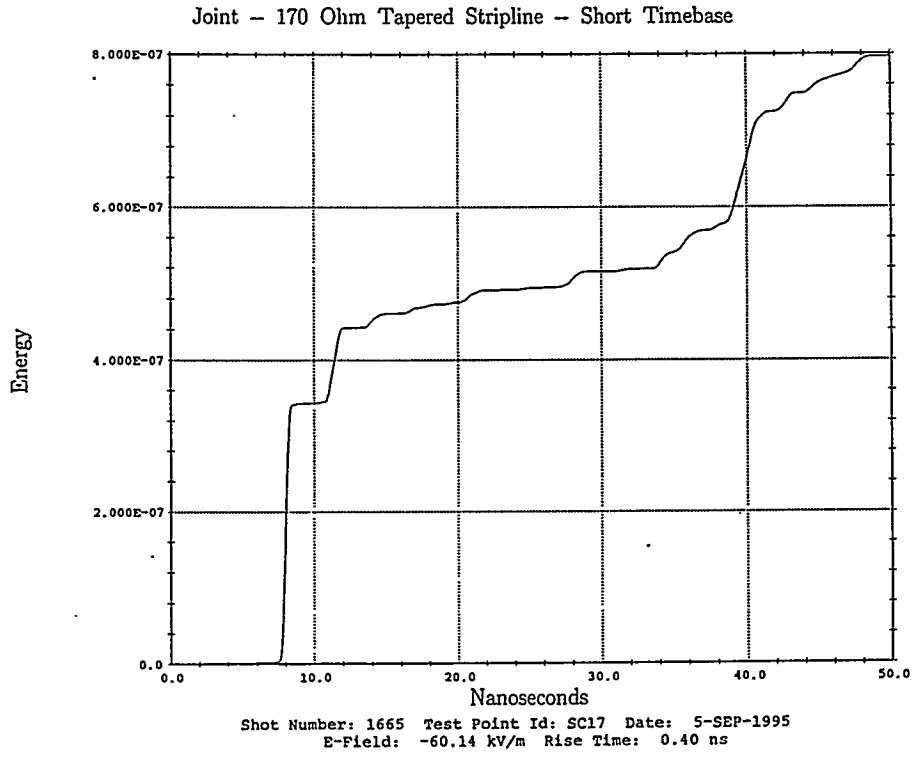

(b) integral of the square of the output voltage

Figure 23. Measured output for bolted joint fixture with tapered stripline cable and matched (170 ohm) load.

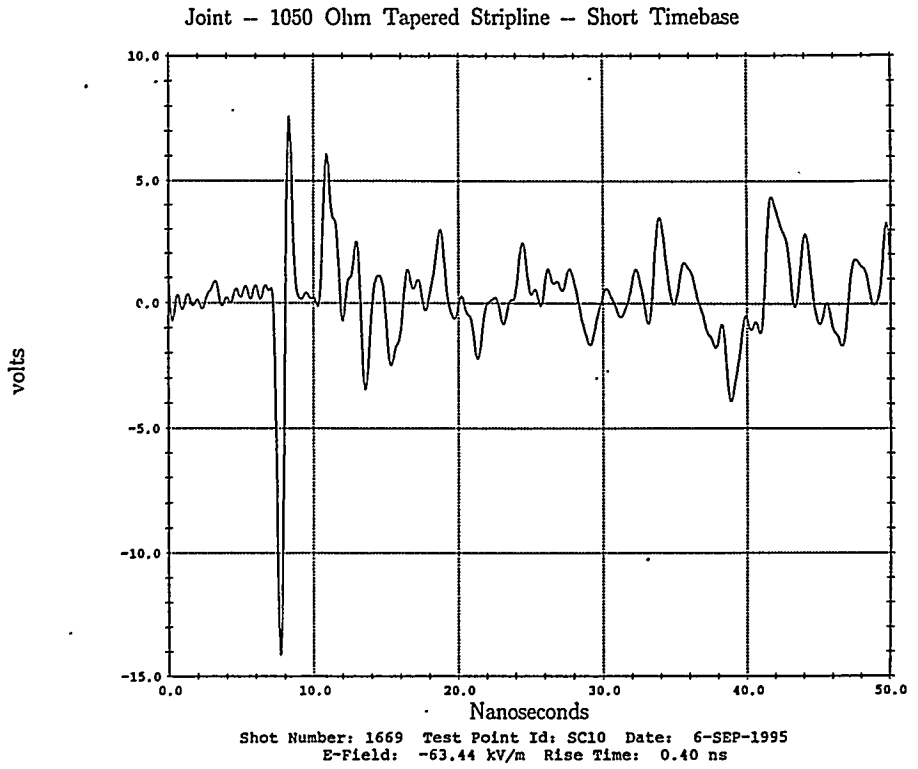

Figure 24. Measured output voltage (into 50-ohm measurement system) for bolted joint fixture with high impedance load (nominal 1050 ohm but parasitic capacitance lowers value) load.

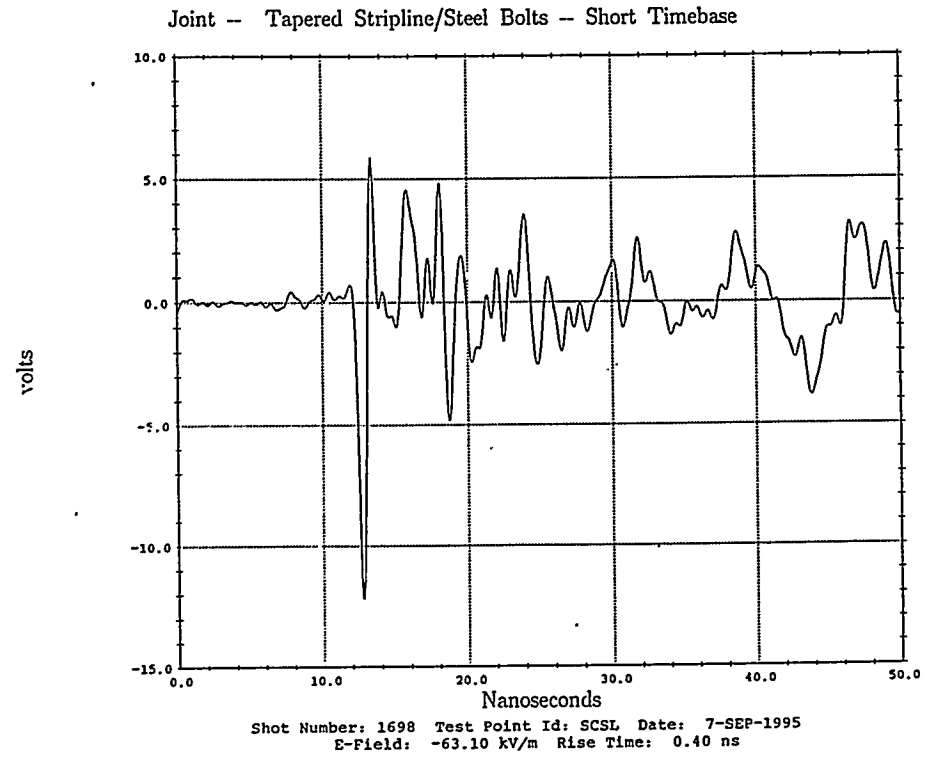

Figure 25. Measured output voltage (into 50-ohm measurement system) for bolted joint fixture with high impedance load (nominal 1050 ohm but parasitic capacitance lowers value) load and ferrous steel bolts.

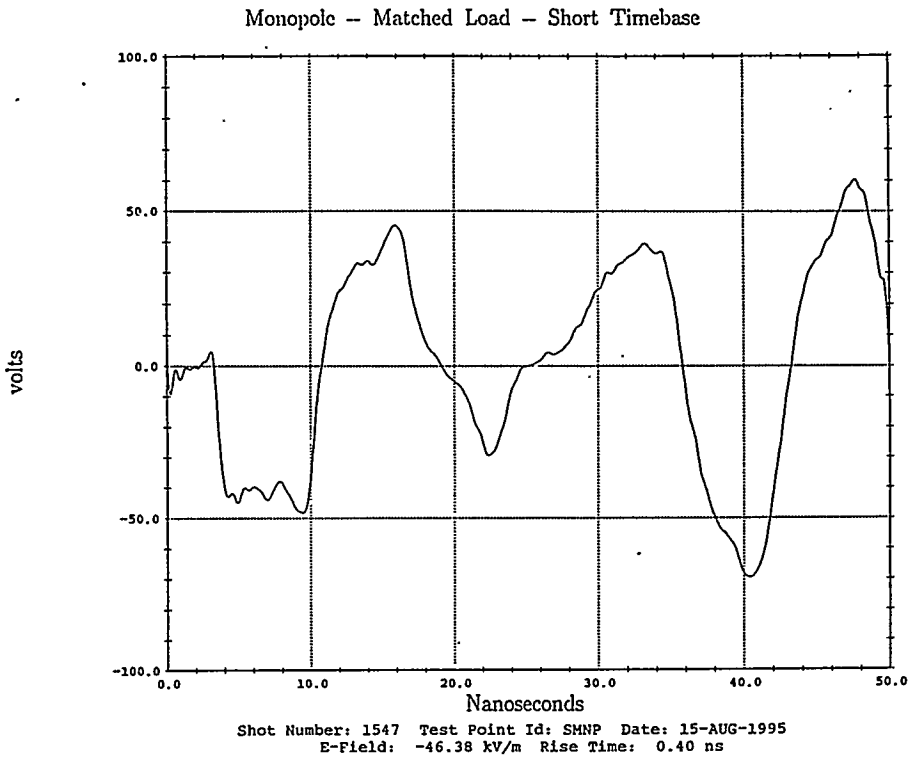

(a) voltage waveform into 50-ohm measurement system

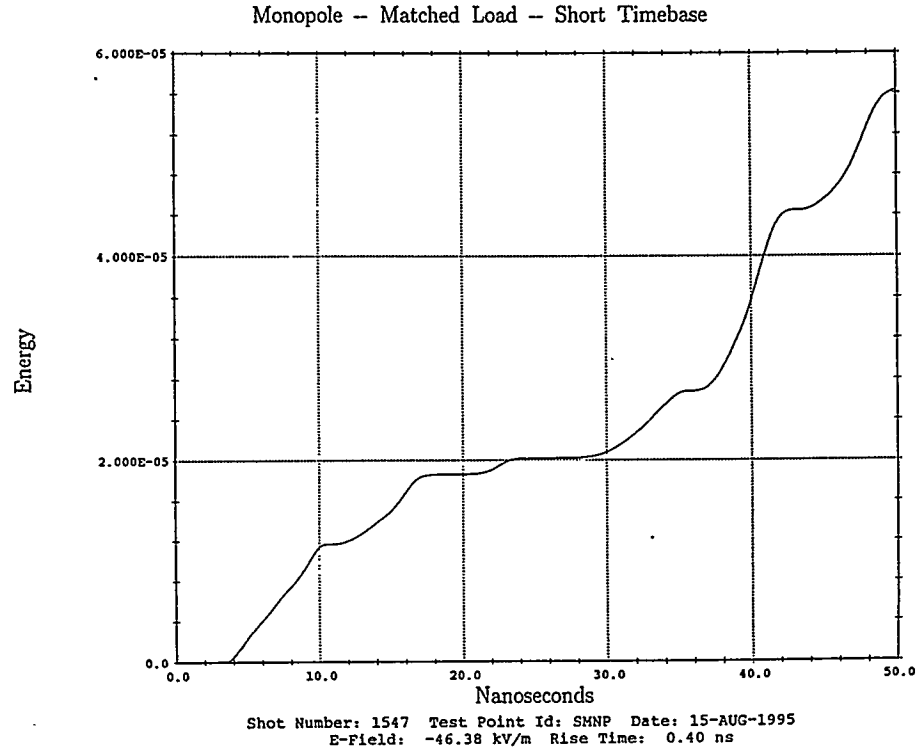

(b) integral of the square of the output voltage

Figure 26. Measured output for monopole fixture with centered wire and matched (200 ohm) load.

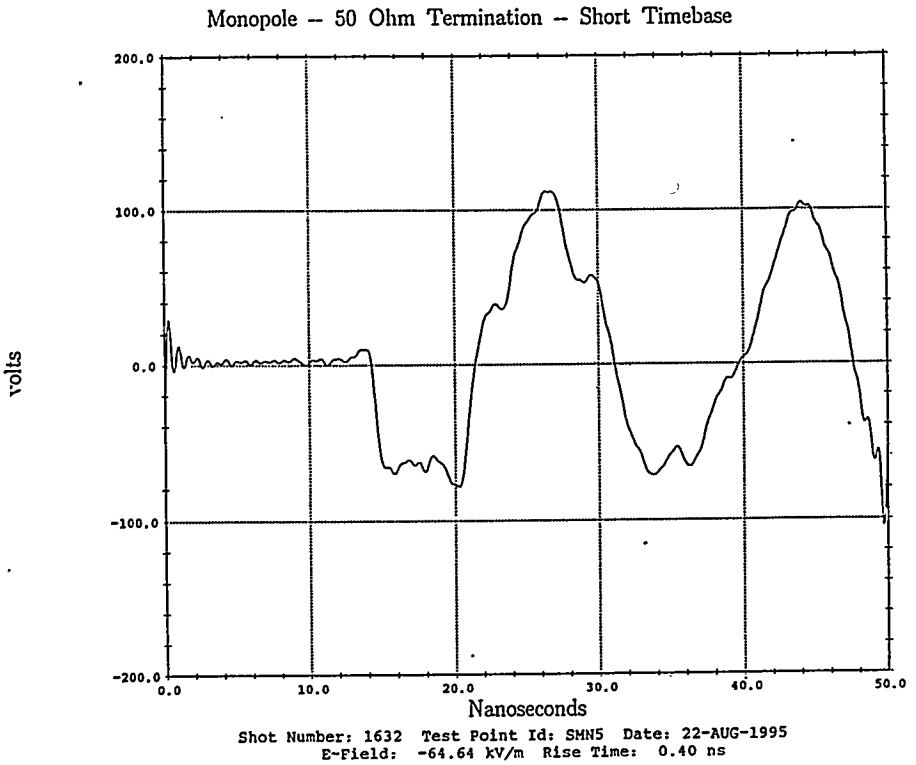

(a) voltage waveform into 50-ohm measurement system

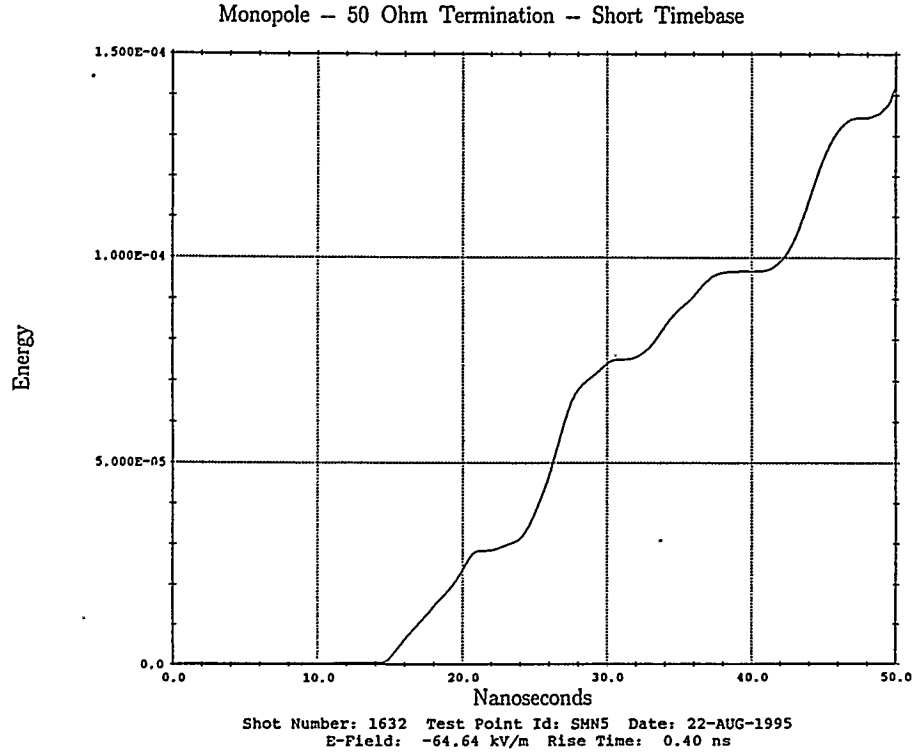

(b) integral of the square of the output voltage

Figure 27. Measured output for monopole fixture with centered wire and low impedance (50 ohm) load.

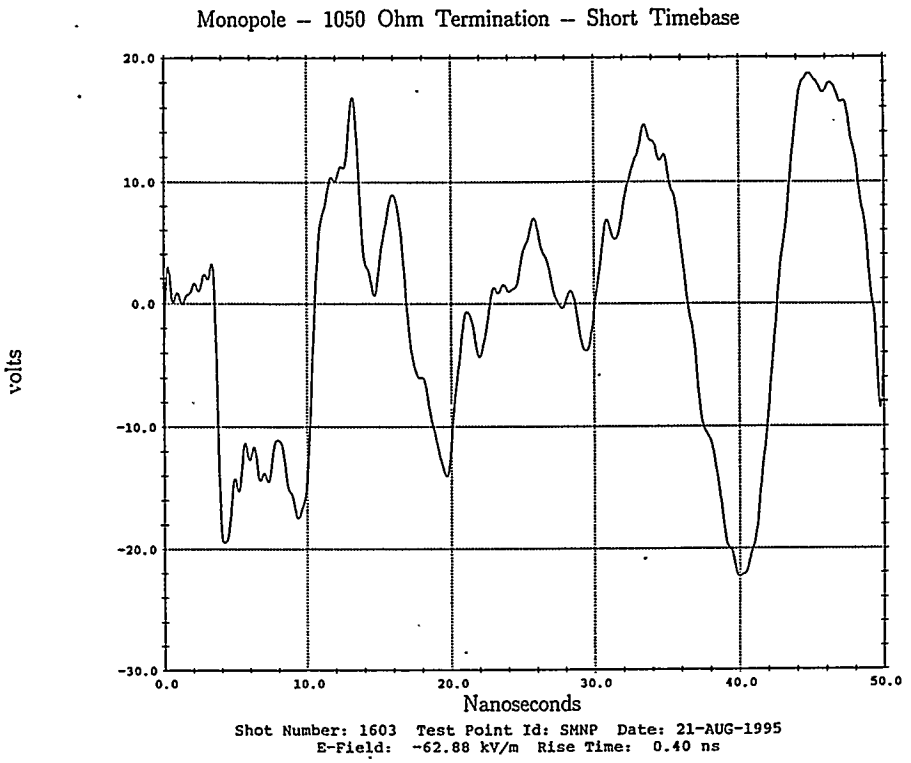

(a) voltage waveform into 50-ohm measurement system

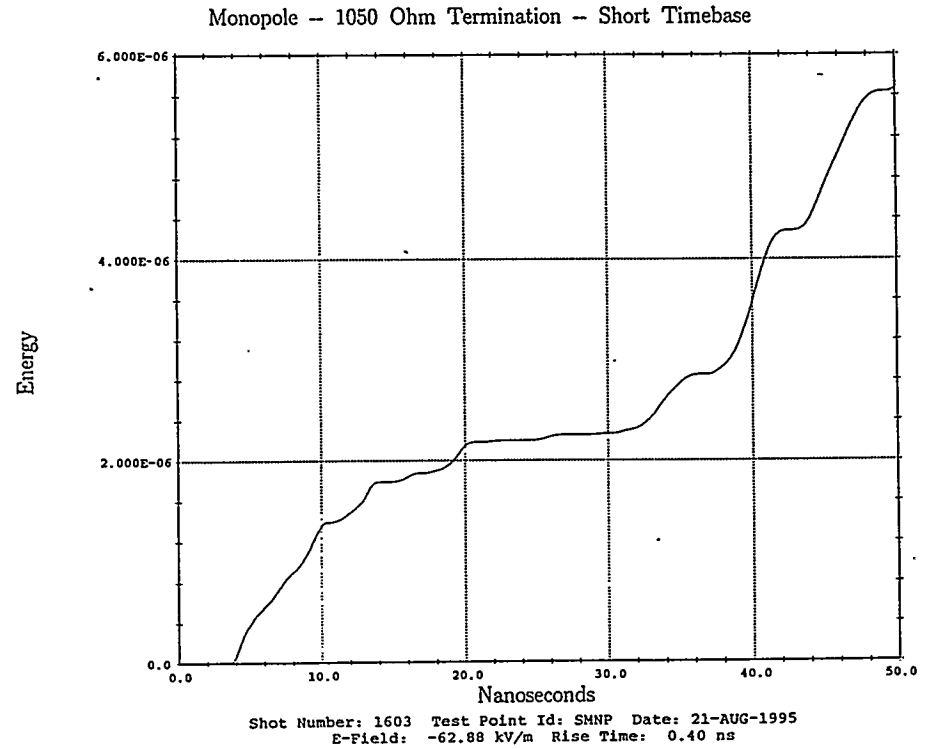

(b) integral of the square of the output voltage

Figure 28. Measured output for monopole fixture with centered wire and high impedance (nominal 1050 ohm) load.

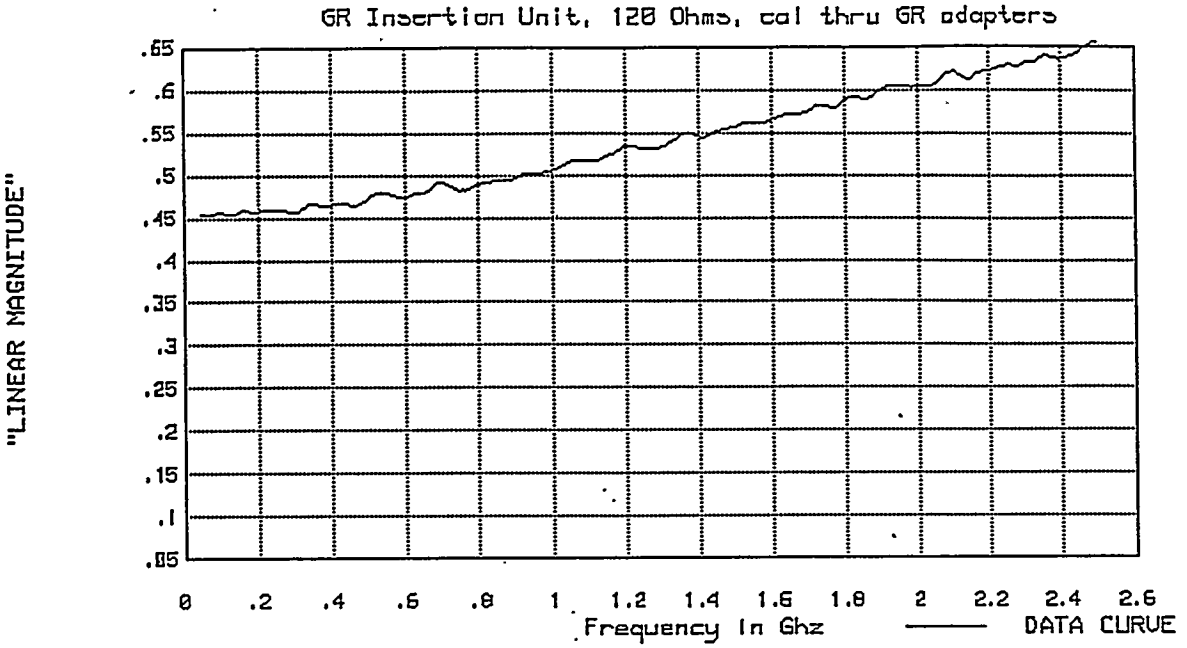

FILE = "GR 120"
"S21","LINEAR MAGNITUDE","STEP",100 AVG
13 Sep 1995 16:25:45

(a) 120-ohm resistor

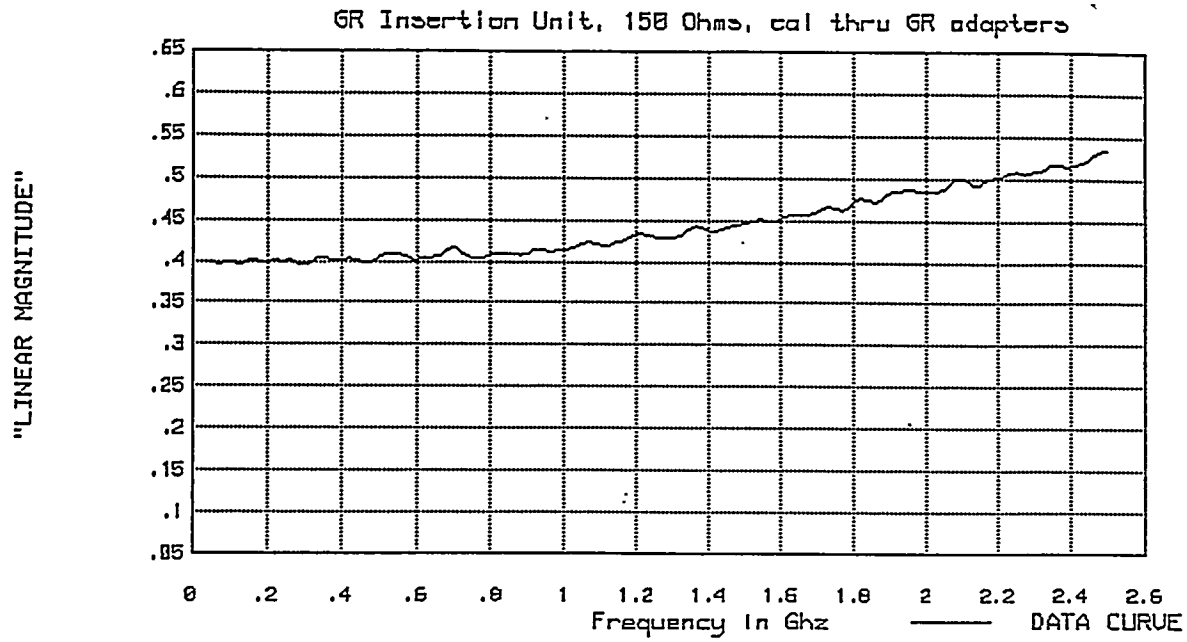

FILE = "GR 150"
"S21","LINEAR MAGNITUDE","STEP",100 AVG
13 Sep 1995 16:15:24

(b) 150-ohm resistor

Figure 29. Calibration (S_{21}) measurements of load resistors (used in series with 50-ohm measurement system).

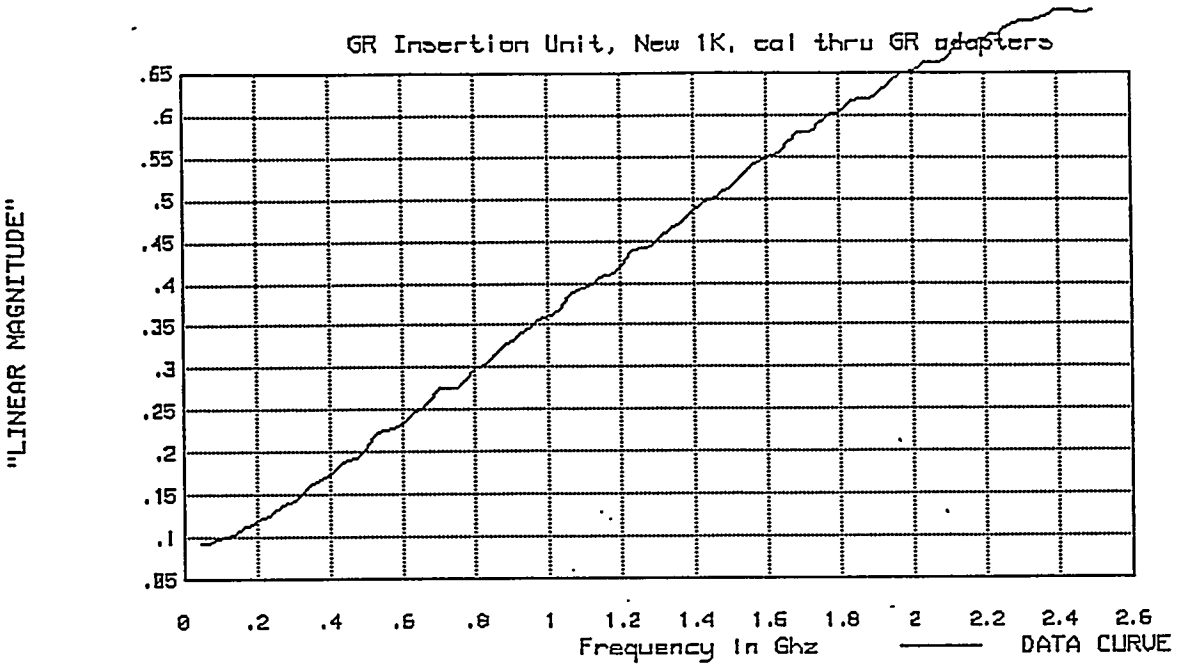

(c) 1000-ohm resistor

Figure 29. Calibration (S_{21}) measurements of load resistors (used in series with 50-ohm measurement system) (continued).

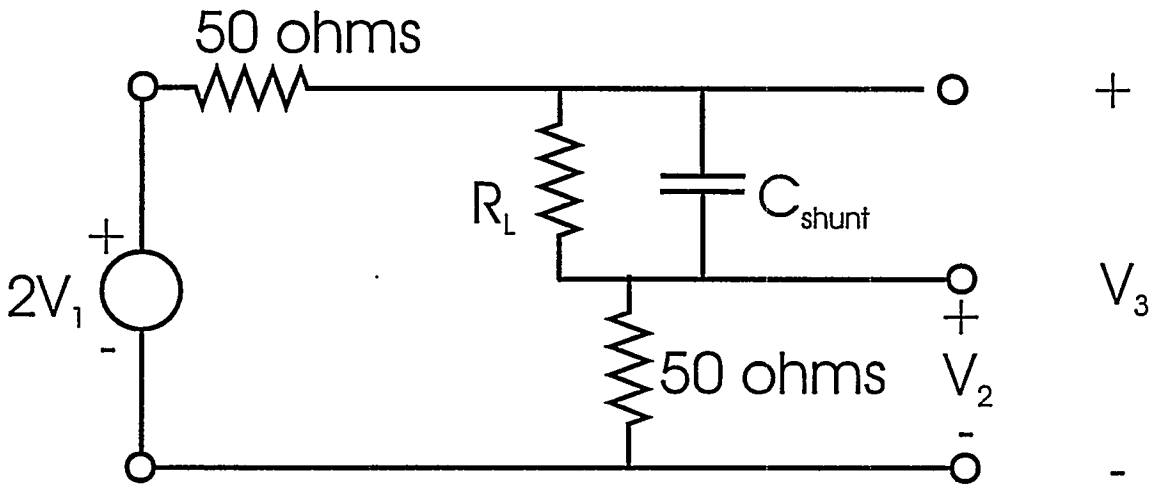

Figure 30. Assumed circuit to represent parasitic shunt capacitance present in calibration measurements (the 50-ohm resistors represent the insertion unit input and output transmission lines).

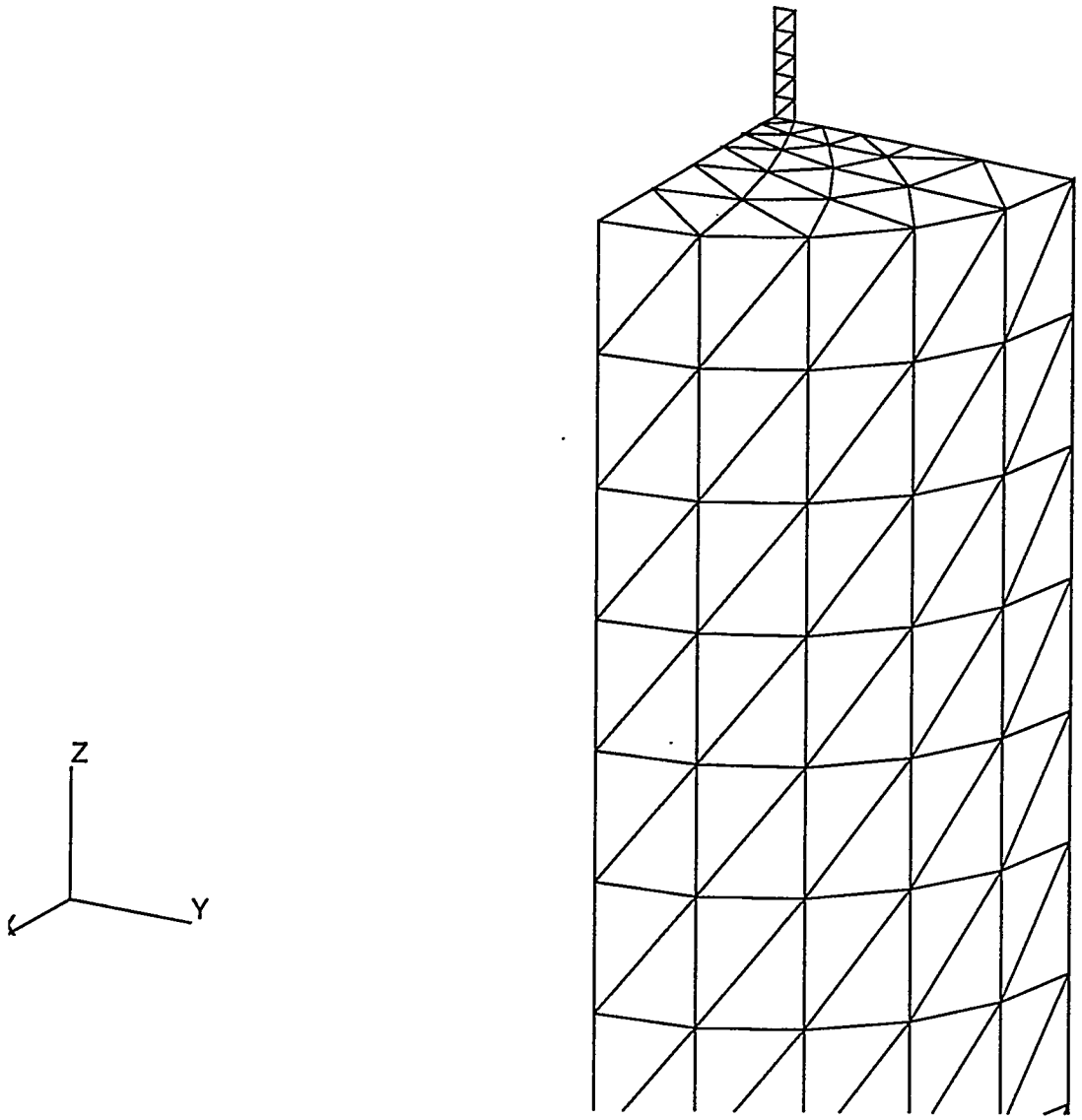

(a) monopole exterior grid (monopole modeled by strip)

Figure 31. PATCH models of monopole fixture (perfect magnetic conductor symmetry planes allow gridding of only one quarter of the structure).

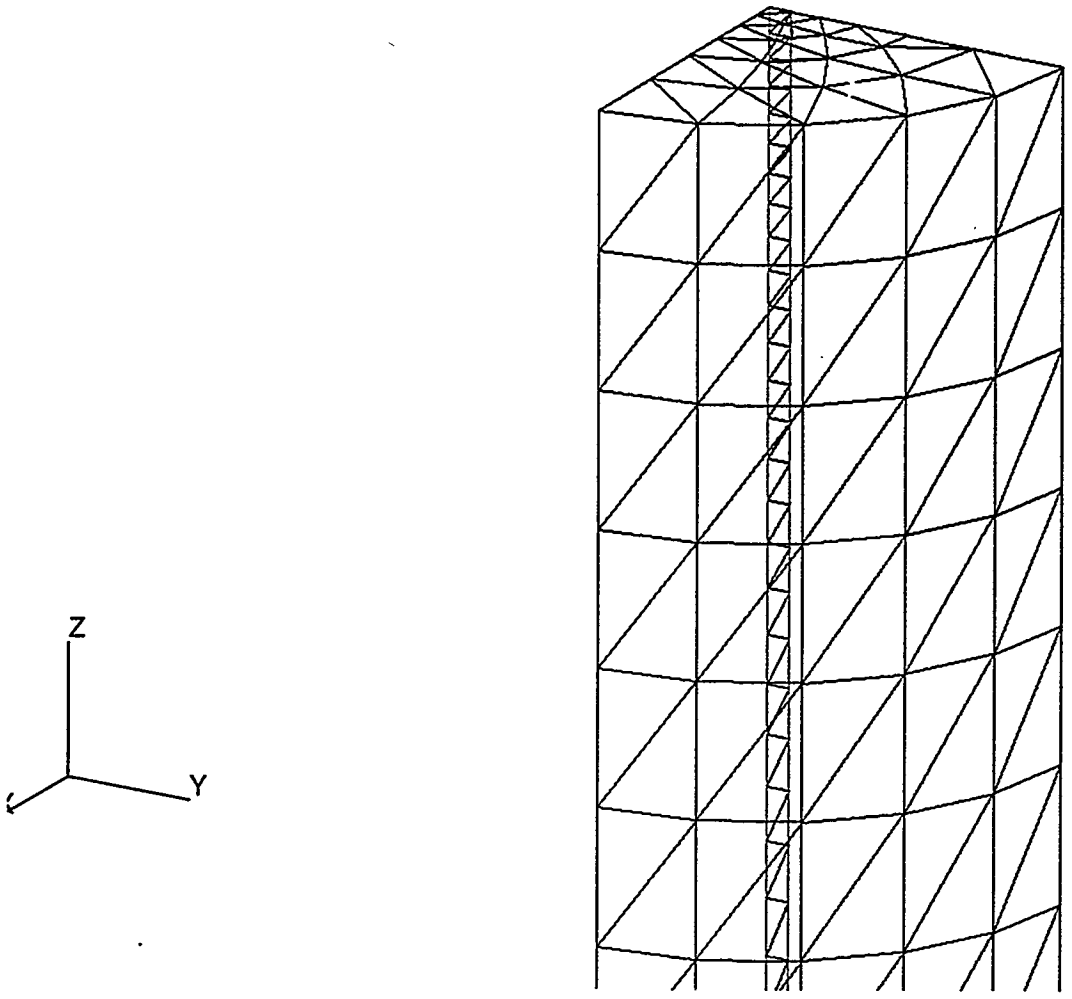

(b) monopole interior surface grid with centered wire (modeled by strip) and 50-ohm load, driven by exterior Thevenin equivalent circuit (second step of two-step coupling procedure).

Figure 31. PATCH models of monopole fixture (perfect magnetic conductor symmetry planes allow gridding of only one quarter of the structure) (continued).

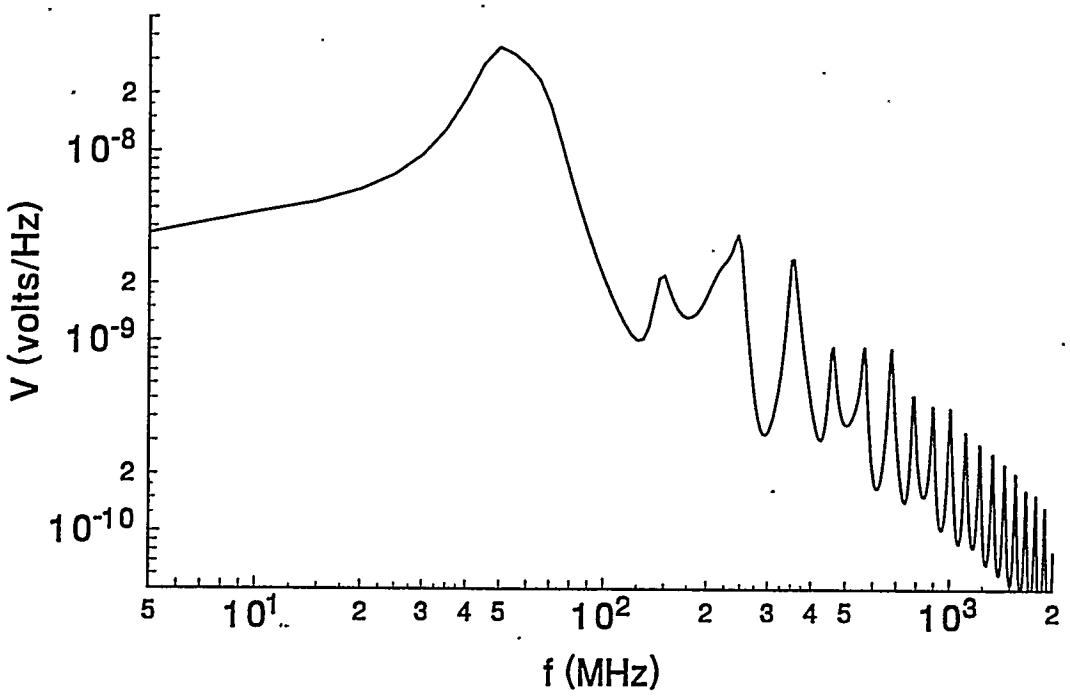

(a) frequency domain load voltage

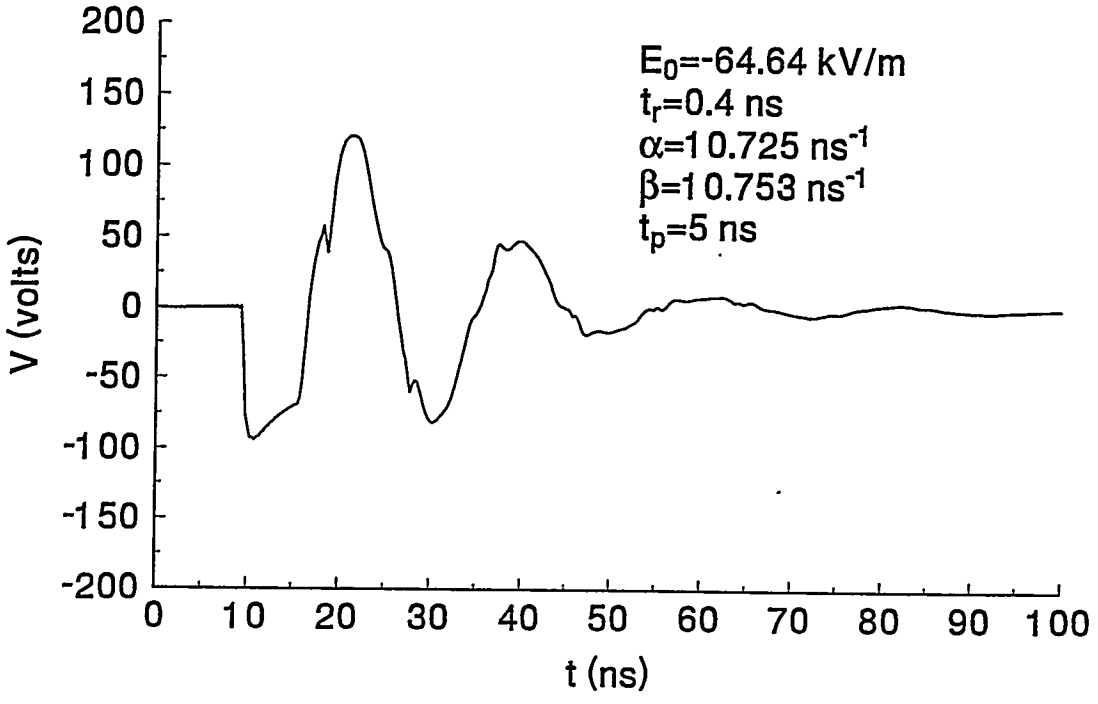

(b) time domain load voltage (predicted voltage into 50-ohm measurement system)

Figure 32. Monopole fixture PATCH code output into 50-ohm load.

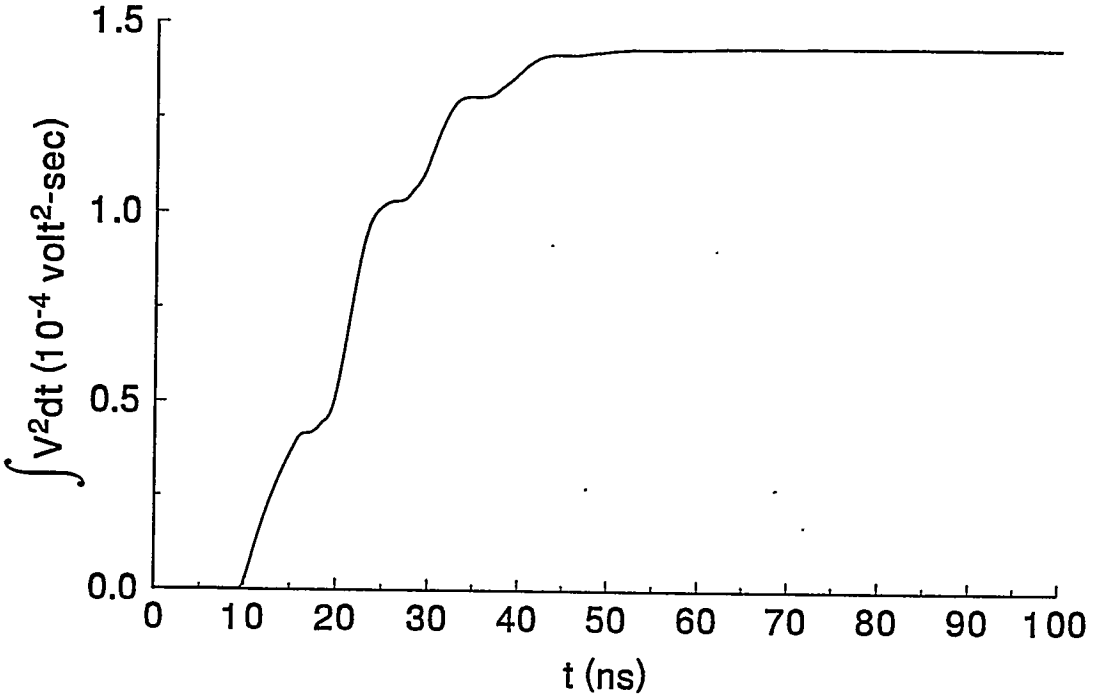

(c) time integral of the square of 50-ohm voltage

Figure 32. Monopole fixture PATCH code output into 50-ohm load.

Distribution

1 Kaman Science
Attn: K. S. H. Lee
2800 28th St.
Santa Monica, CA 90405

1	MS 0483	J. G. Lewis, 2165
5	MS 0492	K. C. Chen, 12332
5	MS 0865	M.E. Morris, 9753
5	MS 0865	K. O. Merewether, 9753
1	MS 0865	P. Holmes, 9753
5	MS 0865	R. E. Jorgenson, 9753
1	MS 0865	J. R. Stake
1	MS 0865	W. Derr, 9753
1	MS 0865	J. E. Solberg, 9753
15	MS 0865	L. K. Warne, 9753
1	MS 9018	Central Technical Files, 8523-2
5	MS 0899	Technical Library, 4414
2	MS 0619	Review & Approval Desk, 12630 for DOE/OSTI